CONFIDENTIAL

Copy 301
RM L56C23b

NACA

RESEARCH MEMORANDUM

WIND-TUNNEL INVESTIGATION OF THE STATIC LONGITUDINAL AND LATERAL STABILITY OF A 1/62-SCALE MODEL OF THE X-1E AT SUPERSONIC SPEEDS

By Arthur Henderson, Jr.

Langley Aeronautical Laboratory
Langley Field, Va.

CLASSIFIED DOCUMENT

This material contains information affecting the National Defense of the United States within the meaning of the espionage laws, Title 18, U.S.C., Secs. 793 and 794, the transmission or revelation of which in any manner to an unauthorized person is prohibited by law.

NATIONAL ADVISORY COMMITTEE
FOR AERONAUTICS

WASHINGTON

May 7, 1956

CONFIDENTIAL

NATIONAL ADVISORY COMMITTEE FOR AERONAUTICS

RESEARCH MEMORANDUM

WIND-TUNNEL INVESTIGATION OF THE STATIC LONGITUDINAL AND LATERAL STABILITY OF A 1/62-SCALE MODEL OF THE X-1E AT SUPERSONIC SPEEDS

By Arthur Henderson, Jr.

SUMMARY

An investigation to determine the static longitudinal and lateral stability characteristics of a 1/62-scale model of the X-1E has been conducted in the Langley 9-inch supersonic tunnel. Tests were made at Mach numbers of 1.62, 1.94, 2.22, 2.40, and 2.62 on the wing-body, wing—body—vertical-tail, and complete model configurations. Detailed analysis of the test results has not been made.

INTRODUCTION

The X-1E is a thin-wing version of the original X-1 series and has been designed to operate in approximately the same speed range as the Bell X-1A. In view of the handling difficulties encountered by the X-1A (wind-tunnel tests of a model of the X-1A are presented in ref. 1), it was deemed advisable to obtain as much preflight knowledge of the anticipated aerodynamic characteristics of the X-1E as possible. This paper presents the aerodynamic characteristics of a 1/62-scale model of the X-1E at Mach numbers of 1.62, 1.94, 2.22, 2.41, and 2.62. Tests were conducted on the complete configuration with three different stabilizer settings (0°, 5°, -10°), the model with horizontal tail off, and the model with horizontal and vertical tails off. Tests were made through an angle-of-attack range at zero sideslip angle and through an angle-of-sideslip range at zero angle of attack. Detailed analysis of the test results is omitted in order to expedite release of this information.

SYMBOLS

A	axial force, lb
b	wing span, in.

B	body
$\bar{c}$	wing mean aerodynamic chord
c.g.	center of gravity (located at 20.0 percent mean aerodynamic chord)
C_A	axial force coefficient, A/qS
C_D	drag coefficient, D/qS
C_{D_o}	minimum drag coefficient
C_{F_N}	normal-force coefficient, F_N/qS
C_L	lift coefficient, L/qS
C_l	rolling-moment coefficient, L'/qSb
C_m	pitching-moment coefficient, $M/qS\bar{c}$
C_n	yawing-moment coefficient, N/qSb
C_Y	side-force coefficient, Y/qS
D	drag, lb
F_N	normal force, lb
L	lift, lb
L'	rolling moment about an axis 0.049 inch above and parallel to body axis, ft-lb
M	pitching moment about center of gravity, ft-lb; or Mach number
N	yawing moment about center of gravity, ft-lb
q	dynamic pressure, lb/sq ft
R	Reynolds number based on $\bar{c}$
S	wing area, sq in.; or stabilizer

T vertical tail

W wing

x longitudinal distance ahead or behind center of gravity, in.

$x/\bar{c}$ longitudinal center-of-pressure location measured from the center of gravity in terms of $\bar{c}$

α angle of attack of body center line, deg

β angle of sideslip, deg

$C_{L_\alpha} = \left(\frac{\partial C_L}{\partial \alpha}\right)_{\alpha=0}$

$C_{m_\alpha} = \left(\frac{\partial C_m}{\partial \alpha}\right)_{\alpha=0}$

$\frac{\partial C_m}{\partial C_L}$ longitudinal aerodynamic-center location measured from the center of gravity in terms of $\bar{c}$ at $\alpha = 0$, $\frac{\partial C_m}{\partial C_L} = \frac{\left(C_{m_\alpha}\right)_{\alpha=0}}{\left(C_{L_\alpha}\right)_{\alpha=0}}$

$C_{Y_\beta} = \frac{\partial C_Y}{\partial \beta}$

$C_{l_\beta} = \frac{\partial C_l}{\partial \beta}$

$C_{n_\beta} = \frac{\partial C_n}{\partial \beta}$

$\frac{\partial C_n}{\partial C_Y}$ direction aerodynamic-center location measured from the center of gravity in terms of b at $\beta = 0$, $\frac{\partial C_n}{\partial C_Y} = \frac{C_{n_\beta}}{C_{Y_\beta}}$

APPARATUS AND TESTS

Wind Tunnel

The Langley 9-inch supersonic tunnel is a closed-throat, single-return, continuous-operating tunnel in which the test section is approximately 9 inches square. Different test Mach numbers are achieved through the use of interchangeable nozzle blocks. Eleven fine-mesh turbulence-damping screens are installed in the settling chamber ahead of the supersonic nozzle. The pressure, temperature, and humidity can be controlled during the tunnel operation.

Models

The configurations used for the present tests consisted of the complete model with stabilizer settings of 0°, 5°, and -10° ($WBTS_0$, $WBTS_5$, $WBTS_{-10}$, respectively), wing-body-vertical tail (WBT), and wing-body (WB). A three-view drawing of the complete model is shown in figure 1.

Six-Component Balance and Model Support System

The six-component balance and model support system used in these tests are described in reference 2.

Tests

In an attempt to simulate flight boundary-layer conditions, all configurations were investigated with transition strips near the model nose, wing leading edges, vertical-tail leading edges, and stabilizer leading edges. The transition strips were approximately 0.006 inch thick and were made with aluminum oxide particles. The Mach number, Reynolds number, and α and β ranges for each configuration are given in table I. The two Reynolds numbers shown in table I at each of Mach numbers 2.22, 2.40, and 2.62 resulted from increasing the stagnation pressure in order to increase the sensitivity of the balance through the zero α and zero β range at the higher Mach numbers. The lower Reynolds number was that for atmospheric pressure in the stagnation chamber, which allowed the α and β ranges to be extended while keeping the maximum loads on the model consistent with allowable sting stresses.

PRECISION OF DATA

The estimated probable errors in the force and moment coefficients are as follows:

M	R	C_{F_N}	C_A	C_Y	C_l	C_n	C_m	C_L	C_D
1.62	0.39×10^6	±0.0004	±0.0004	±0.0004	±0.0016	±0.0006	±0.0020	±0.0004	±0.0004
1.94	.36	±.0006	±.0005	±.0007	±.0014	±.0010	±.0037	±.0006	±.0005
2.22	.55	±.0003	±.0002	±.0003	±.0012	±.0006	±.0018	±.0003	±.0002
	.32	±.0007	±.0003	±.0006	±.0007	±.0007	±.0024	±.0007	±.0003
2.41	.49	±.0005	±.0002	±.0004	±.0006	±.0006	±.0013	±.0005	±.0002
	.28	±.0005	±.0002	±.0006	±.0012	±.0012	±.0028	±.0005	±.0002
2.62	.55	±.0005	±.0002	±.0003	±.0013	±.0008	±.0011	±.0005	±.0002
	.26	±.0006	±.0005	±.0011	±.0015	±.0013	±.0036	±.0006	±.0004

SUMMARY OF RESULTS

The static longitudinal and lateral force and moment characteristics of the configurations tested are presented in figures 2 to 26 as follows:

Configuration	Figures for Mach number of -				
	1.62	1.94	2.22	2.40	2.62
WB	2	3	4	5	6
WBT	7	8	9	10	11
$WBTS_0$	12	13	14	15	16
$WBTS_5$	17	18	19	20	21
$WBTS_{-10}$	22	23	24	25	26

Figures 2 to 26 have three parts each: part (a) presents the longitudinal force and moment characteristics about the body-axis system; part (b) presents the longitudinal force characteristics about the stability axis system; part (c) presents the lateral force and moment

characteristics about the body axis system. The flagged symbols on the curves for $M = 2.22$, 2.40, and 2.62 represent the atmospheric stagnation pressure data, while the unflagged symbols are for stagnation pressures greater than atmospheric.

Figure 27 presents the static longitudinal and lateral stability derivatives and the minimum-drag coefficients of the configurations as a function of Mach number. The lateral derivatives in figure 27(a) are taken through $\beta = 0^\circ$ at $\alpha = 0^\circ$, whereas those in figure 27(b) are through $\beta = -8^\circ$ at $\alpha = 0^\circ$.

The figure shows that the variation with Mach number of the minimum drag and static longitudinal stability derivatives is qualitatively what would be expected. The general trends with Mach number of the static lateral stability derivatives are also about what would be expected, except that between $M = 2.2$ and 2.4 the X-1E encounters a decrease in effective dihedral. In addition, the directional stability decreases with increasing Mach number up to a Mach number of about 2.4, from which point it begins to increase with Mach number.

Langley Aeronautical Laboratory,
National Advisory Committee for Aeronautics,
Langley Field, Va., March 9, 1956.

REFERENCES

1. Henderson, Arthur, Jr.: Wind-Tunnel Investigation of the Static Longitudinal and Lateral Stability of the Bell X-1A at Supersonic Speeds. NACA RM L55I23, 1955.

2. Rainey, Robert W.: Investigation of the Effects of Bomb-Bay Configuration Upon the Aerodynamic Characteristics of a Body With Circular Cross Section at Supersonic Speeds. NACA RM L55E27, 1955.

TABLE I.- TEST CONDITIONS

M	R	Range of α, deg	Range of β, deg
1.62	0.39×10^6	-6 to 6	-6 to 4
1.94	.36	-6 to 8	-8 to 4
2.22	.55	-6 to 6	-6 to 4
	.32	4 to 10	-10 to -4
2.40	.49	-6 to 8	-8 to 4
	.28	6 to 12	-12 to -6
2.62	.55	-6 to 8	-8 to 4
	.26	6 to ≈13	≈-13 to -6

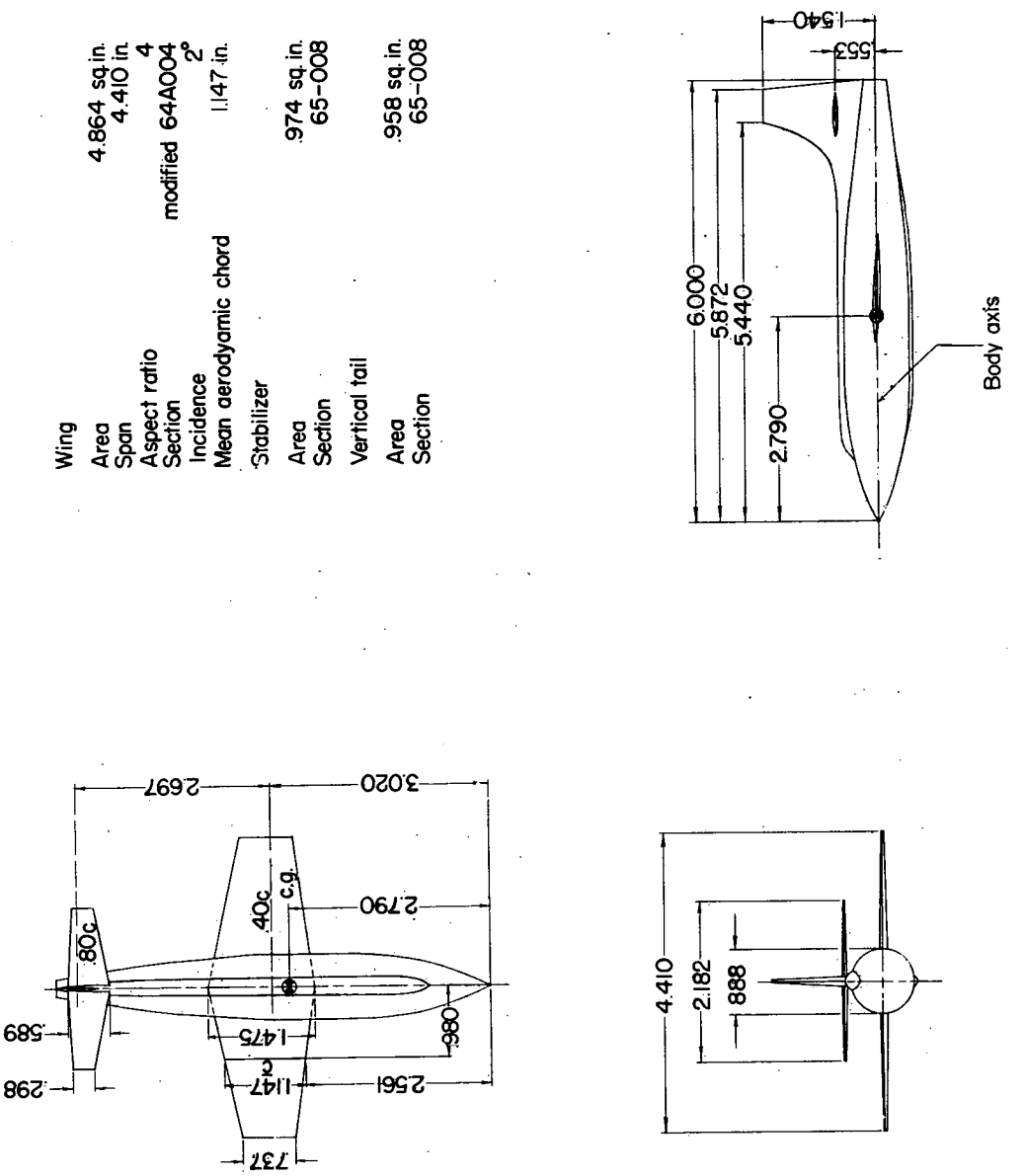

Figure 1.- Three-view drawing of 1/62-scale model of X-1E. All dimensions are in inches.

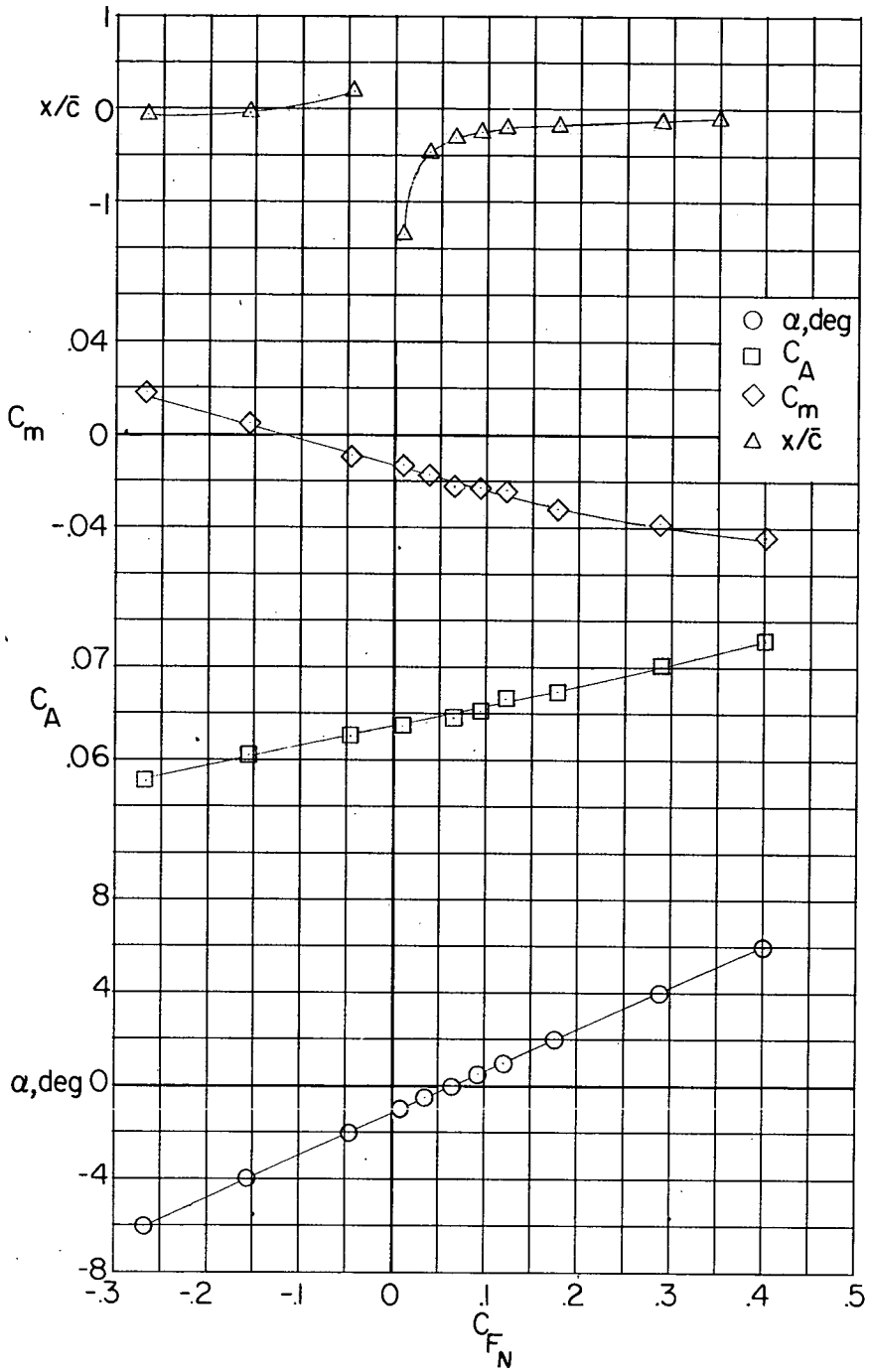

(a) Longitudinal characteristics in body-axis system at $\beta = 0^{\circ}$.

Figure 2.- Wing-body configuration at $M = 1.62$.

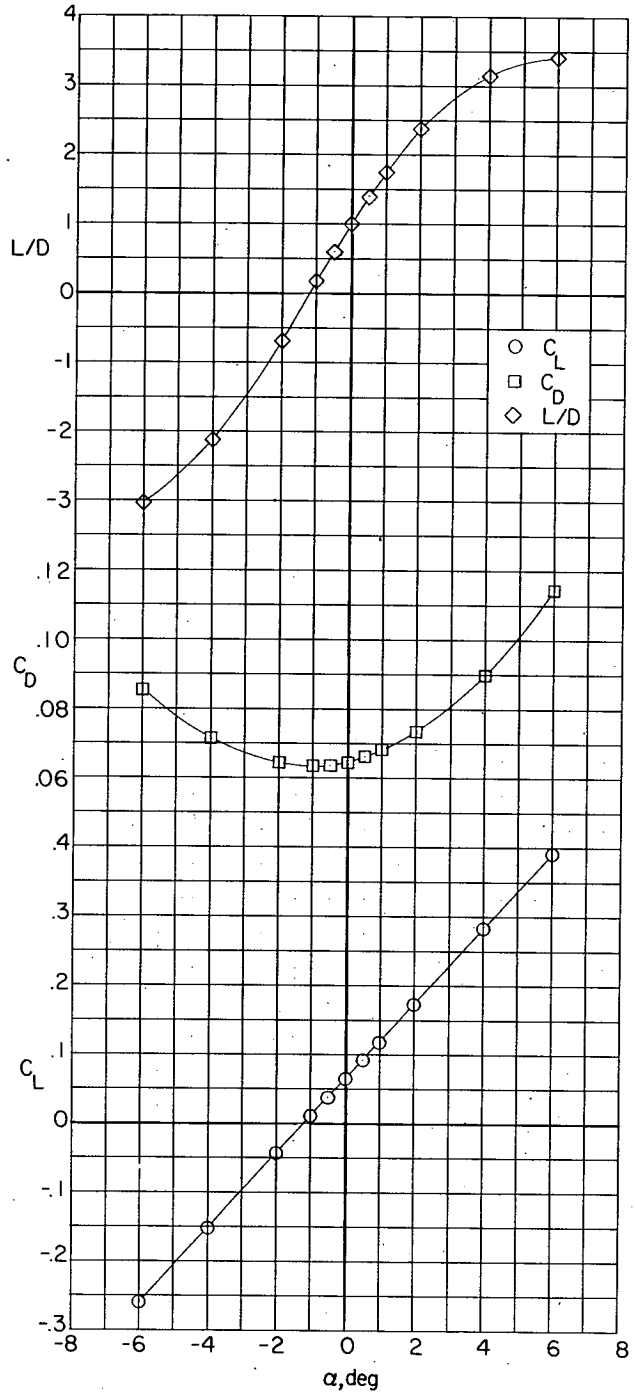

(b) Longitudinal-force characteristics in stability-axis system at $\beta = 0^\circ$.

Figure 2.- Continued.

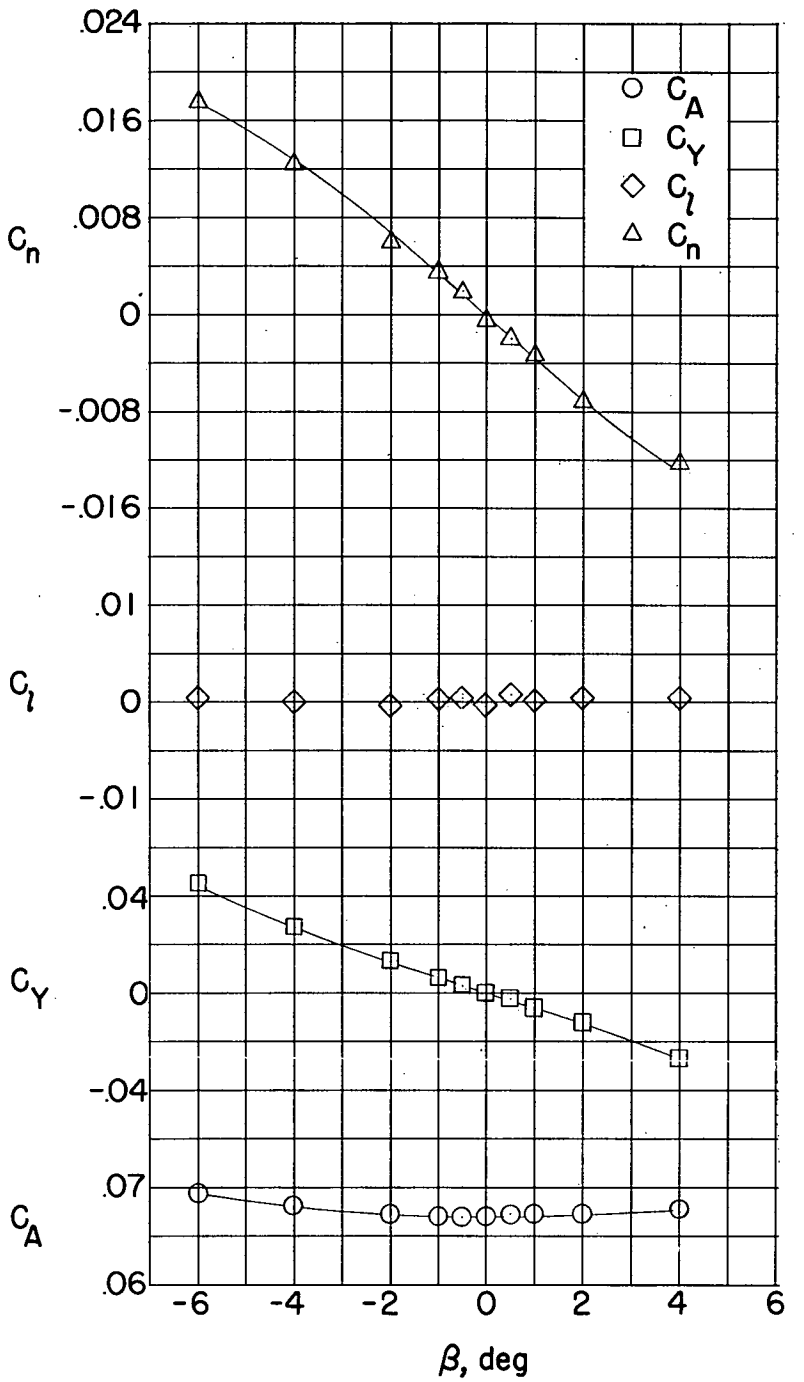

(c) Lateral characteristics in body-axis system at $\alpha = 0^{\circ}$.

Figure 2.- Concluded.

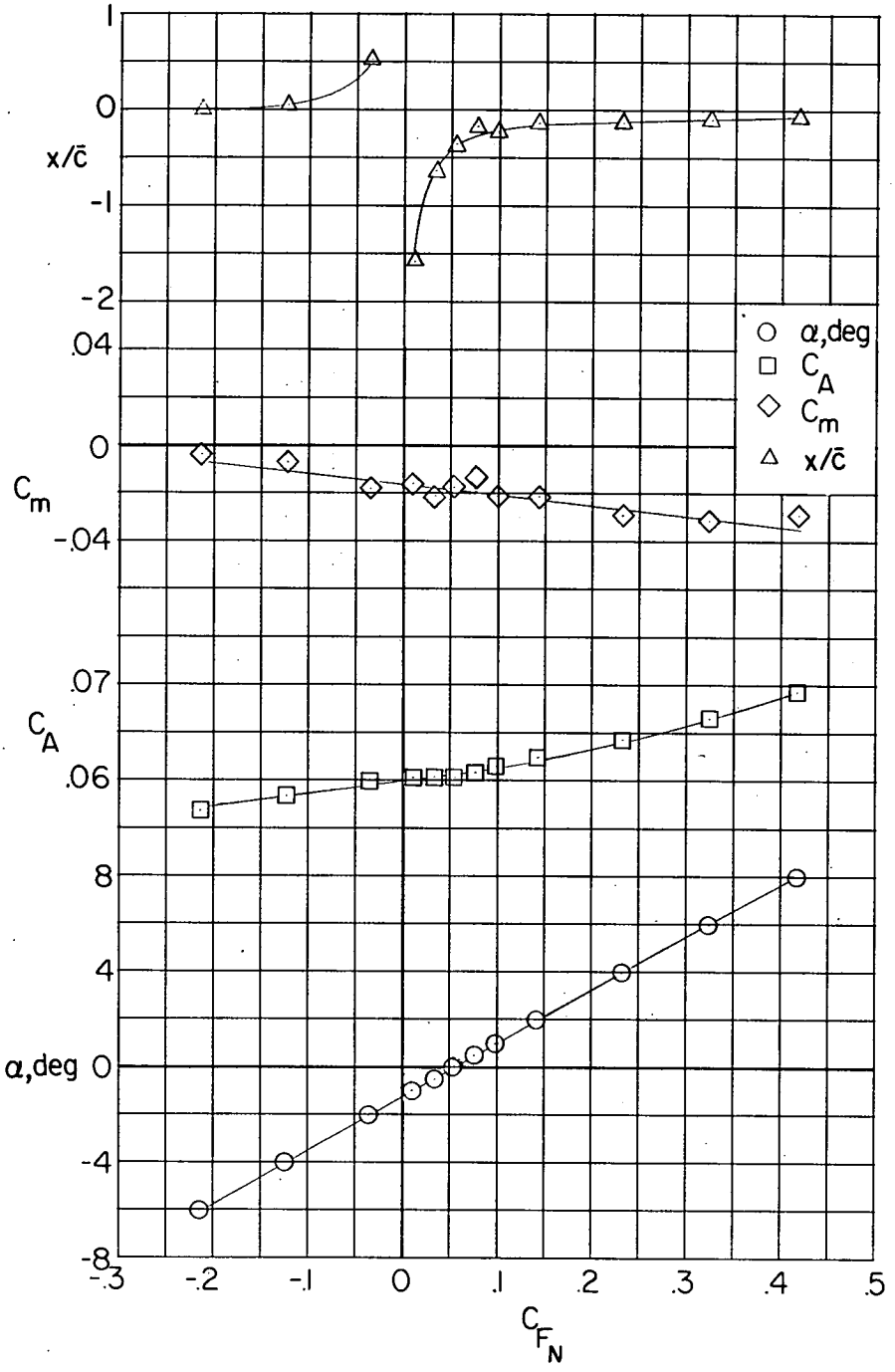

(a) Longitudinal characteristics in body-axis system at $\beta = 0^{\circ}$.

Figure 3.- Wing-body configuration at $M = 1.94$.

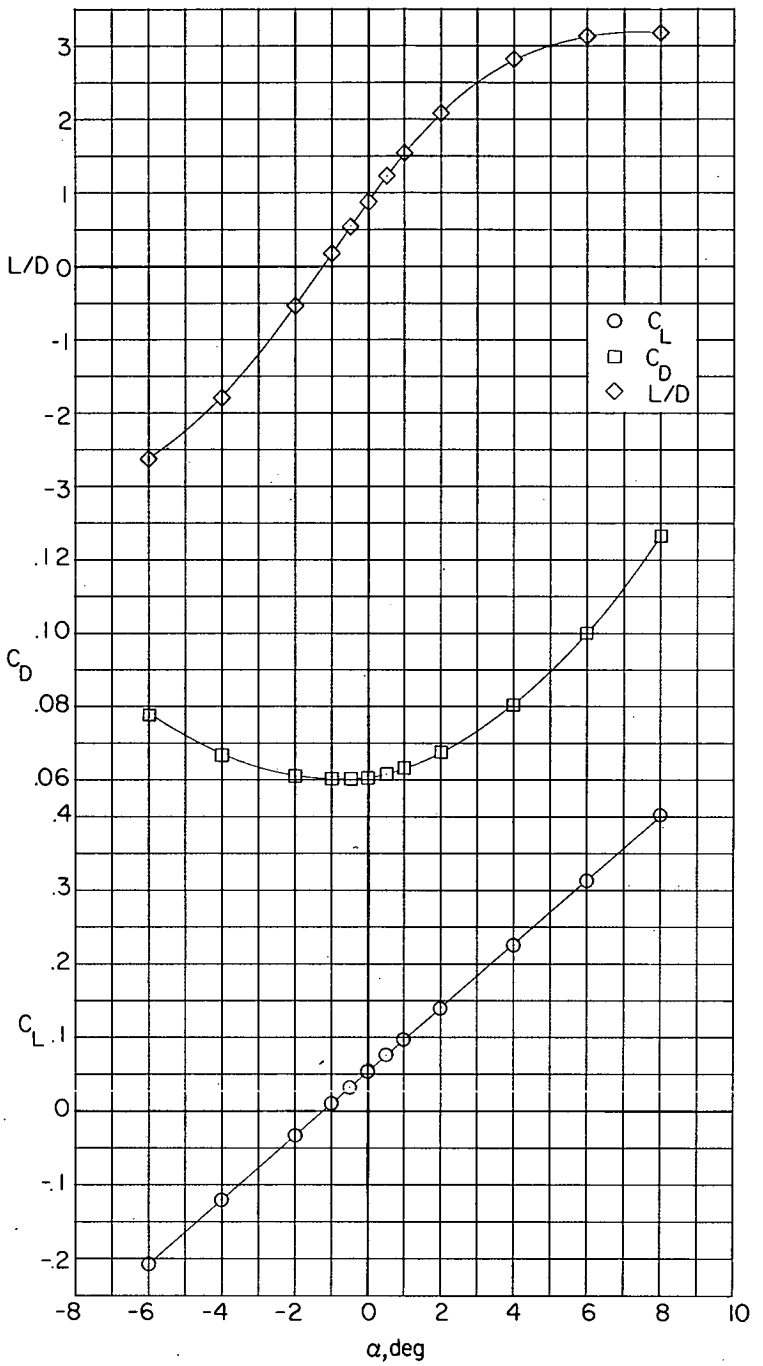

(b) Longitudinal-force characteristics in stability-axis system at $\beta = 0^{\circ}$.

Figure 3.- Continued.

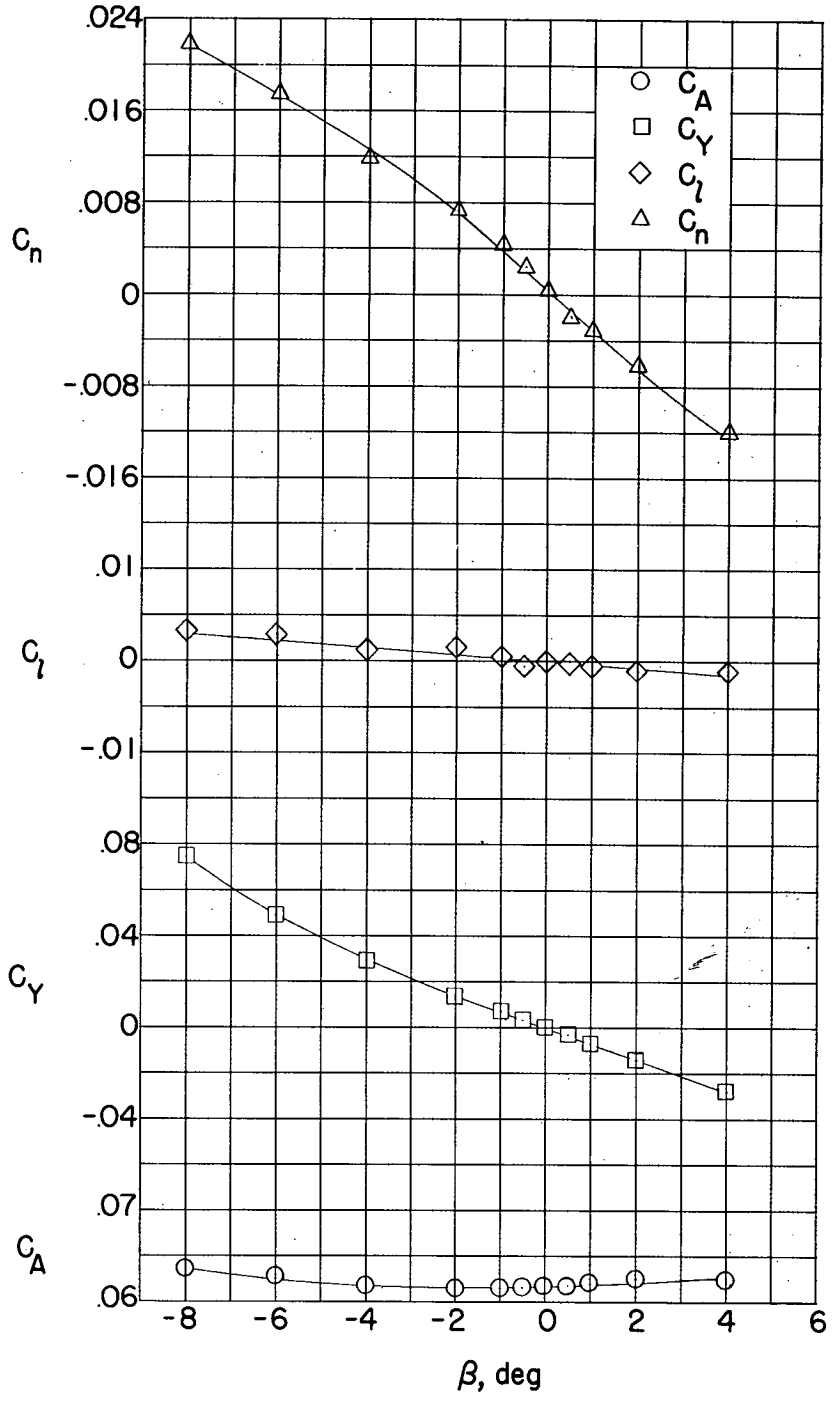

(c) Lateral characteristics in body-axis system at $\alpha = 0^\circ$.

Figure 3.- Concluded.

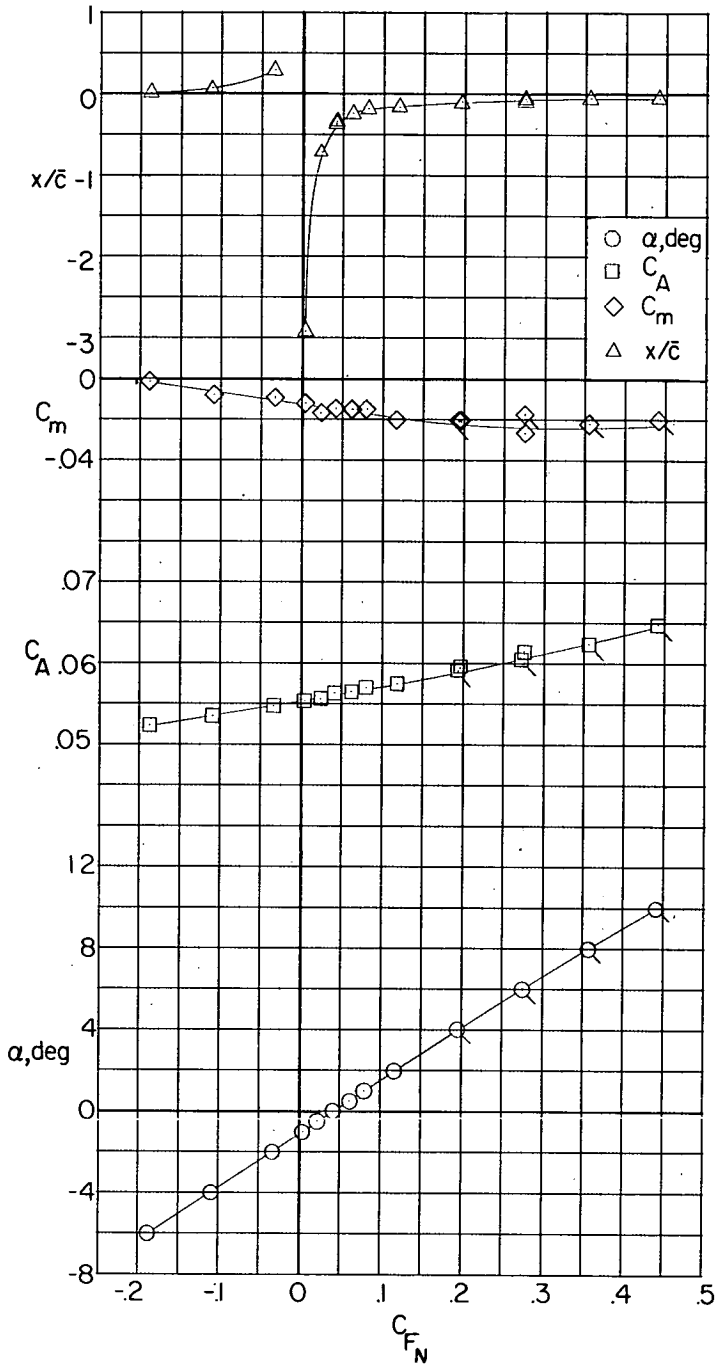

(a) Longitudinal characteristics in body-axis system at $\beta = 0^{\circ}$.

Figure 4.- Wing-body configuration at $M = 2.22$.

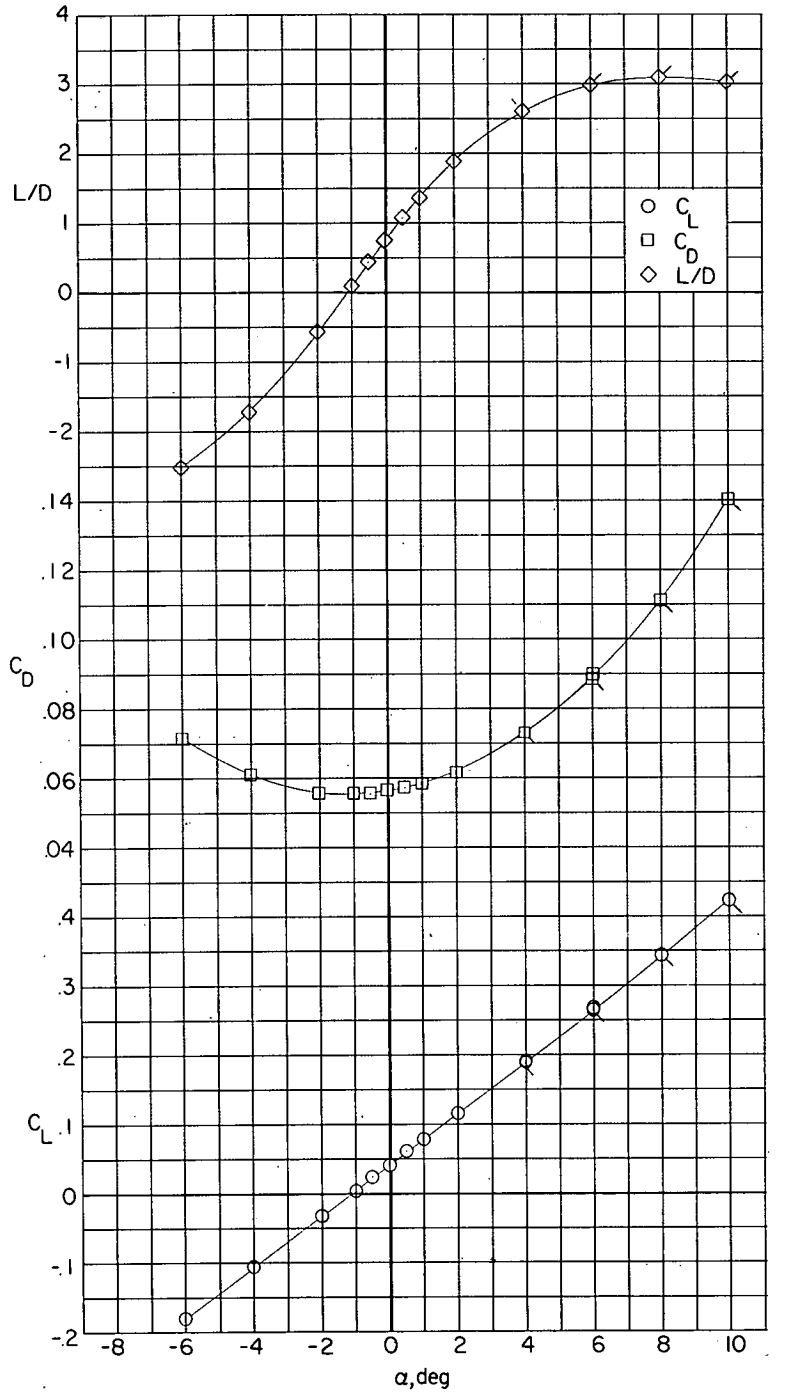

(b) Longitudinal-force characteristics in stability-axis system at $\beta = 0^{\circ}$.

Figure 4.- Continued.

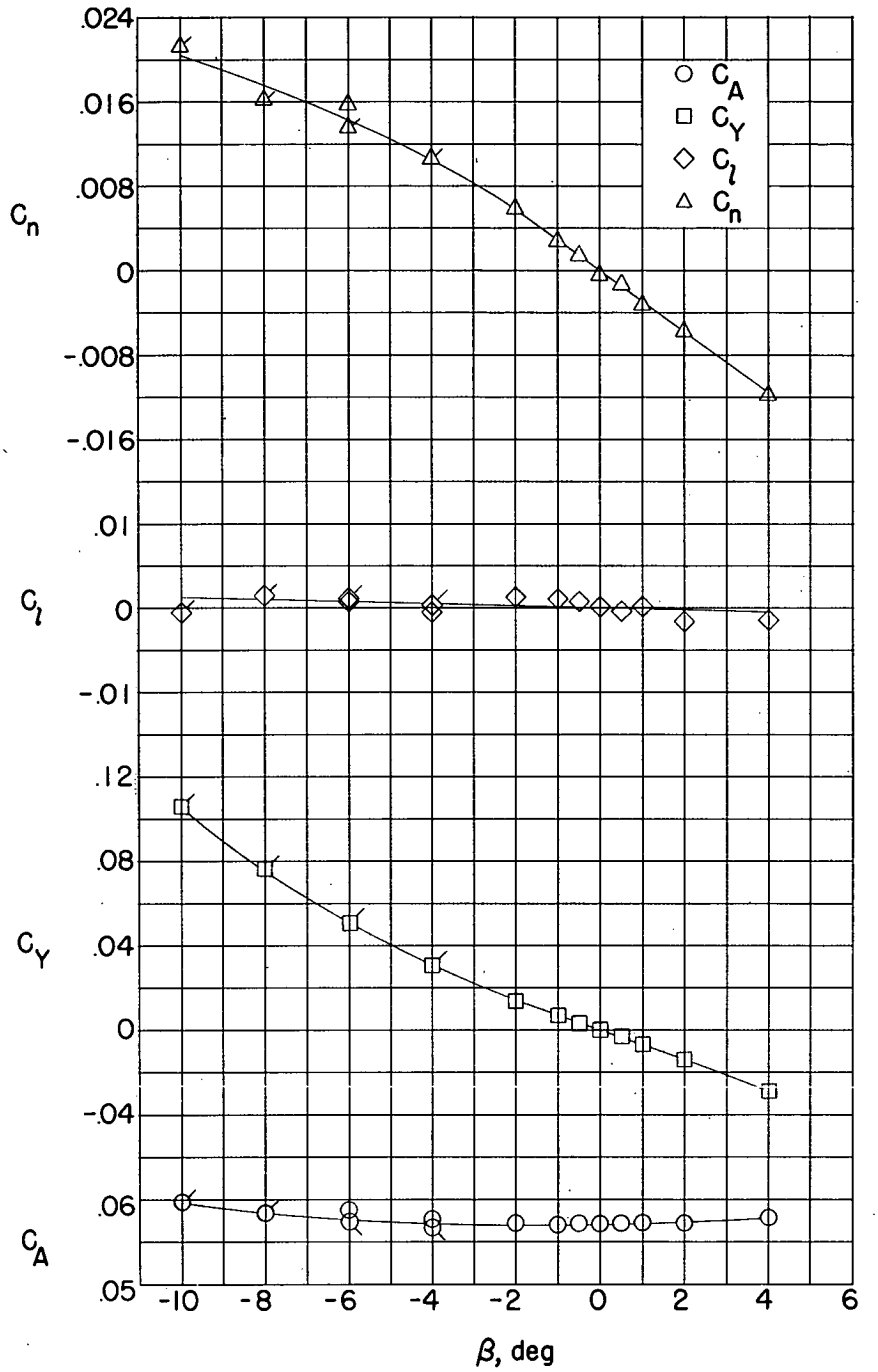

(c) Lateral characteristics in body-axis system at $\alpha = 0^{\circ}$.

Figure 4.- Concluded.

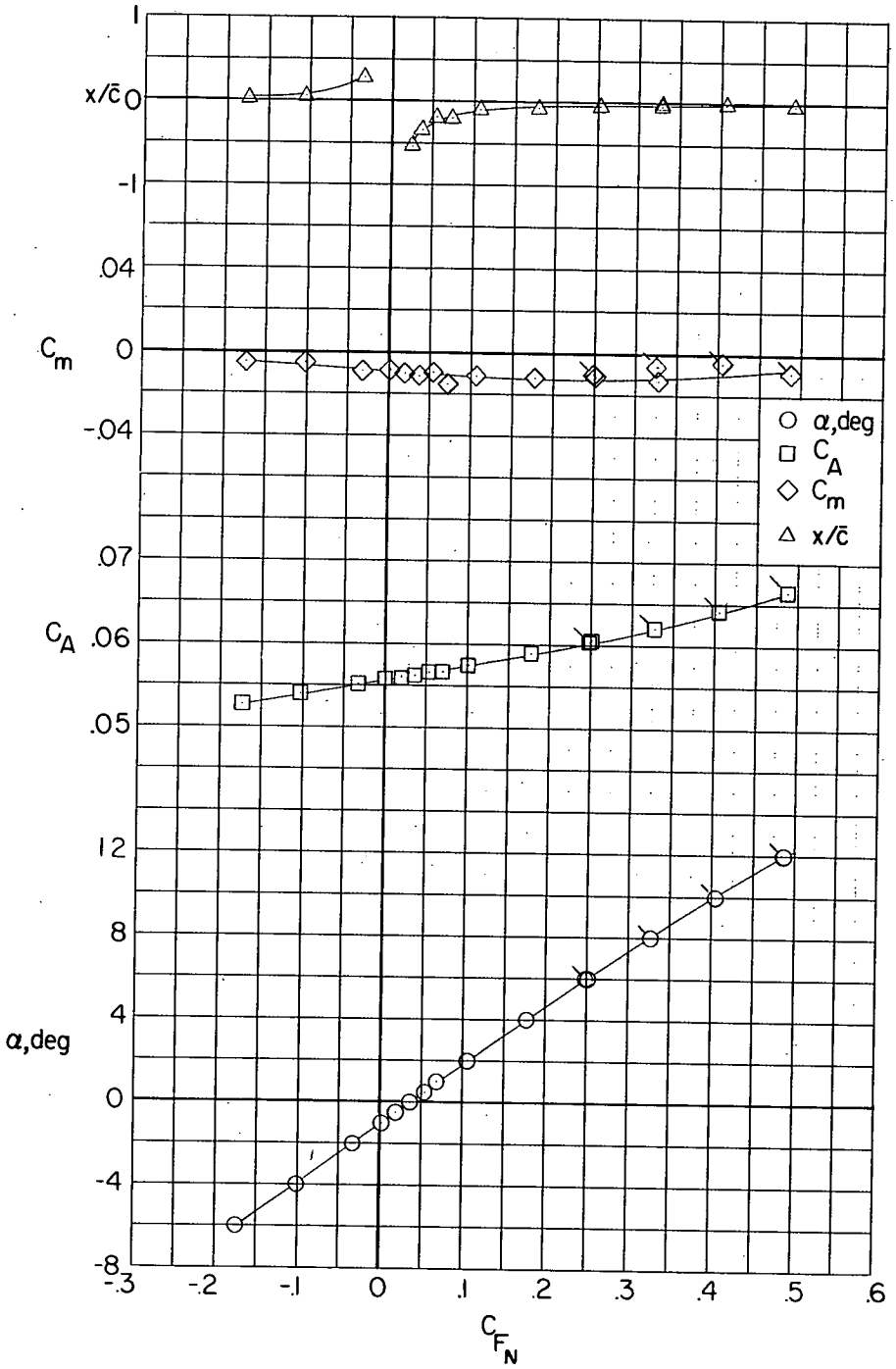

(a) Longitudinal characteristics in body-axis system at $\beta = 0^{\circ}$.

Figure 5.- Wing-body configuration at $M = 2.40$.

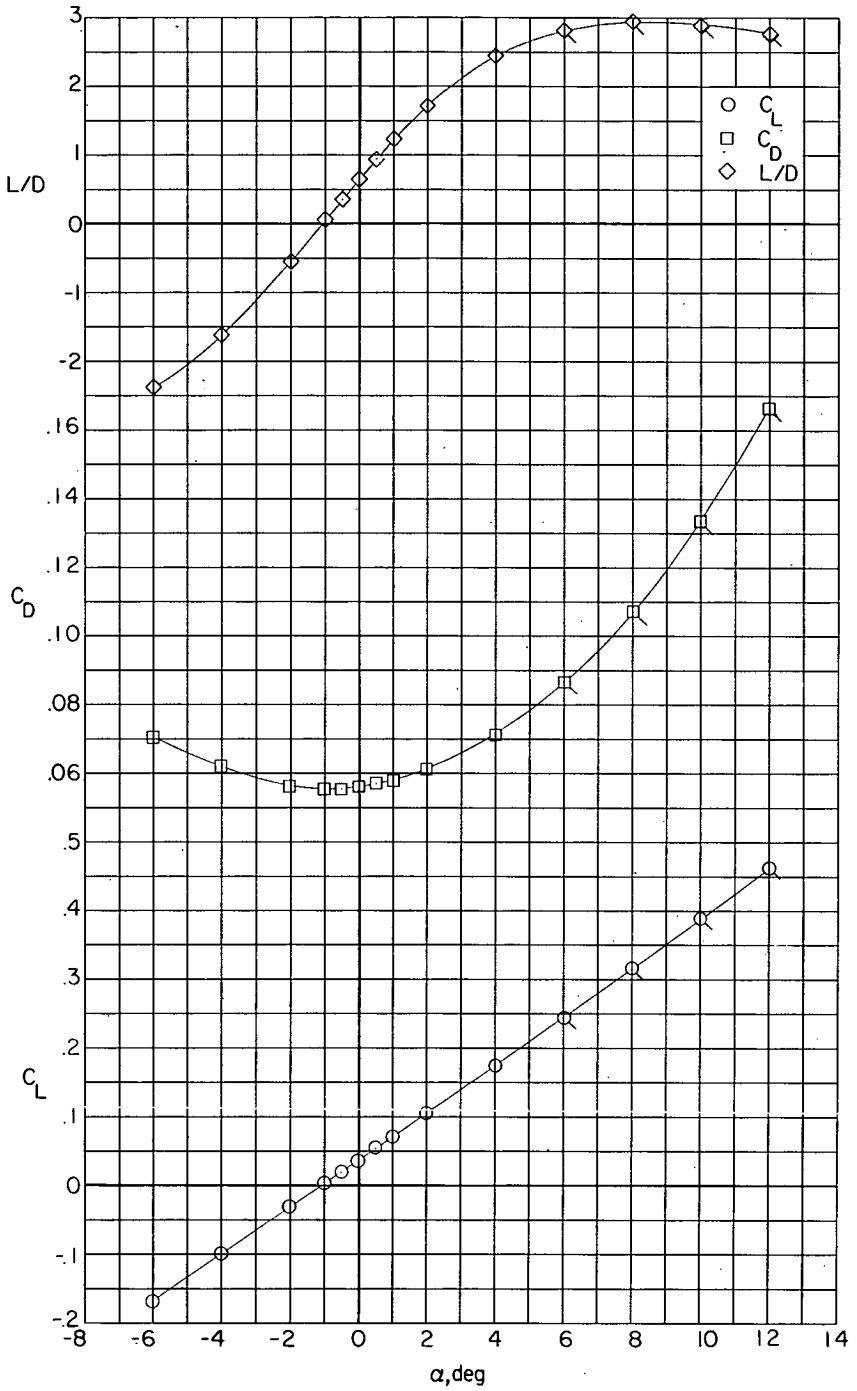

(b) Longitudinal-force characteristics in stability-axis system at $\beta = 0^{\circ}$.

Figure 5.- Continued.

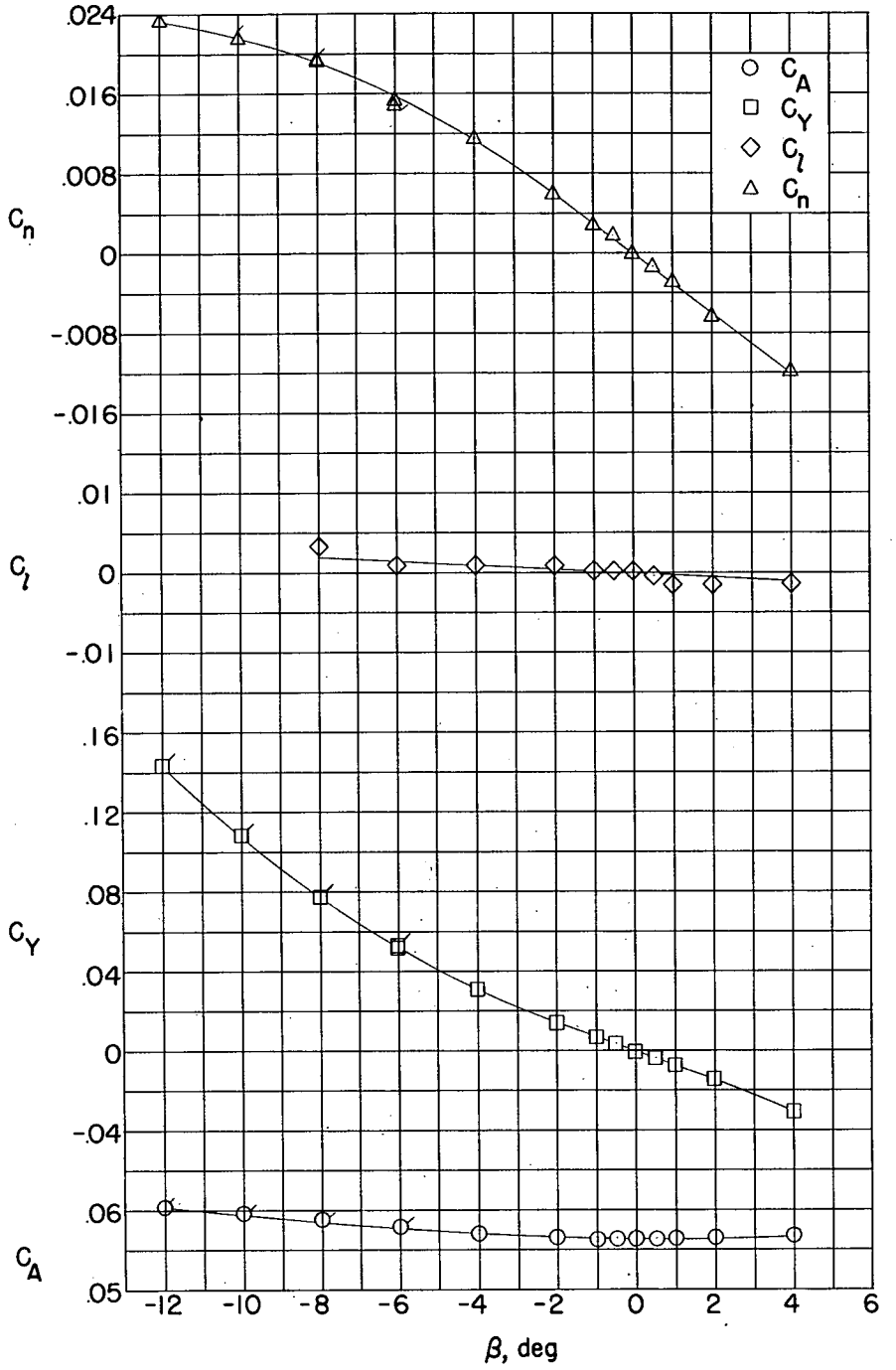

(c) Lateral characteristics in body-axis system at $\alpha = 0^{\circ}$.

Figure 5.- Concluded.

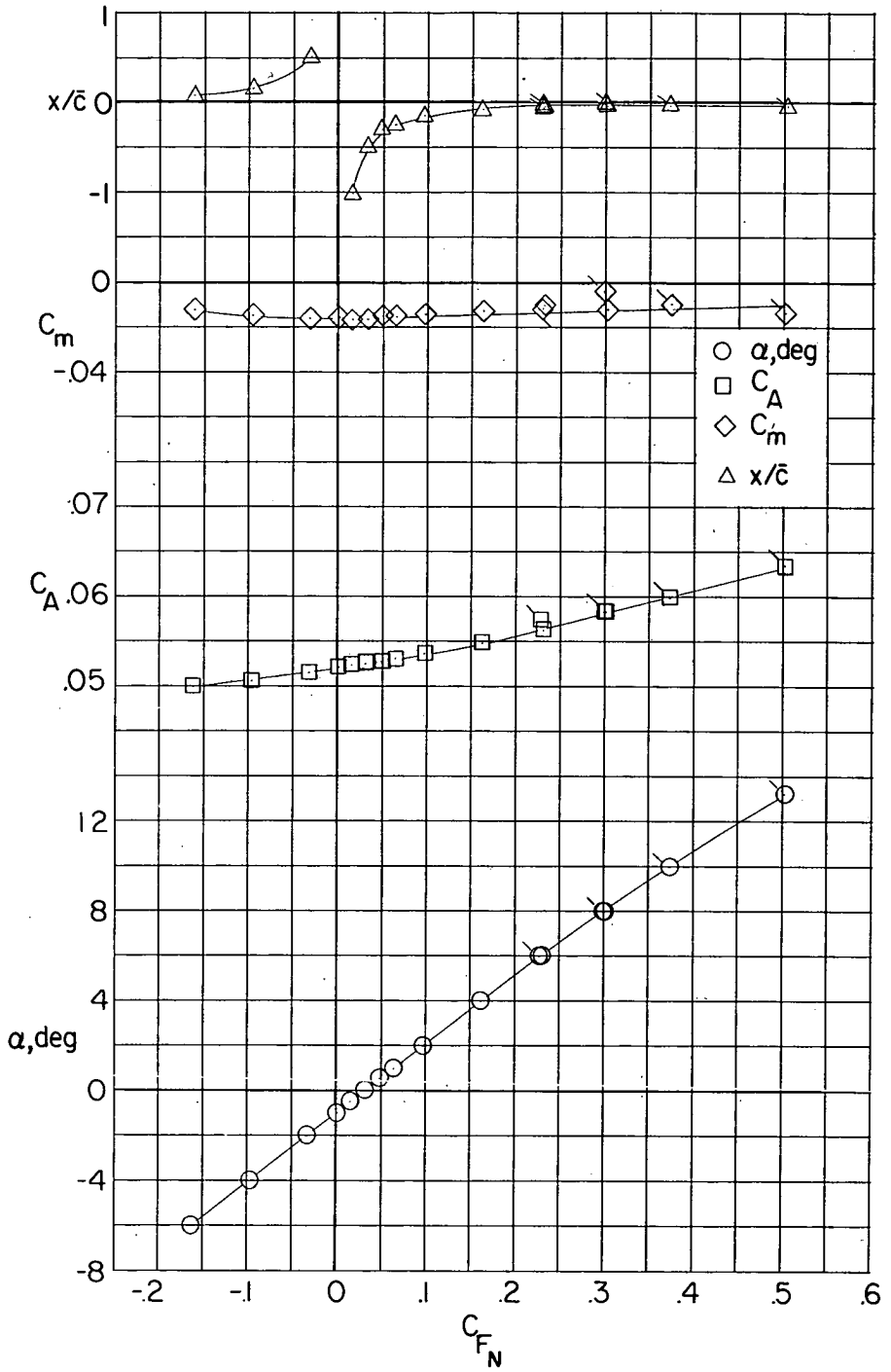

(a) Longitudinal characteristics in body-axis system at $\beta = 0^{\circ}$.

Figure 6.- Wing-body configuration at $M = 2.62$.

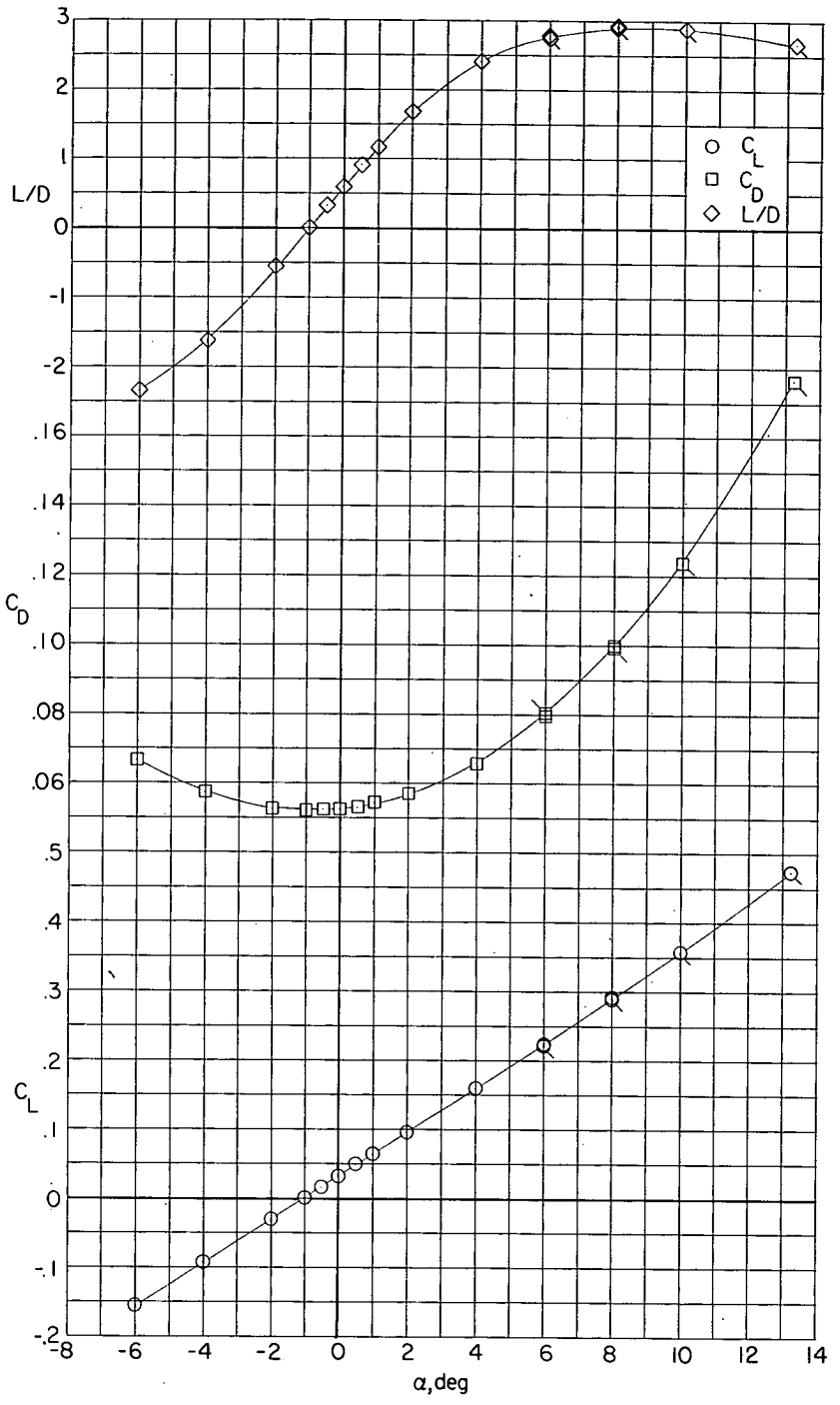

(b) Longitudinal-force characteristics in stability-axis system at $\beta = 0^\circ$.

Figure 6.- Continued.

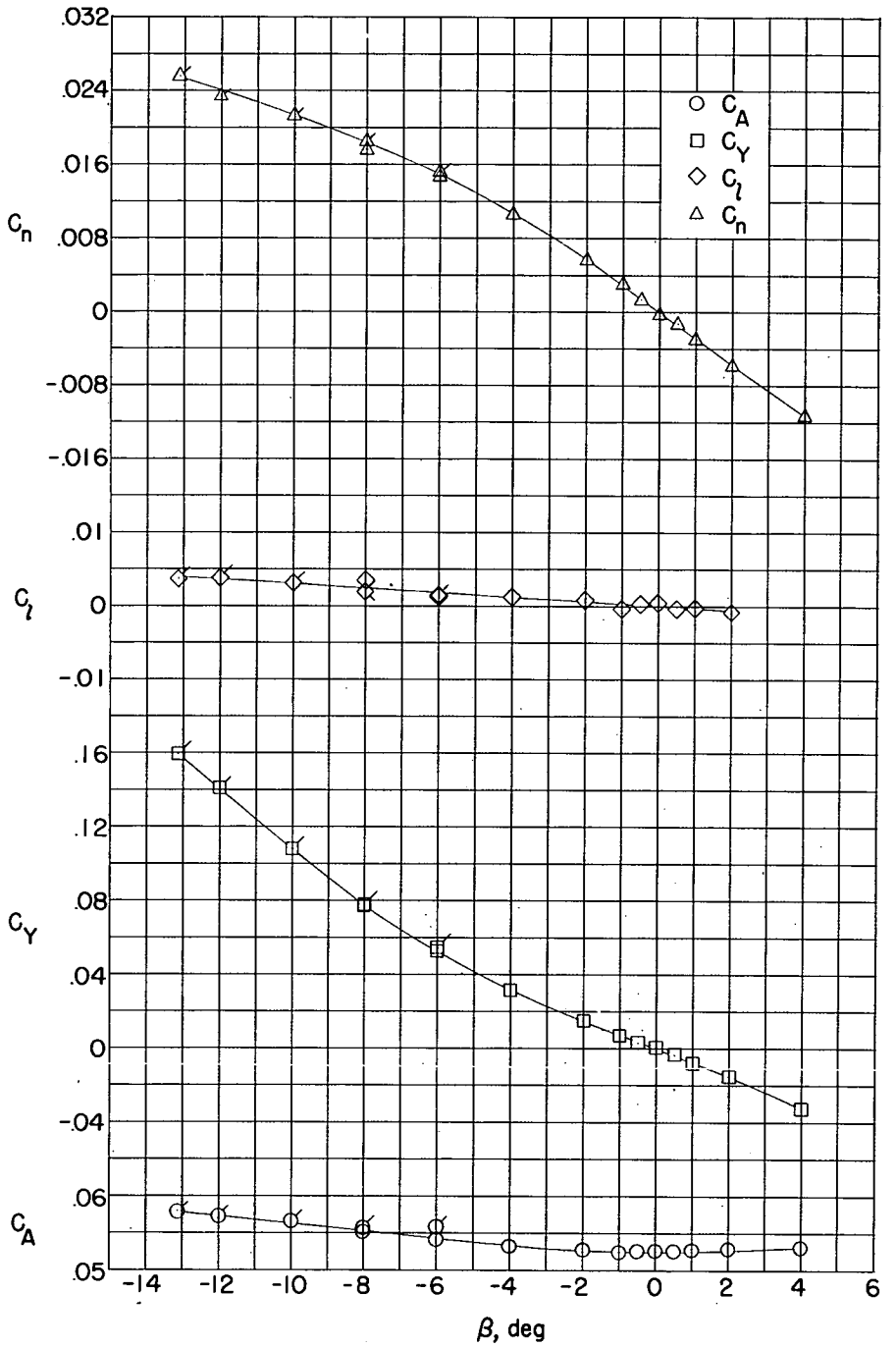

(c) Lateral characteristics in body-axis system at $\alpha = 0^\circ$.

Figure 6.- Concluded.

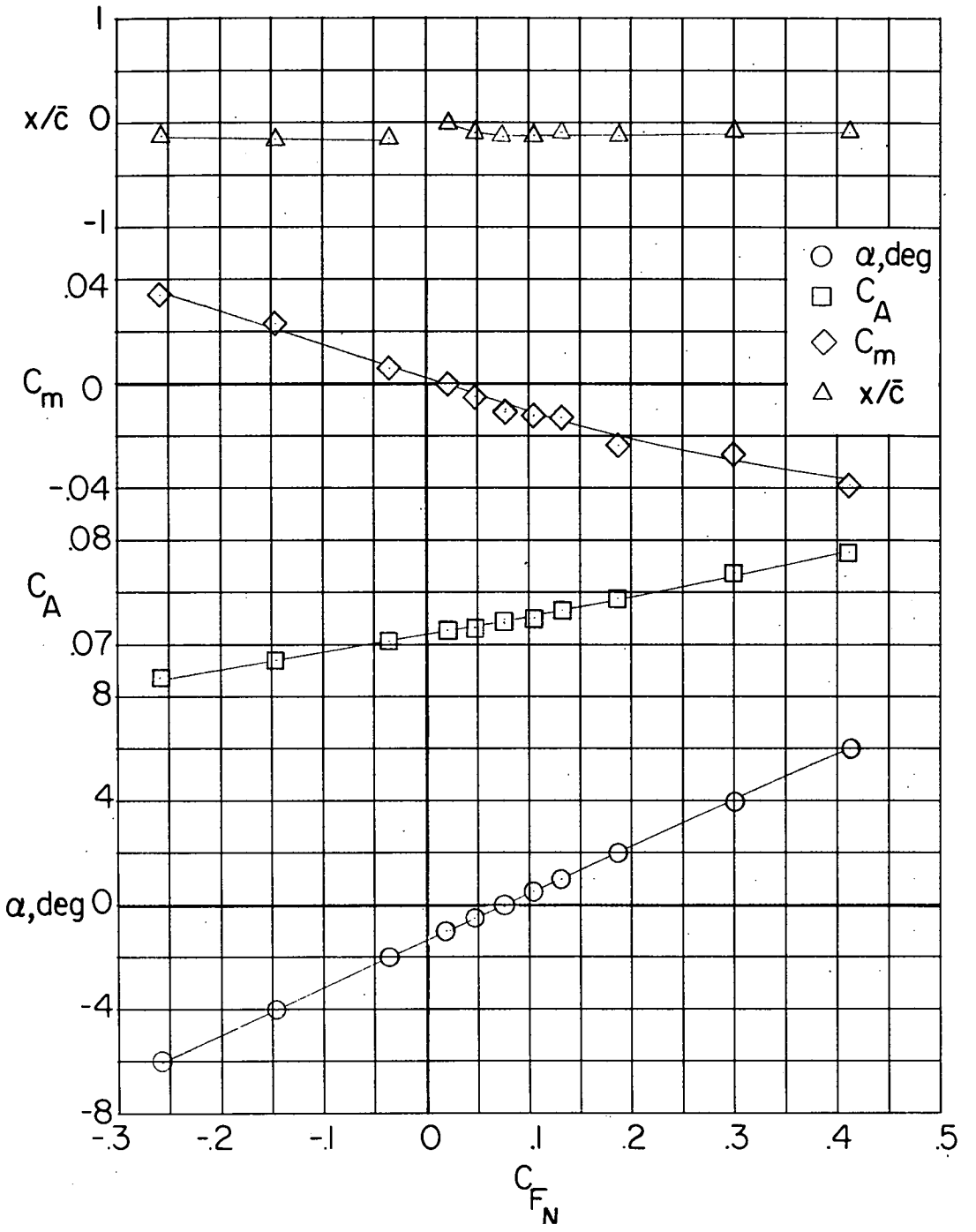

(a) Longitudinal characteristics in body-axis system at $\beta = 0^{o}$.

Figure 7.- Wing—body—vertical-tail configuration at $M = 1.62$.

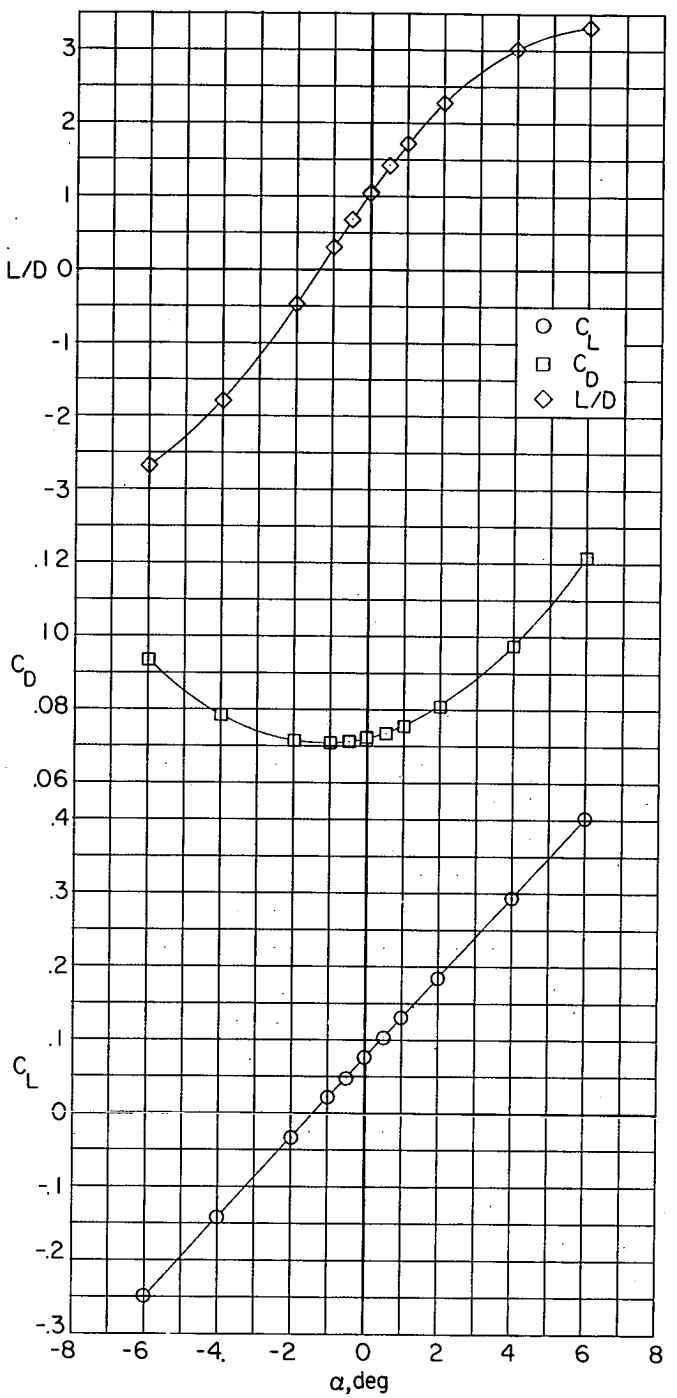

(b) Longitudinal-force characteristics in stability-axis system at $\beta = 0^{\circ}$.

Figure 7.- Continued.

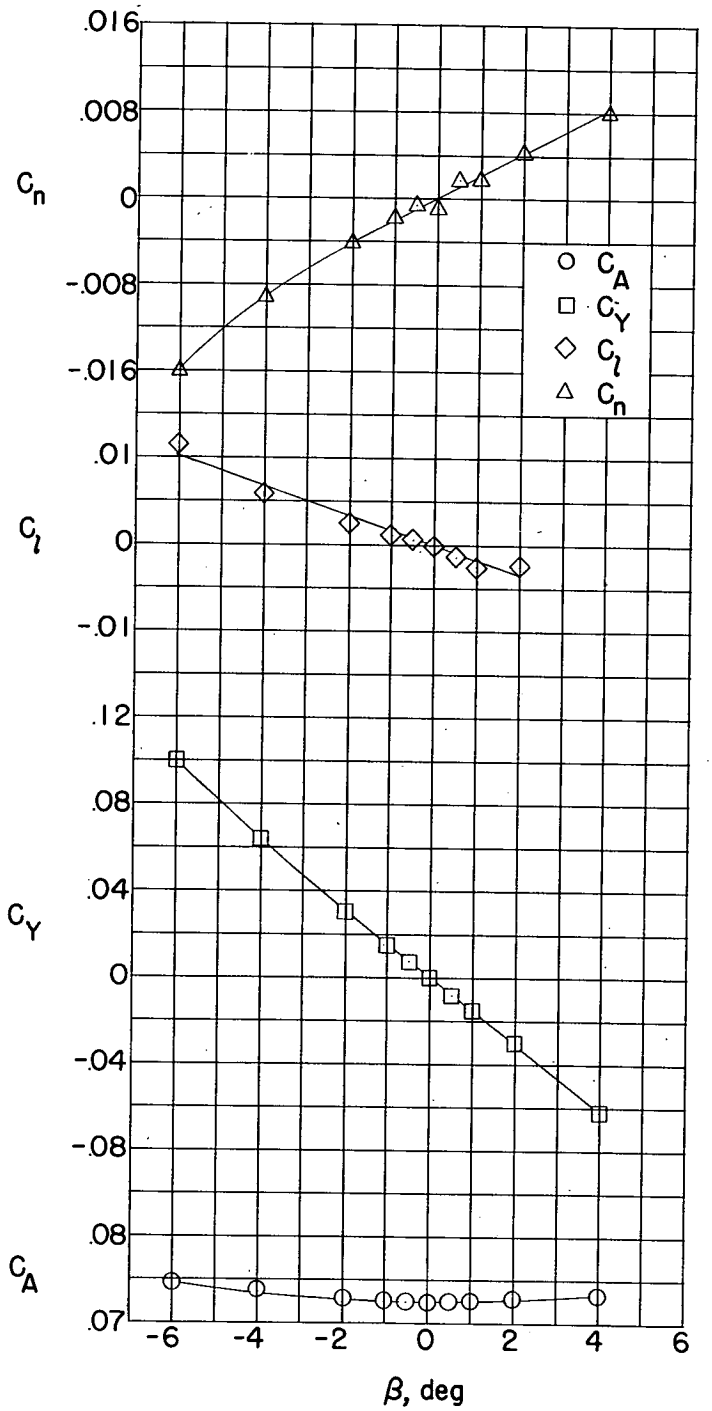

(c) Lateral characteristics in body-axis system at $\alpha = 0^\circ$.

Figure 7.- Concluded.

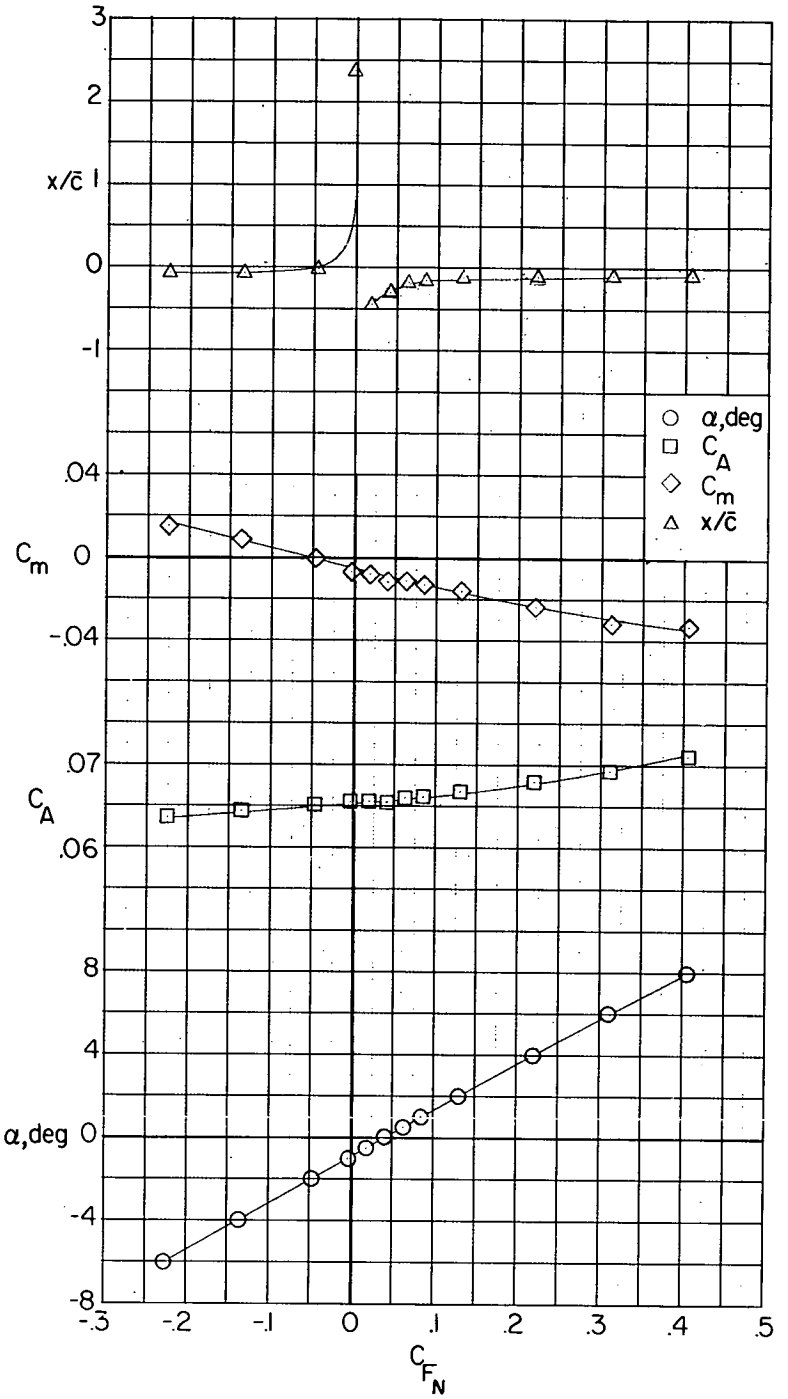

(a) Longitudinal characteristics in body-axis system at $\beta = 0^{\circ}$.

Figure 8.- Wing—body—vertical-tail configuration at $M = 1.94$.

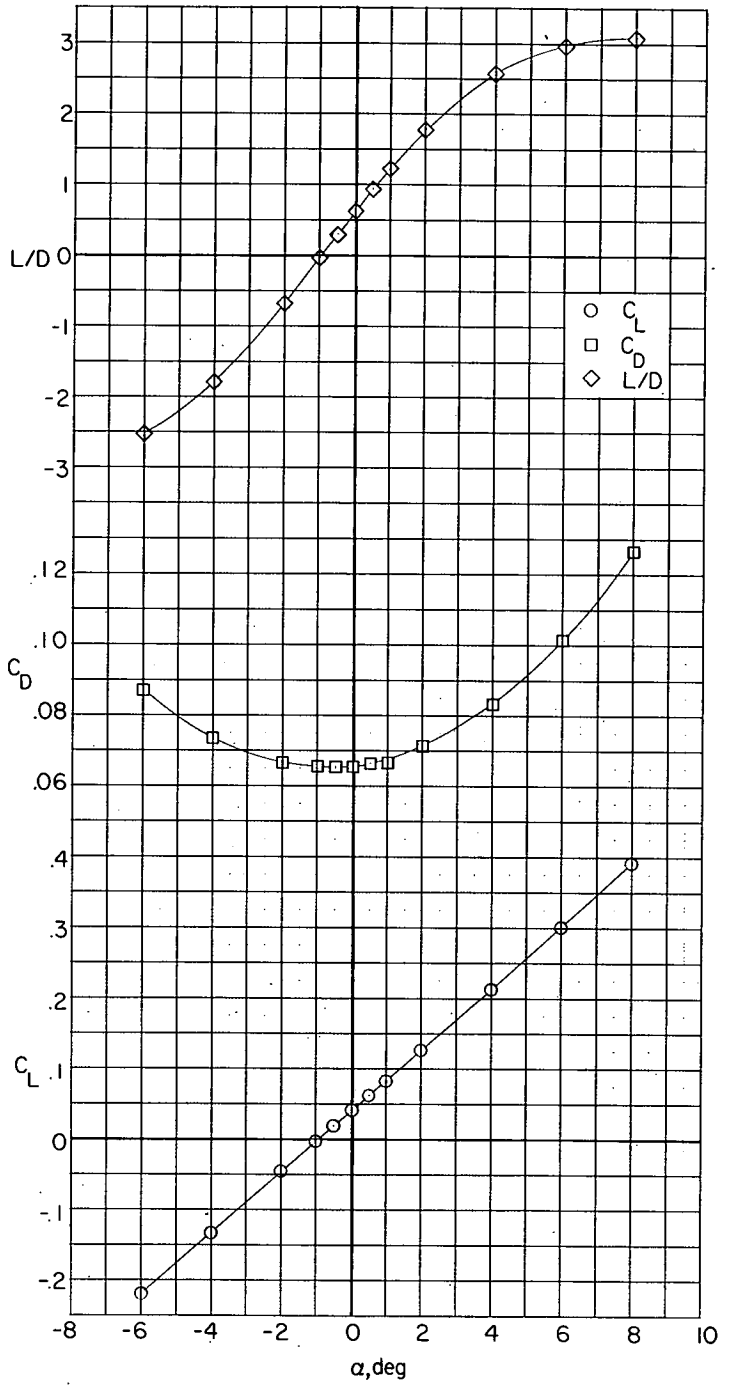

(b) Longitudinal-force characteristics in stability-axis system at $\beta = 0^{\circ}$.

Figure 8.- Continued.

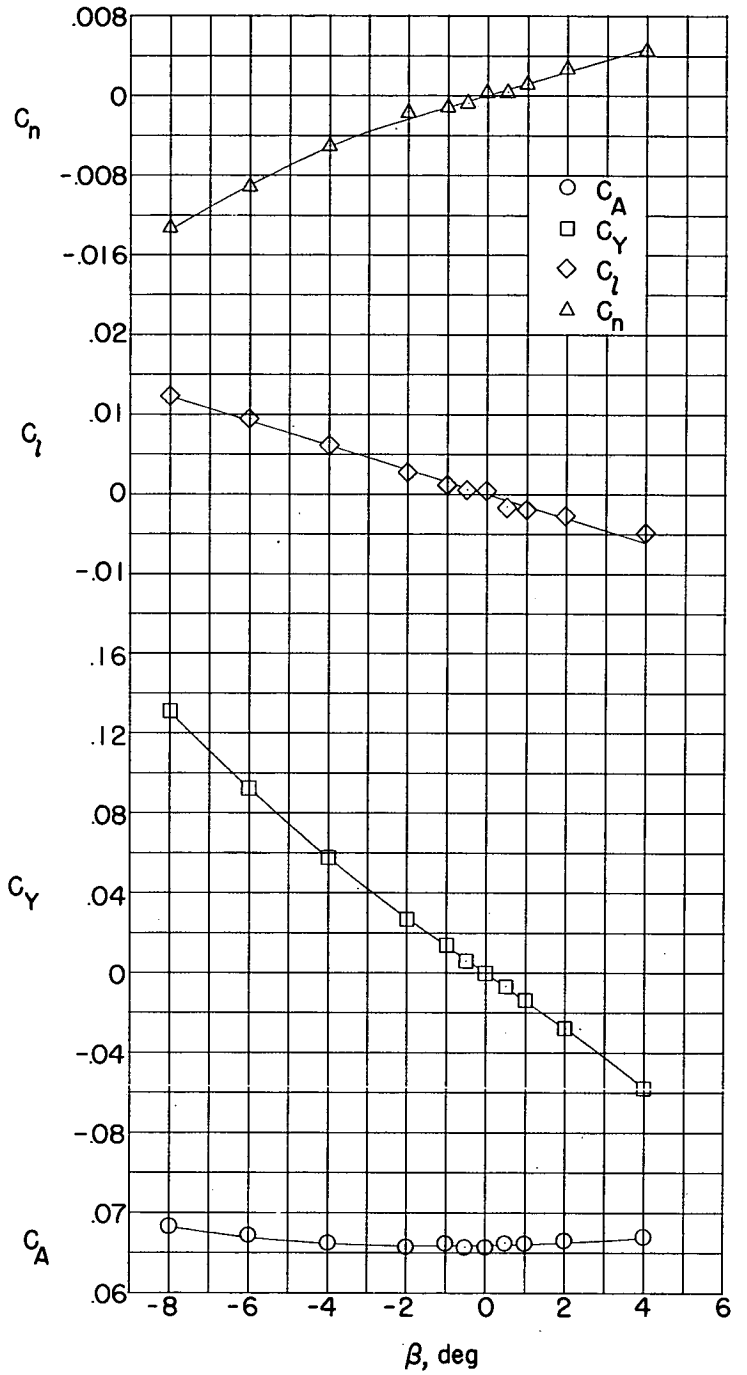

(c) Lateral characteristics in body-axis system at $\alpha = 0^\circ$.

Figure 8.- Concluded.

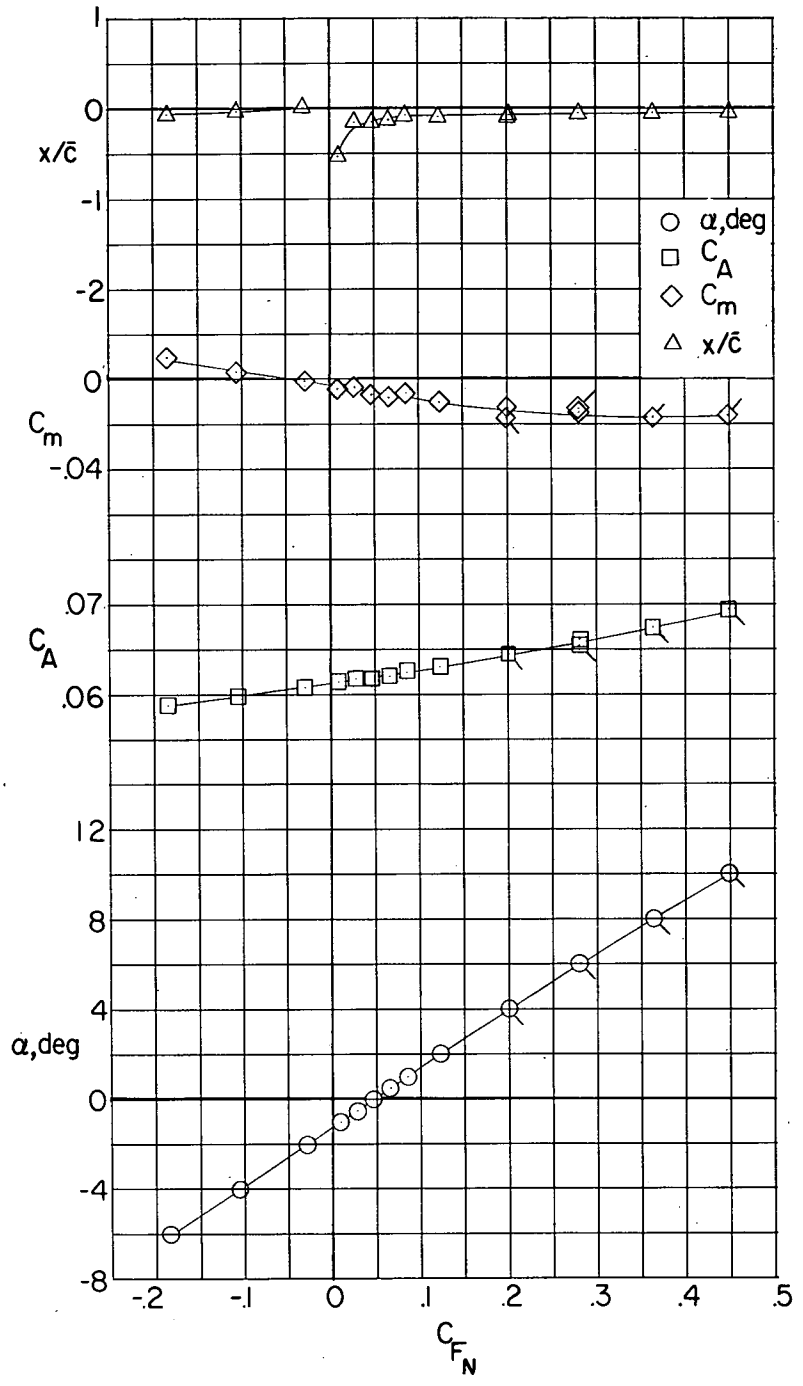

(a) Longitudinal characteristics in body-axis system at $\beta = 0^{\circ}$.

Figure 9.- Wing—body—vertical-tail configuration at $M = 2.22$.

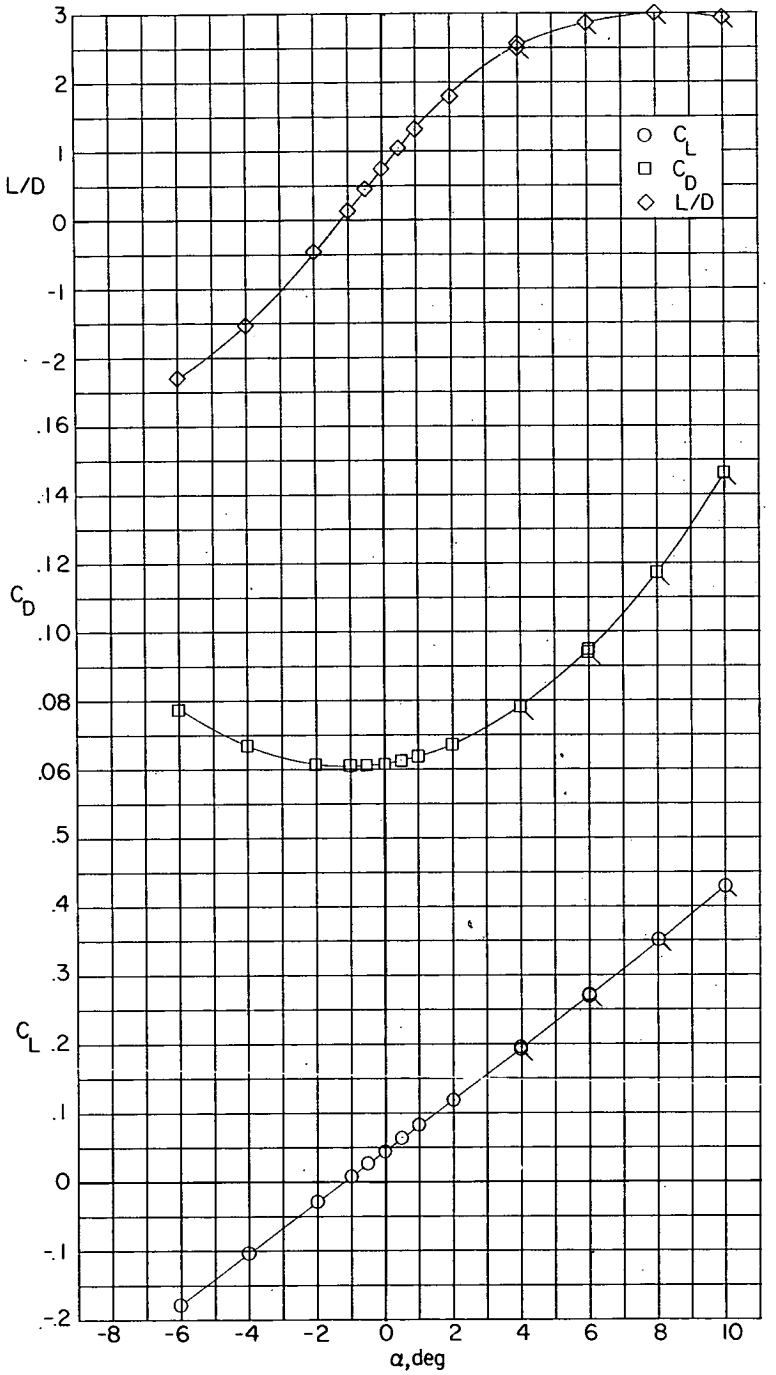

(b) Longitudinal-force characteristics in stability-axis system at $\beta = 0^{\circ}$.

Figure 9.- Continued.

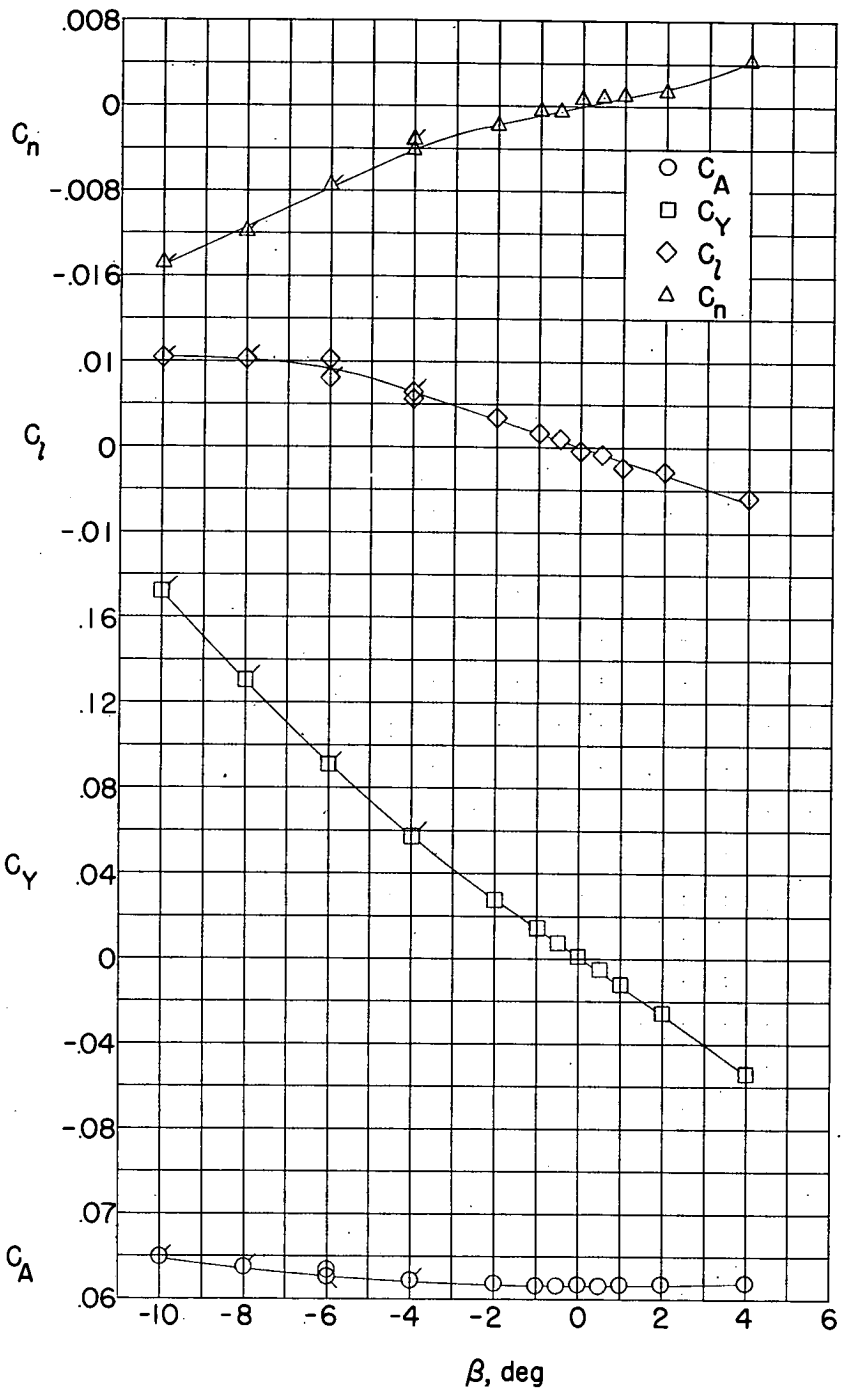

(c) Lateral characteristics in body-axis system at $\alpha = 0^\circ$.

Figure 9.- Concluded.

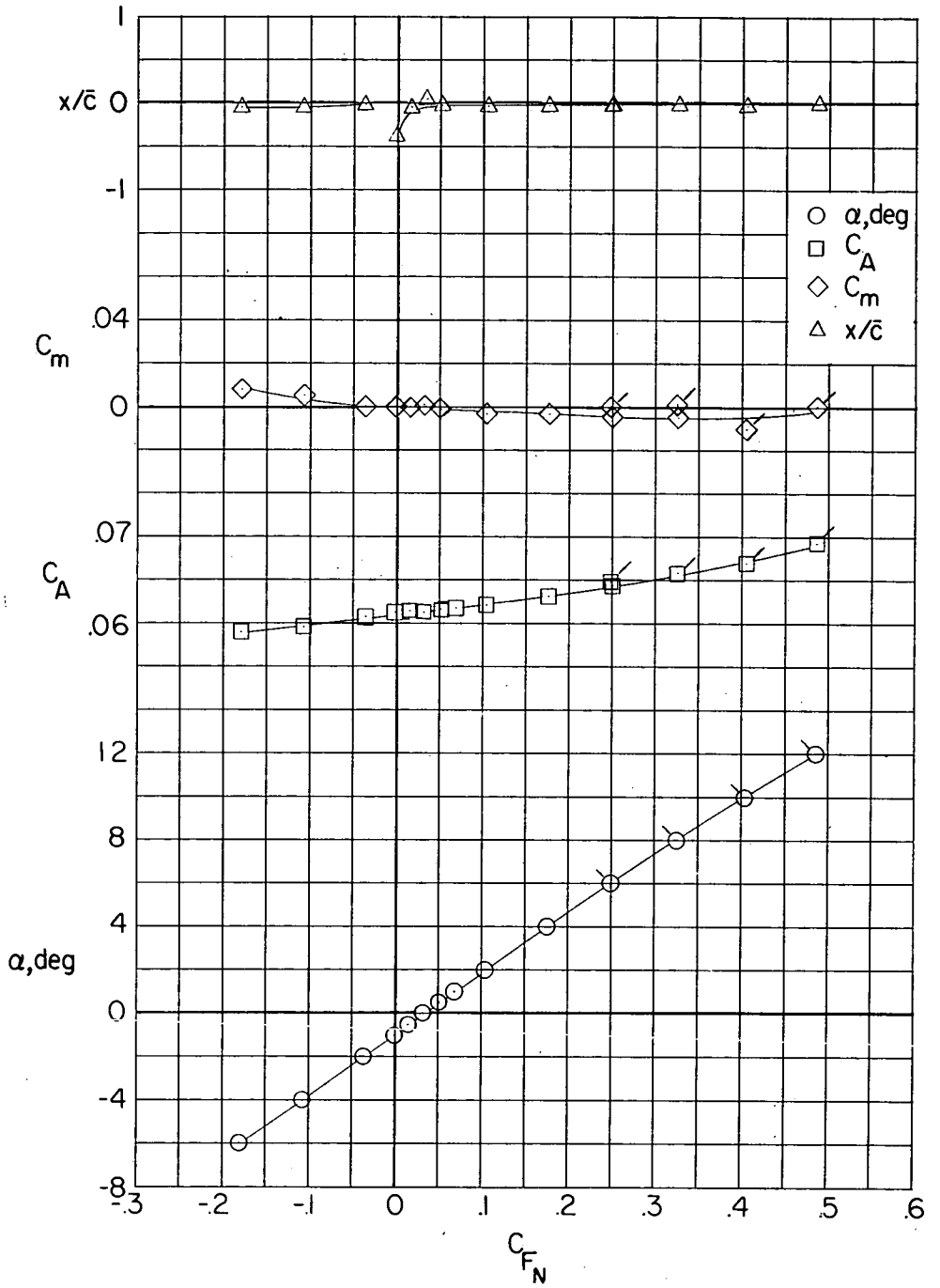

(a) Longitudinal characteristics in body-axis system at $\beta = 0^{\circ}$.

Figure 10.- Wing—body—vertical-tail configuration at $M = 2.40$.

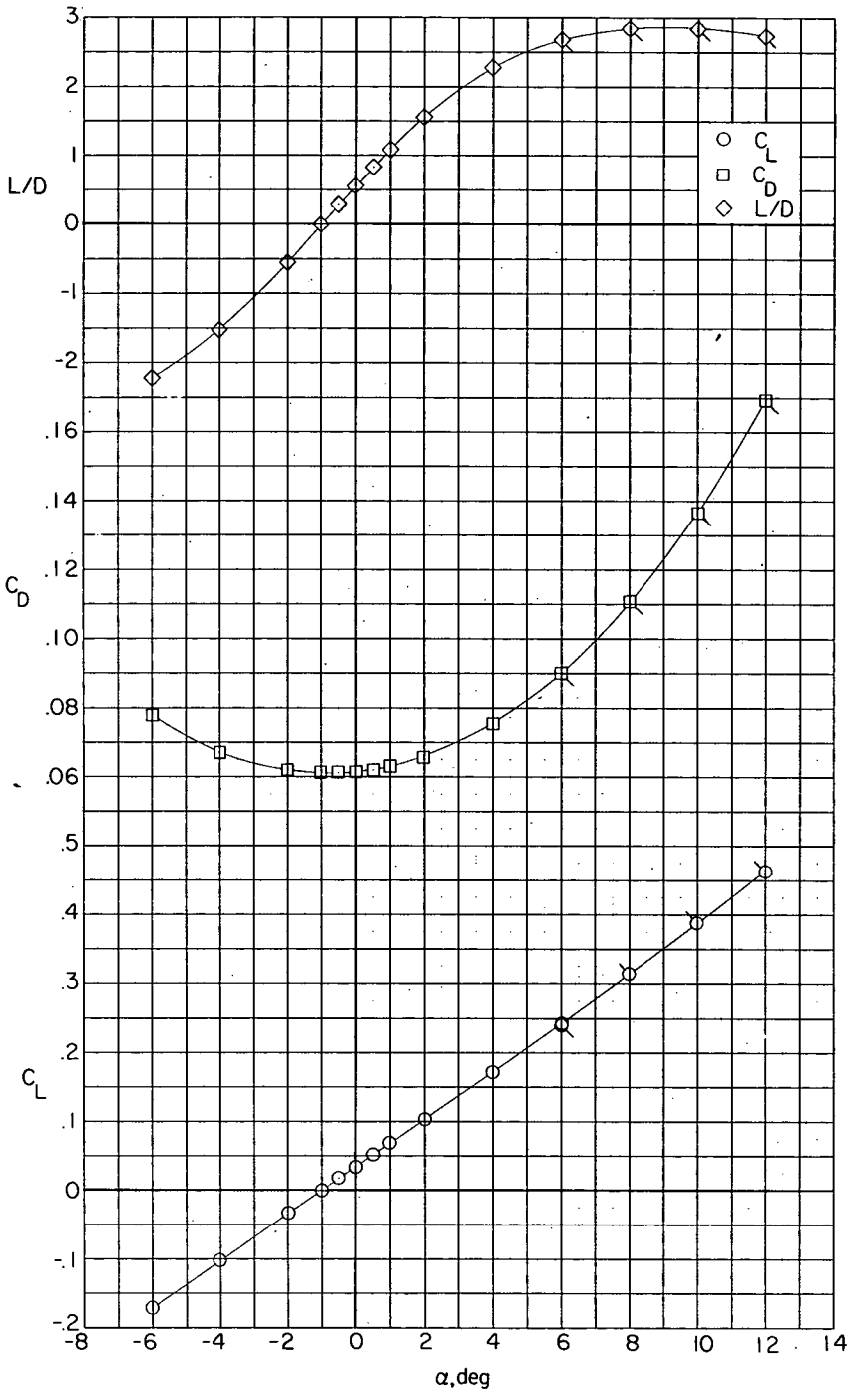

(b) Longitudinal-force characteristics in stability-axis system at $\beta = 0^\circ$.

Figure 10.- Continued.

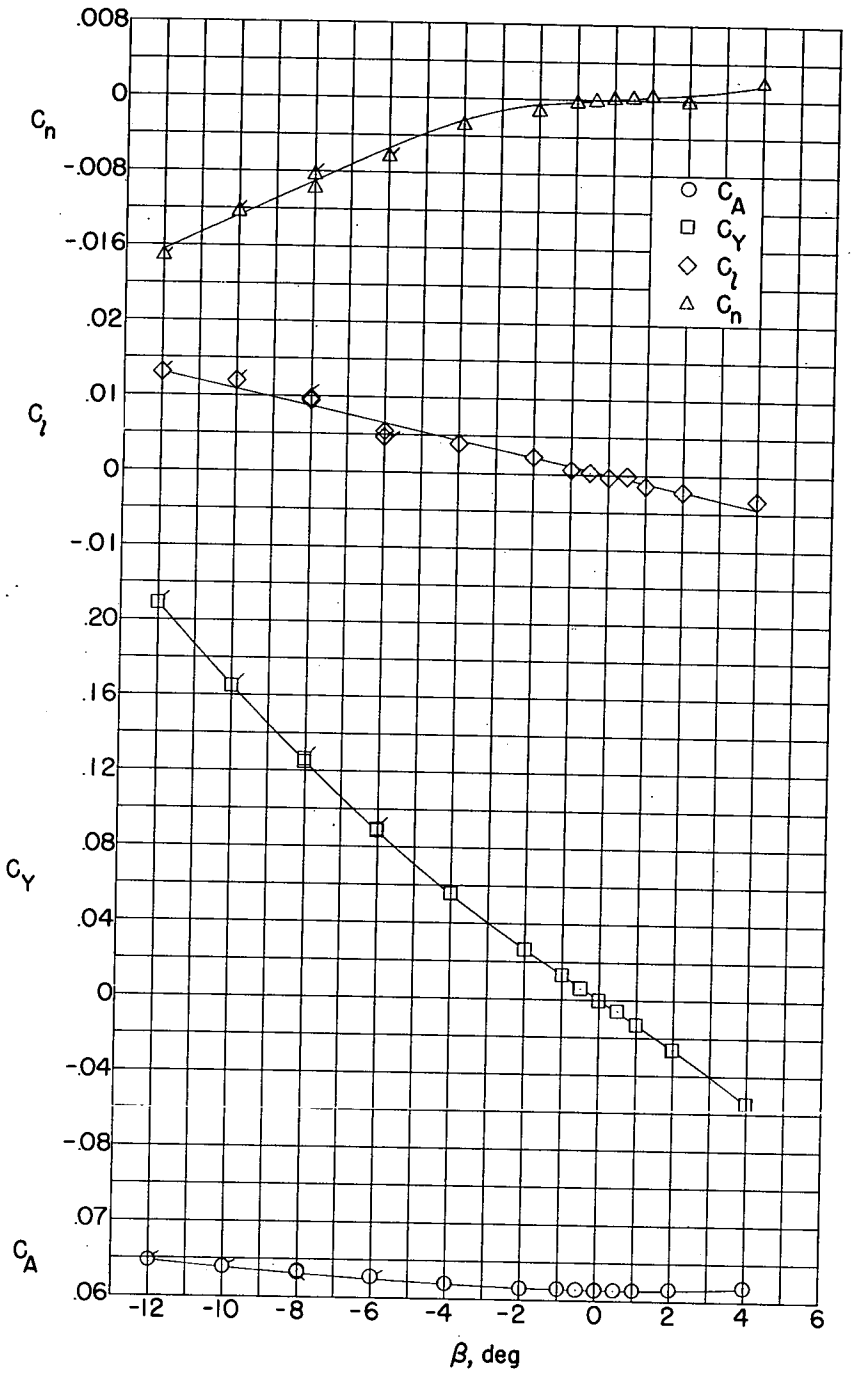

(c) Lateral characteristics in body-axis system at $\alpha = 0^\circ$.

Figure 10.- Concluded.

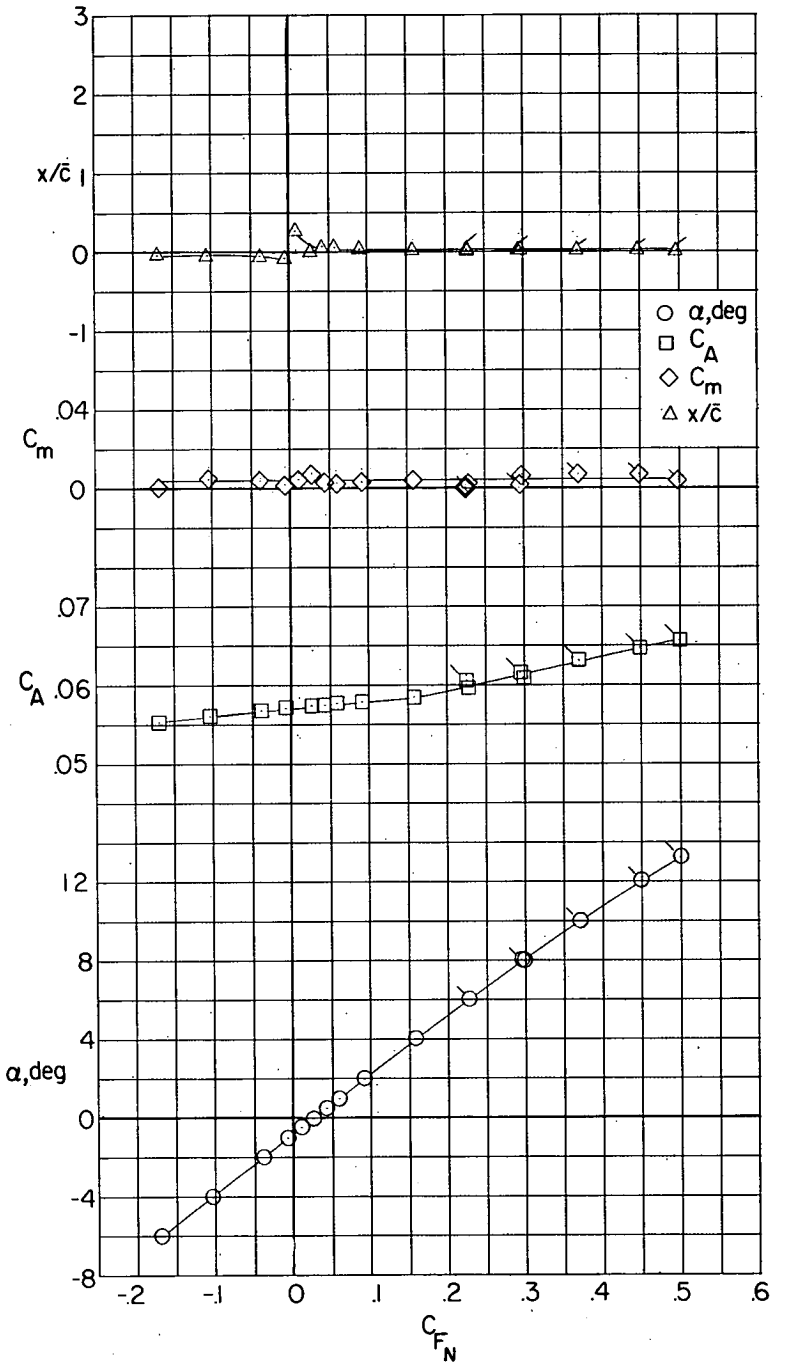

(a) Longitudinal characteristics in body-axis system at $\beta = 0^{\circ}$.

Figure 11.- Wing—body—vertical-tail configuration at $M = 2.62$.

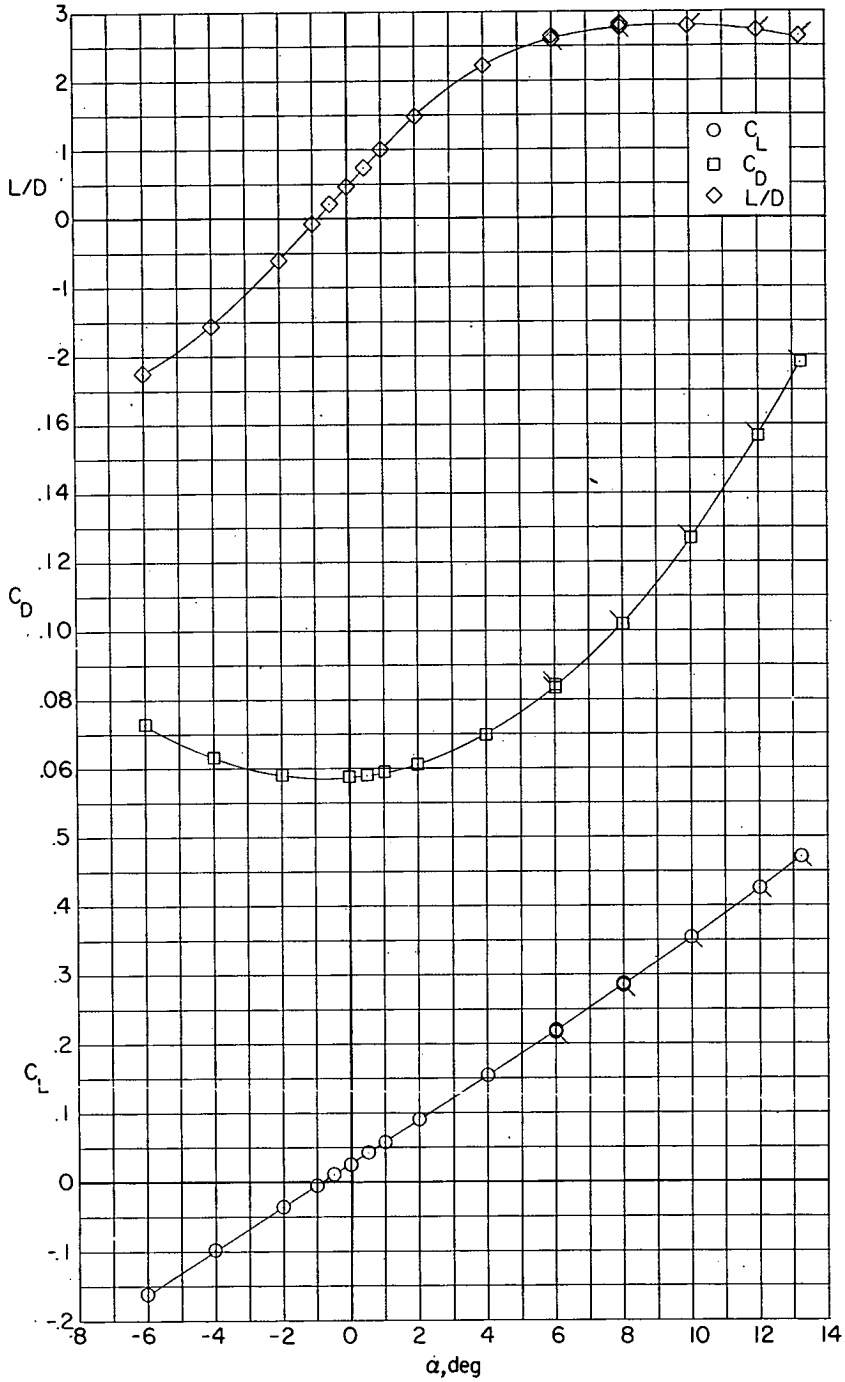

(b) Longitudinal-force characteristics in stability-axis system at $\beta = 0^{\circ}$.

Figure 11.- Continued.

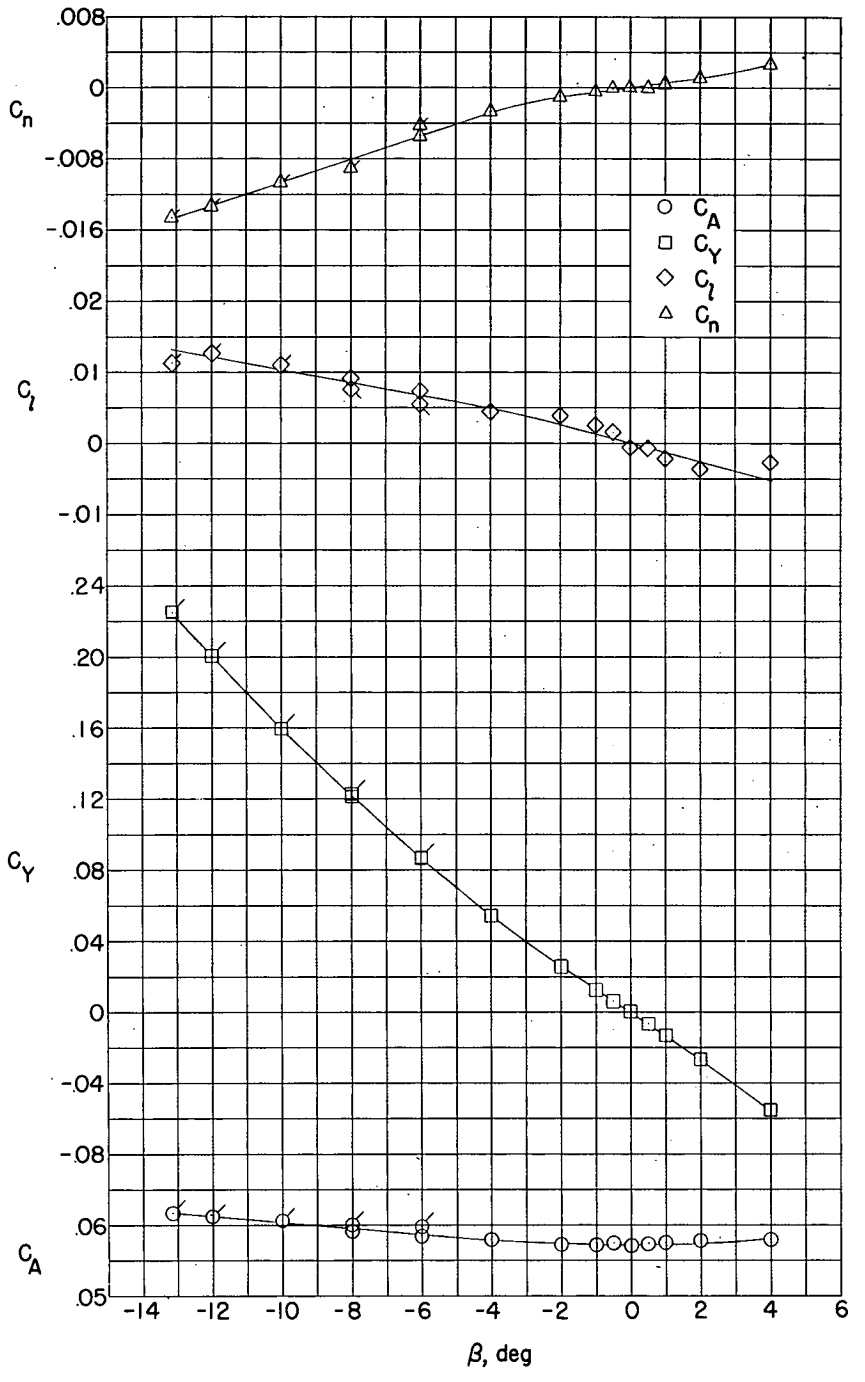

(c) Lateral characteristics in body-axis system at $\alpha = 0^{\circ}$.

Figure 11.- Concluded.

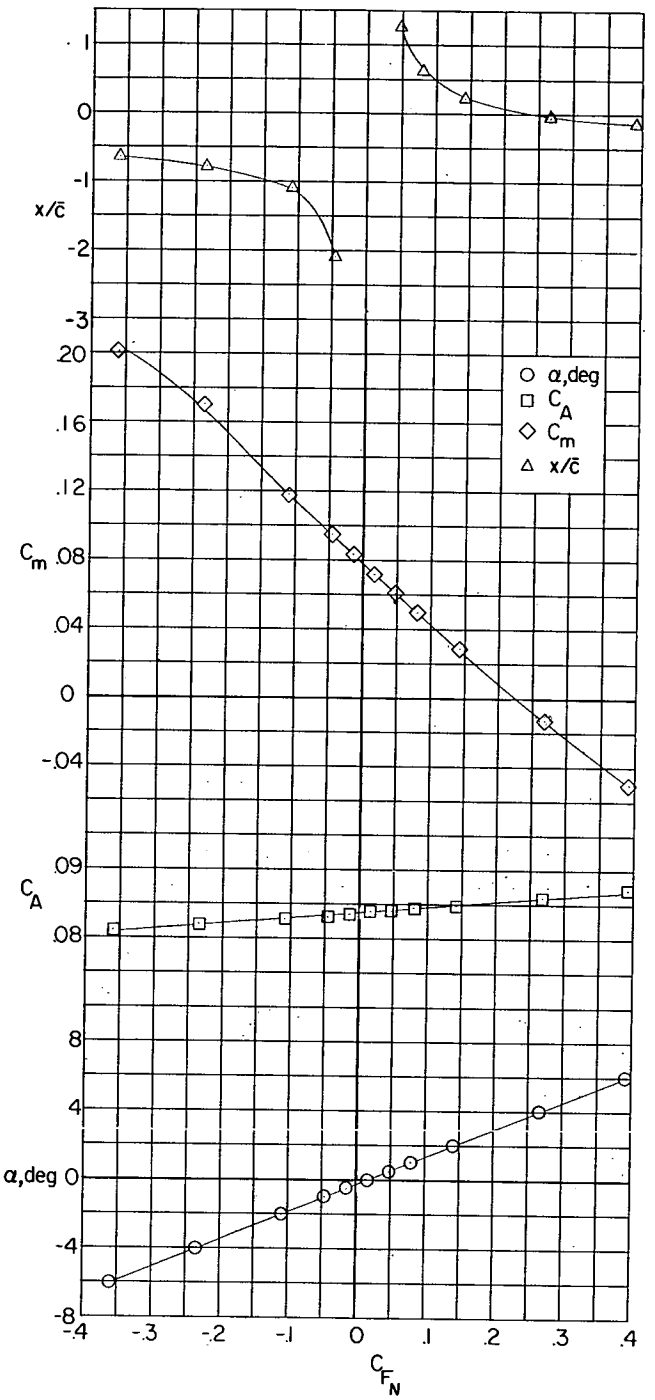

(a) Longitudinal characteristics in body-axis system at $\beta = 0^o$.

Figure 12.- Complete configuration with $i_t = 0^o$ at $M = 1.62$.

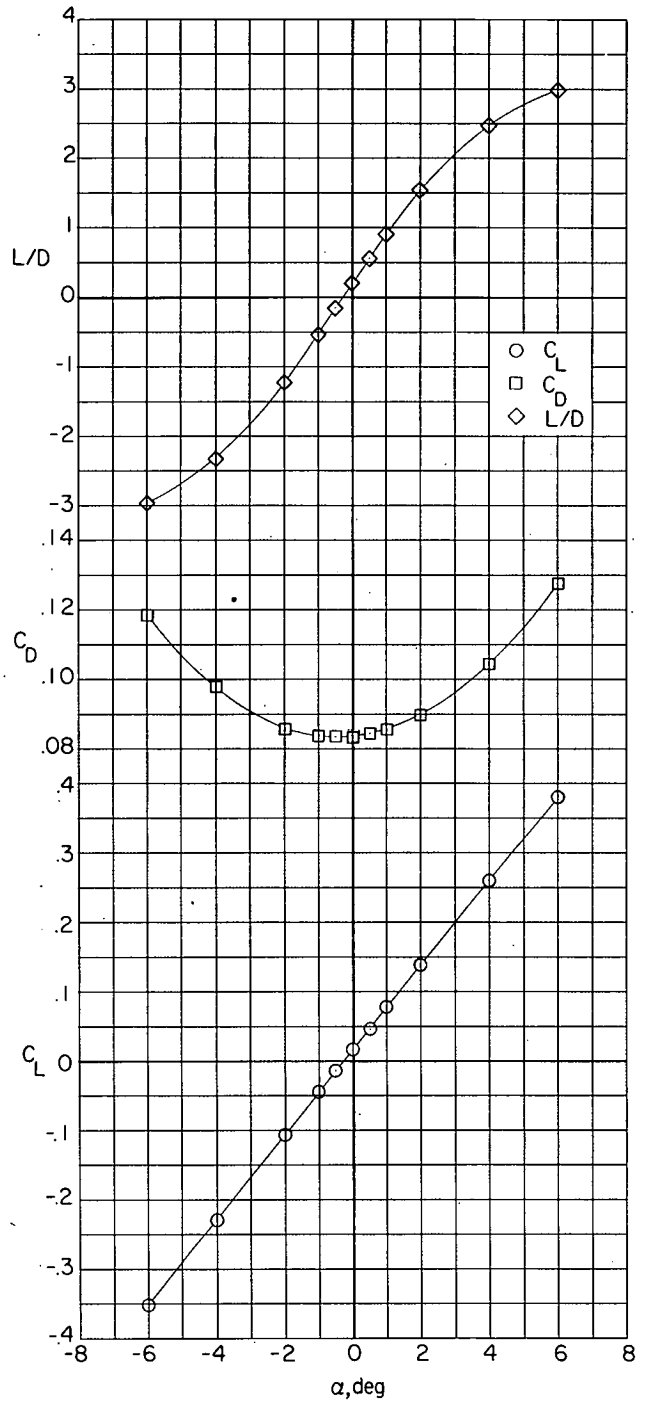

(b) Longitudinal-force characteristics in stability-axis system at $\beta = 0^{\circ}$.

Figure 12.- Continued.

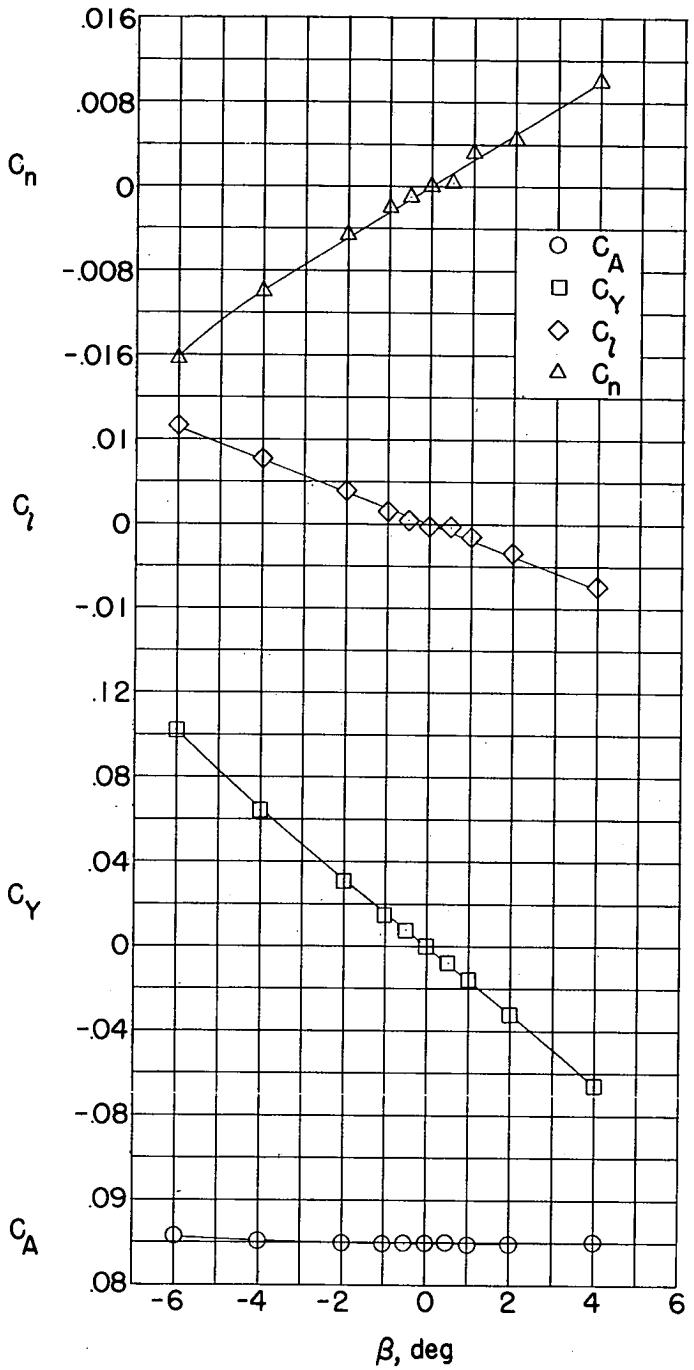

(c) Lateral characteristics in body-axis system at $\alpha = 0^{\circ}$.

Figure 12.- Concluded.

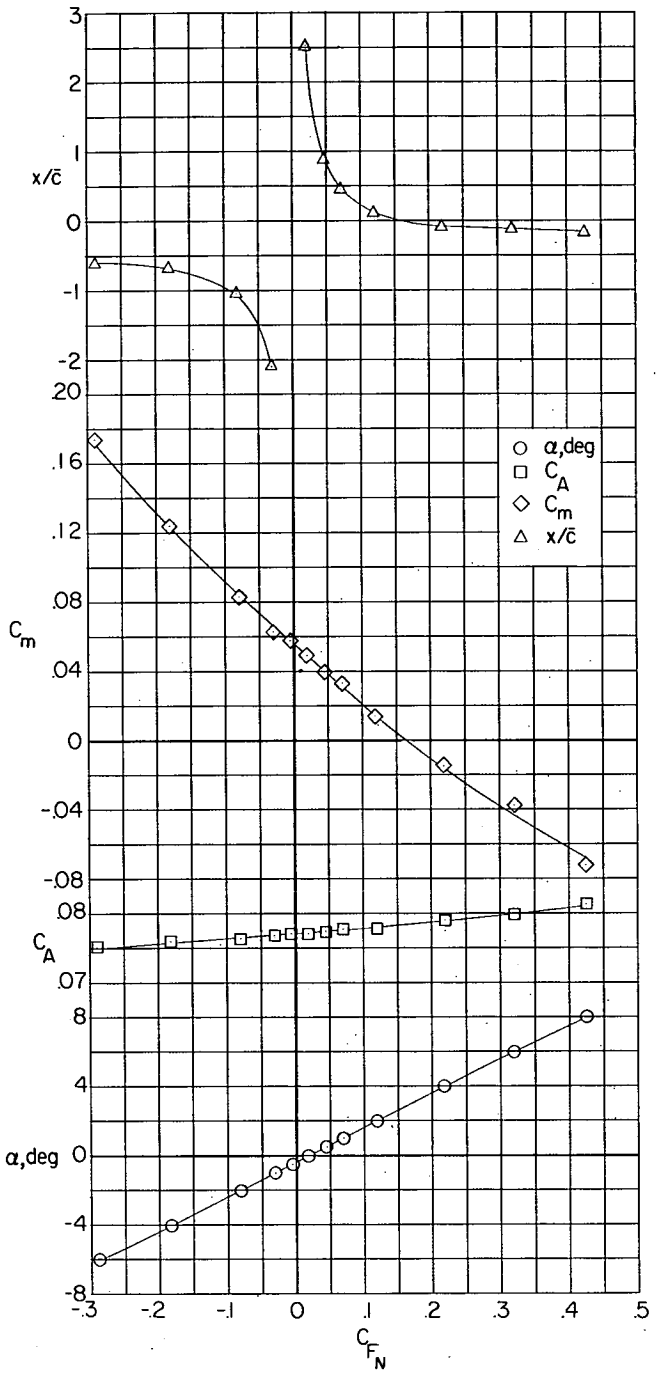

(a) Longitudinal characteristics in body-axis system at $\beta = 0^{\circ}$.

Figure 13.- Complete configuration with $i_t = 0^{\circ}$ at $M = 1.94$.

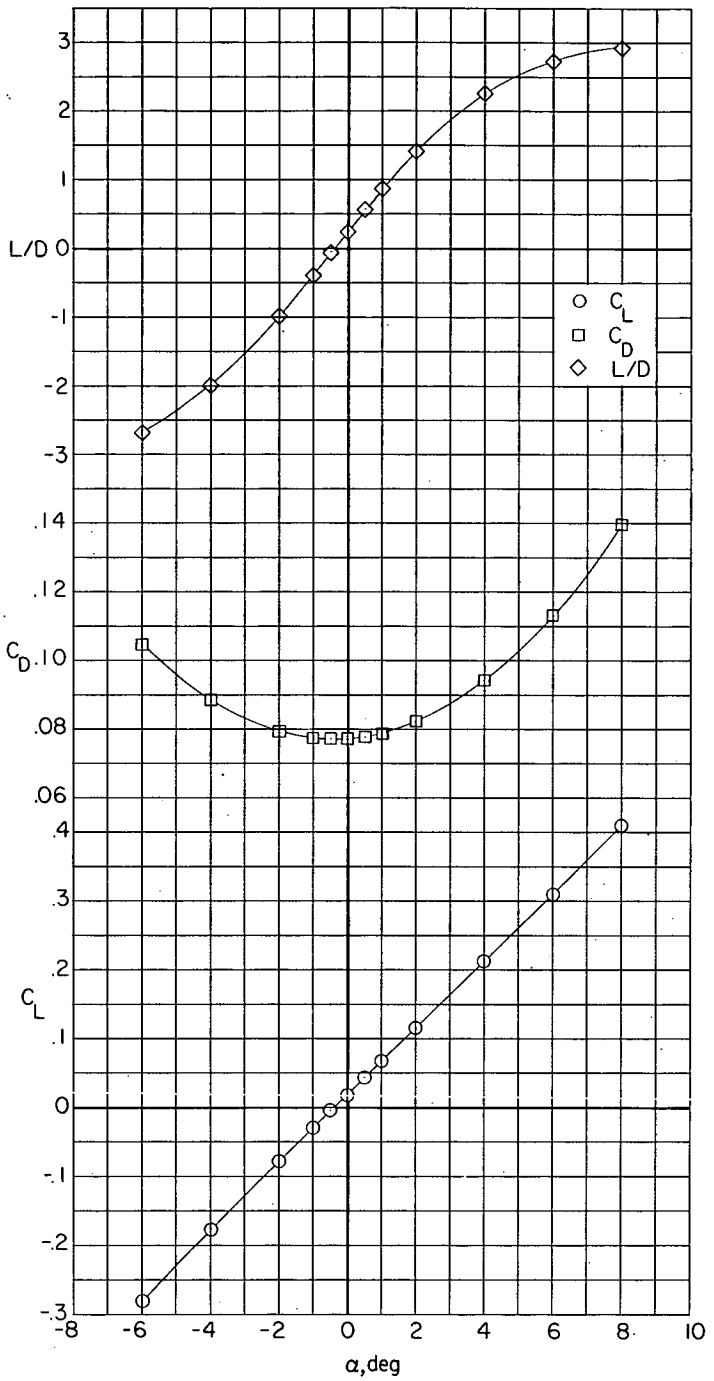

(b) Longitudinal-force characteristics in stability-axis system at $\beta = 0^{\circ}$.

Figure 13.- Continued.

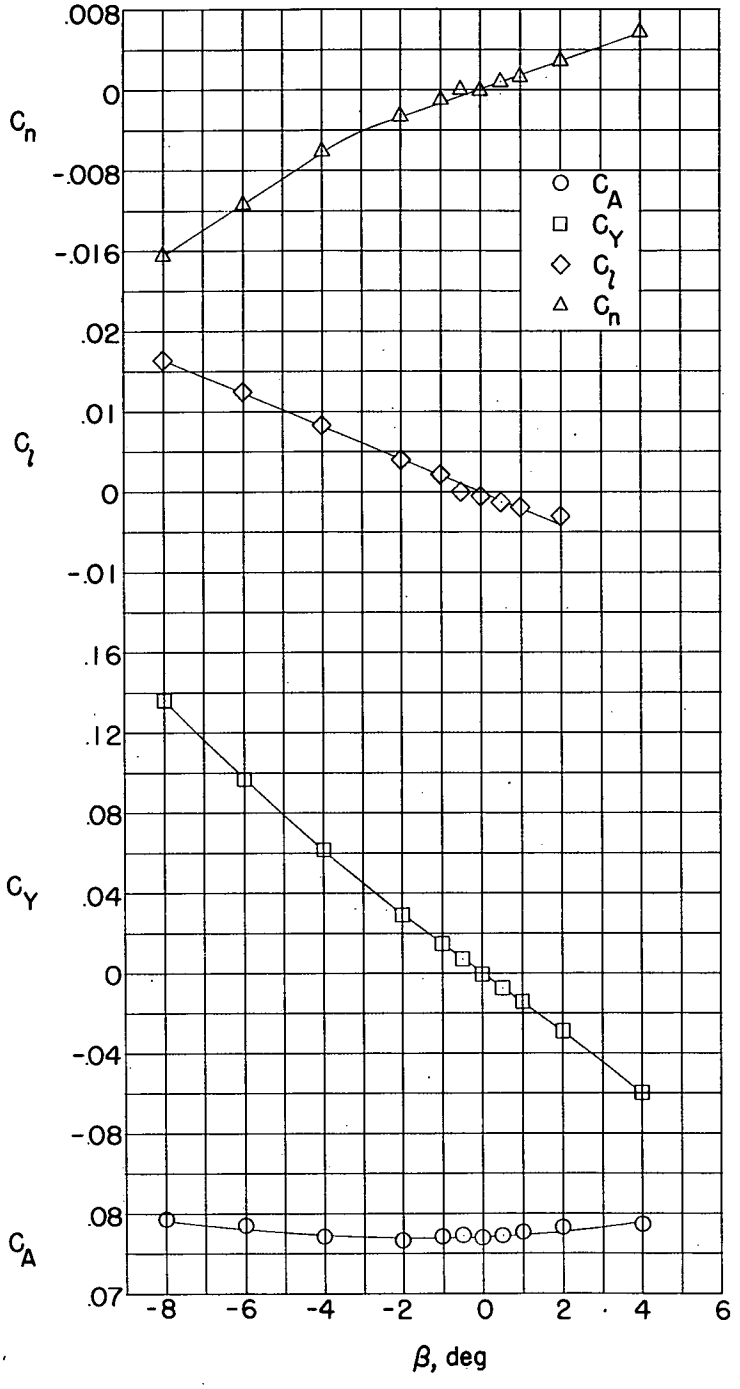

(c) Lateral characteristics in body-axis system at $\alpha = 0^\circ$.

Figure 13.- Concluded.

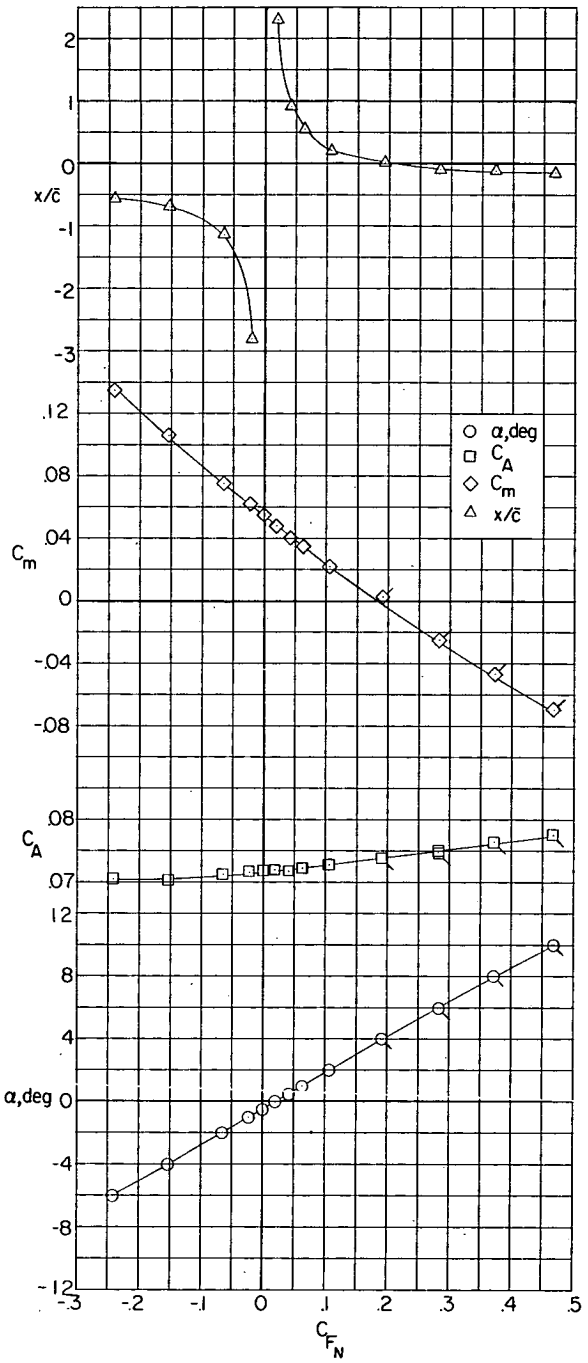

(a) Longitudinal characteristics in body-axis system at $\beta = 0^{\circ}$.

Figure 14.- Complete configuration with $i_t = 0^{\circ}$ at $M = 2.22$.

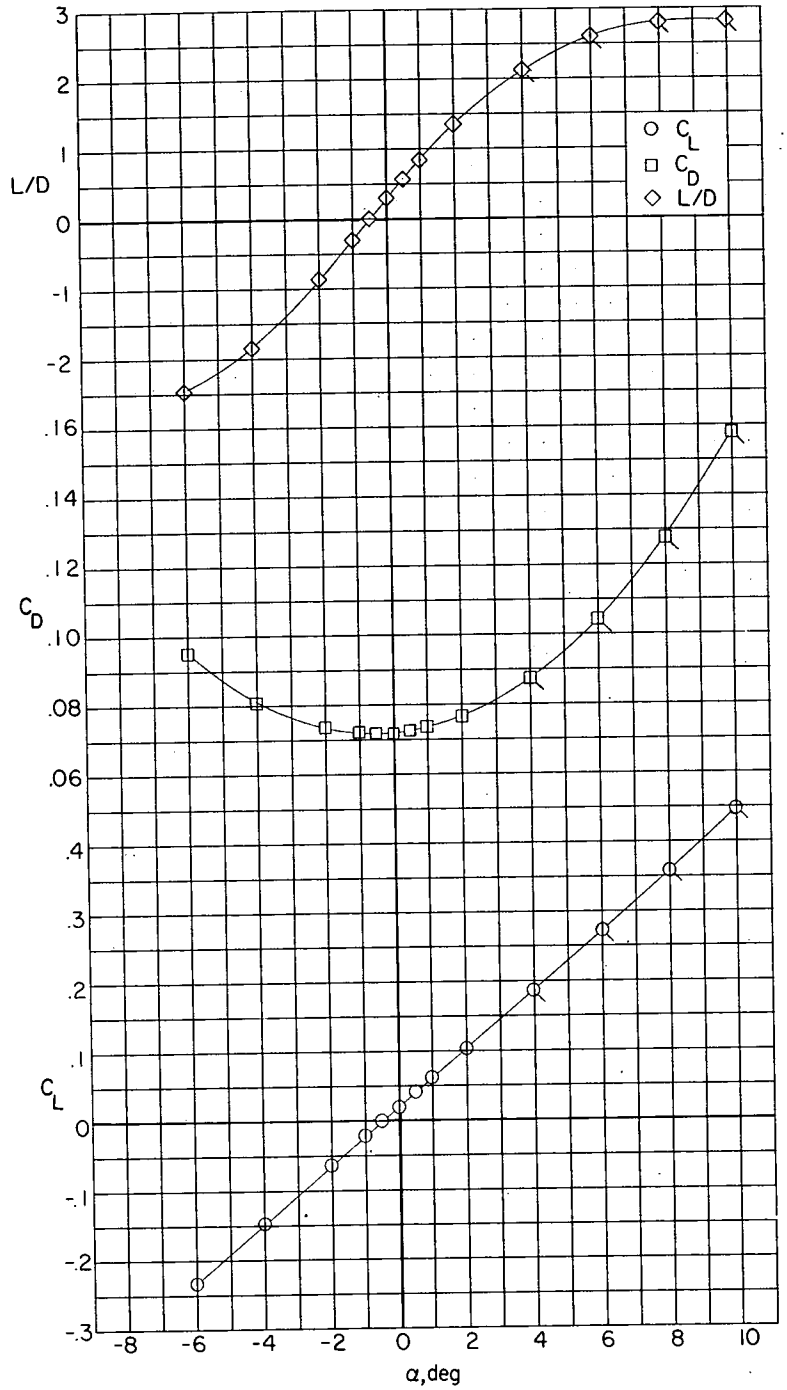

(b) Longitudinal-force characteristics in stability-axis system at $\beta = 0^{\circ}$.

Figure 14.- Continued.

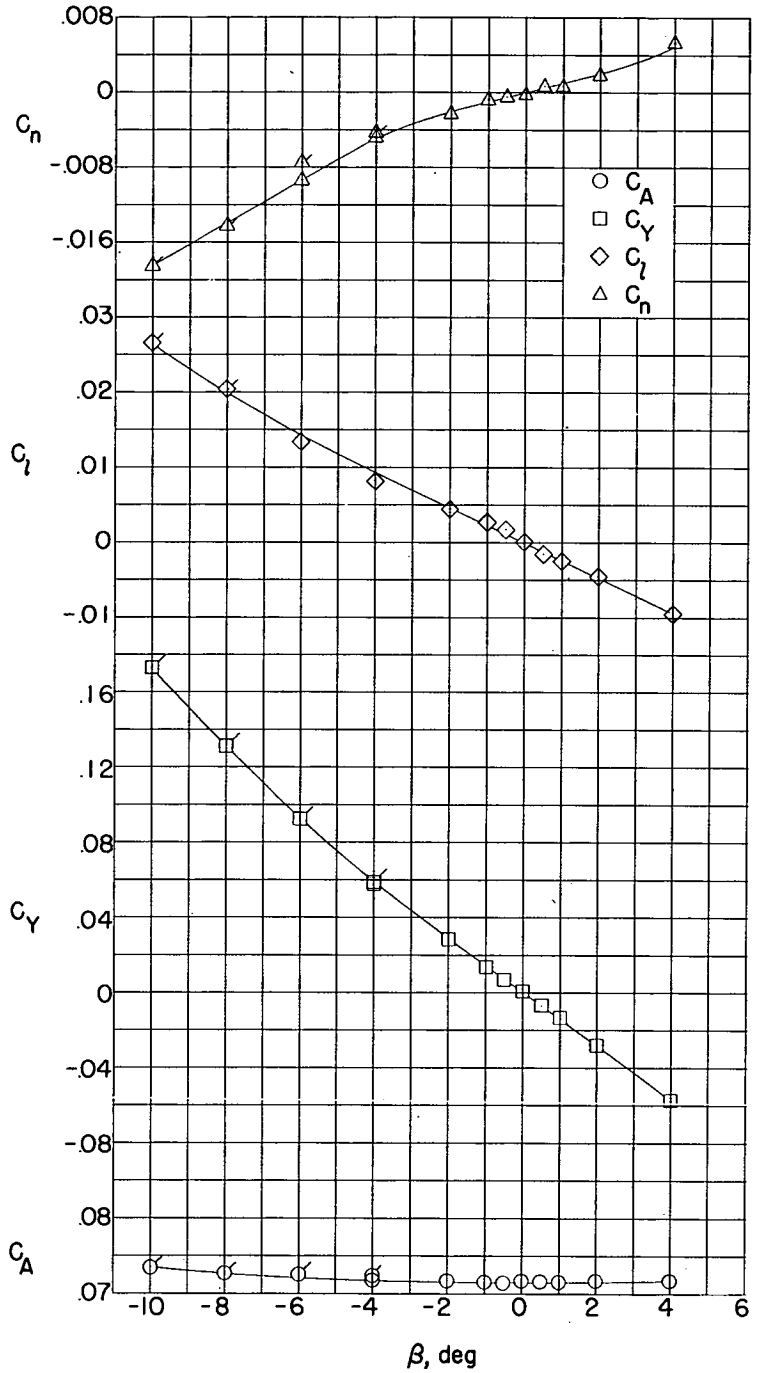

(c) Lateral characteristics in body-axis system at $\alpha = 0^\circ$.

Figure 14.- Concluded.

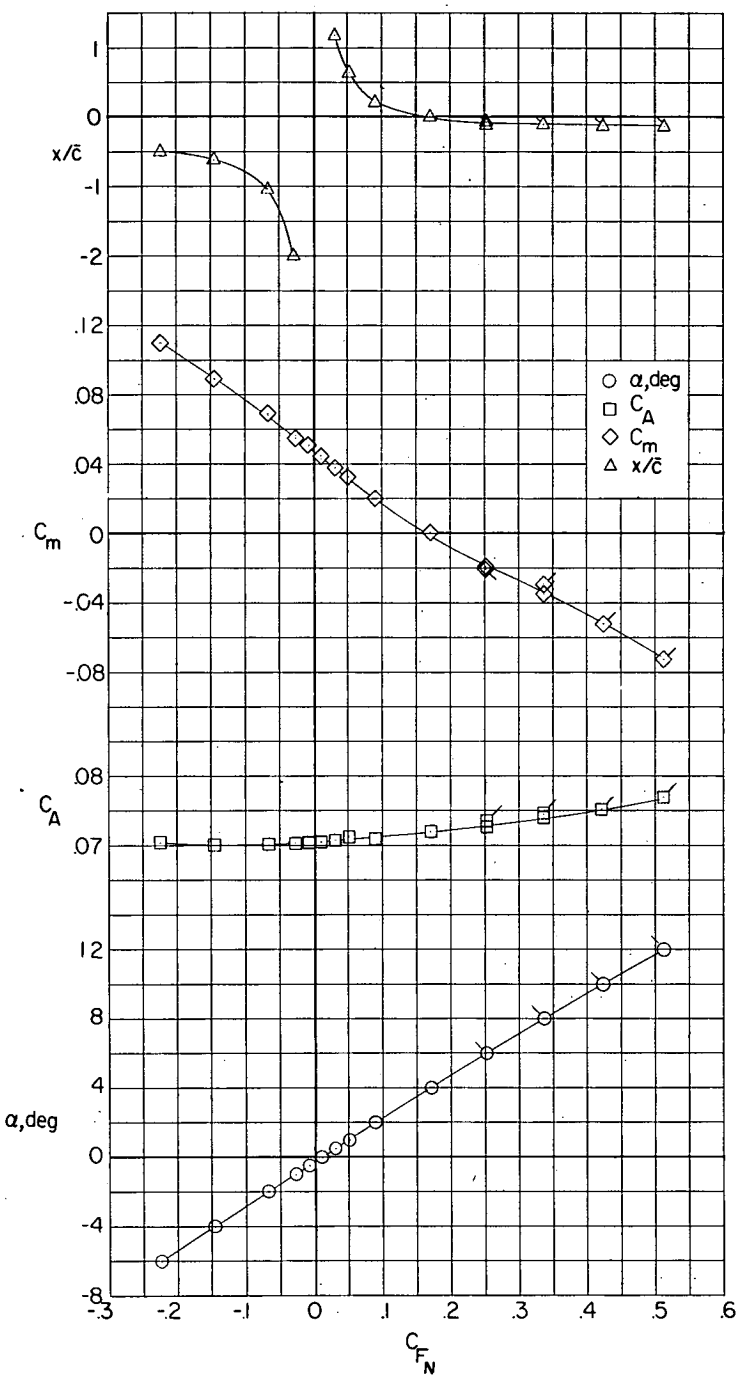

(a) Longitudinal characteristics in body-axis system at $\beta = 0^{\circ}$.

Figure 15.- Complete configuration with $i_t = 0^{\circ}$ at $M = 2.40$.

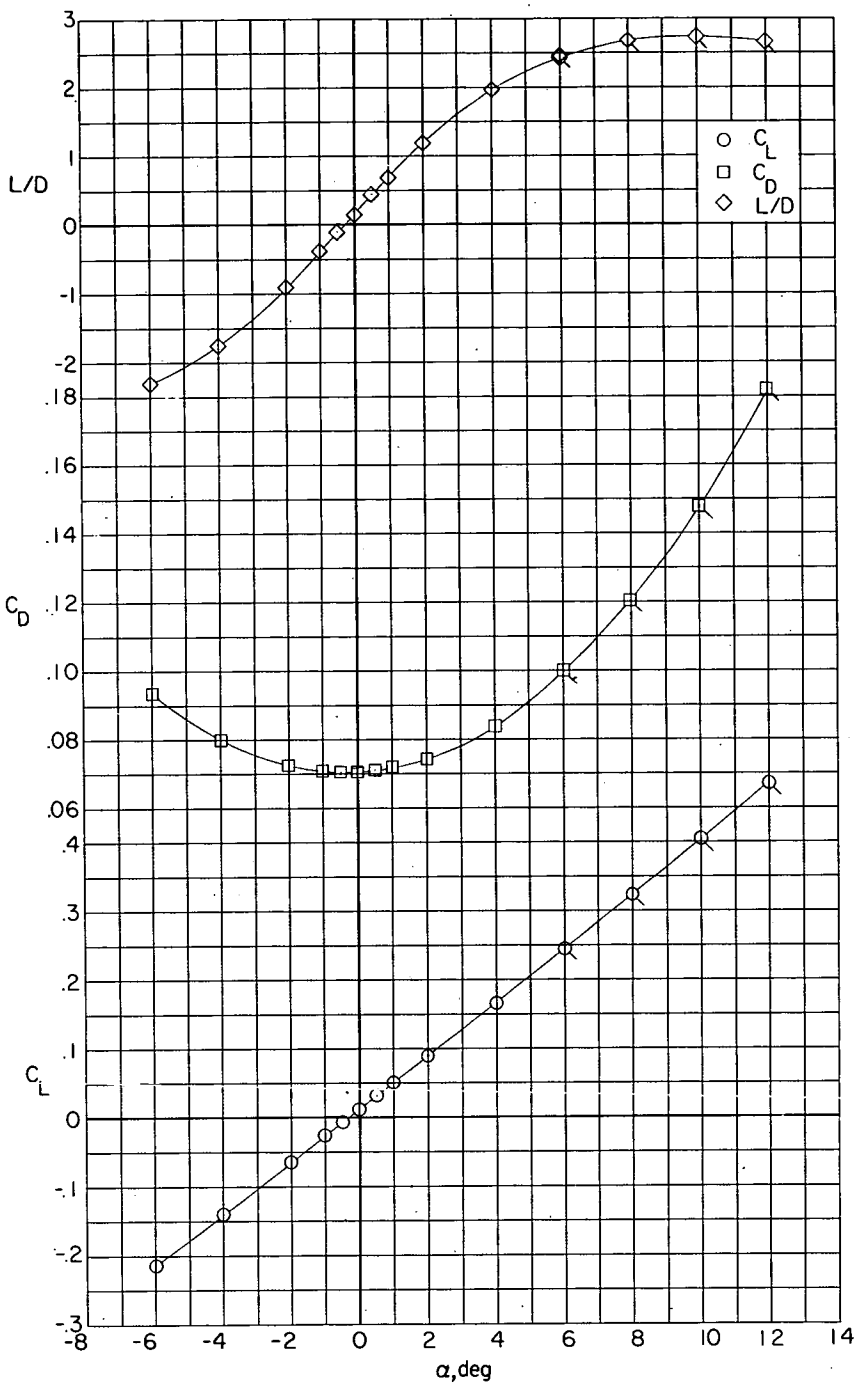

(b) Longitudinal-force characteristics in stability-axis system at $\beta = 0^{\circ}$.

Figure 15.- Continued.

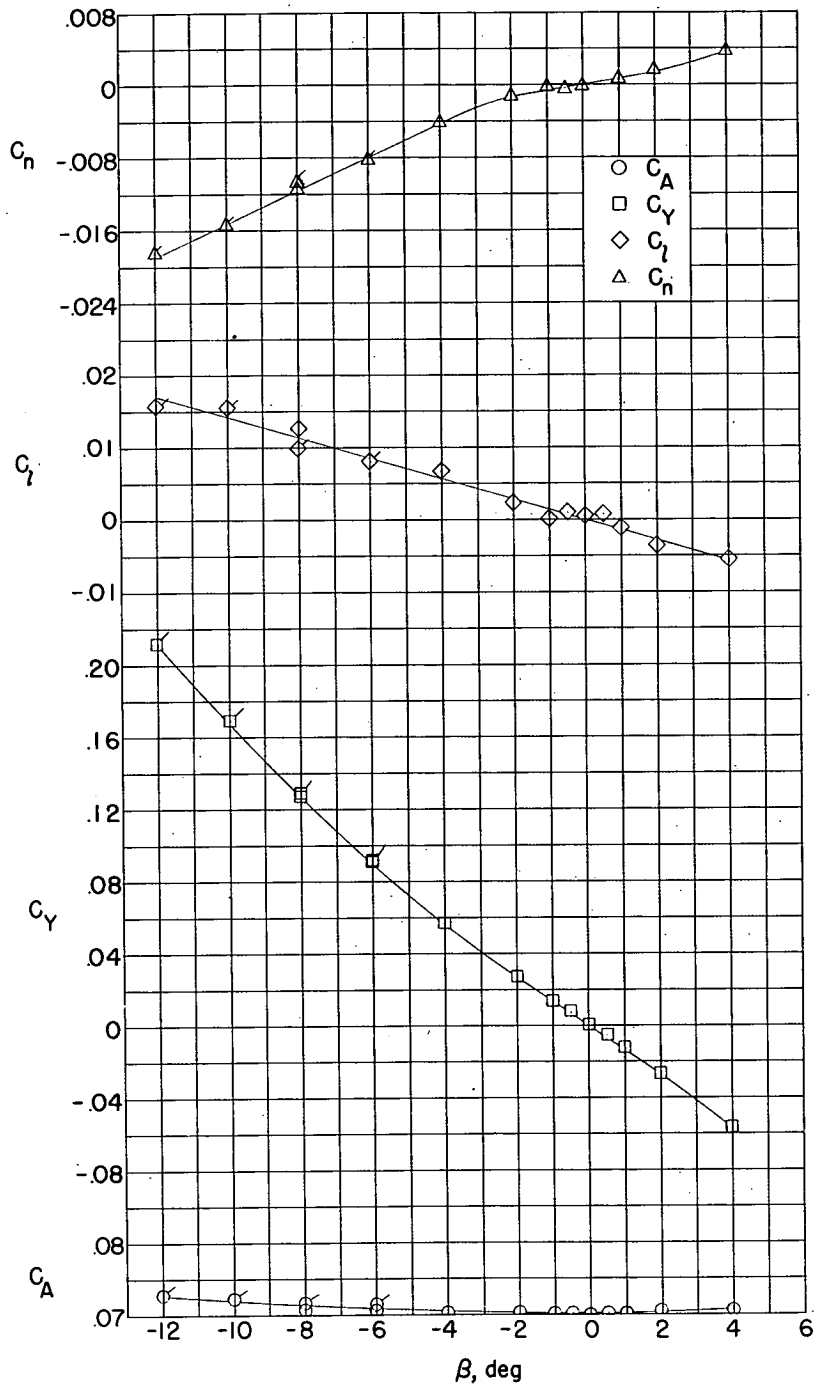

(c) Lateral characteristics in body-axis system at $\alpha = 0^\circ$.

Figure 15.- Concluded.

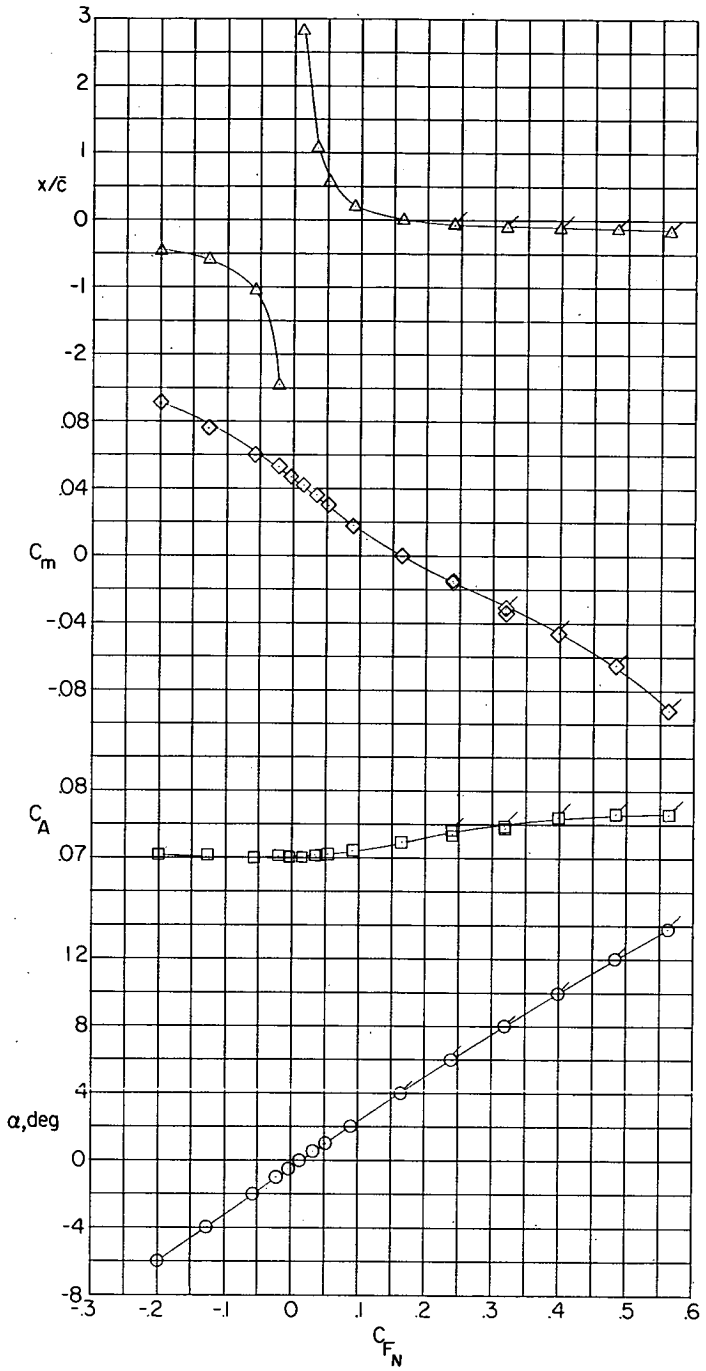

(a) Longitudinal characteristics in body-axis system at $\beta = 0^{\circ}$.

Figure 16.- Complete configuration with $i_t = 0^{\circ}$ at $M = 2.62$.

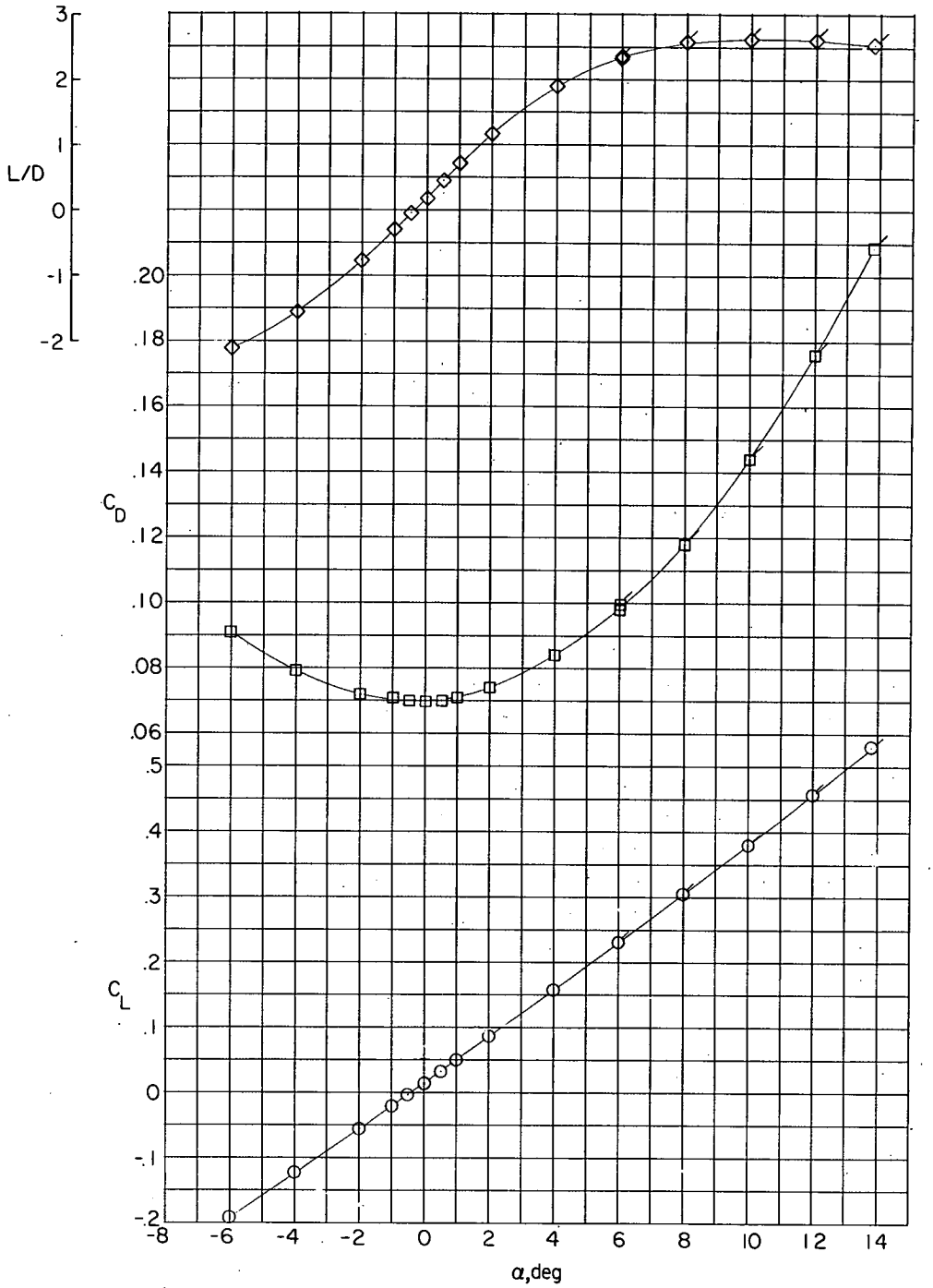

(b) Longitudinal-force characteristics in stability-axis system at $\beta = 0^{\circ}$.

Figure 16.- Continued.

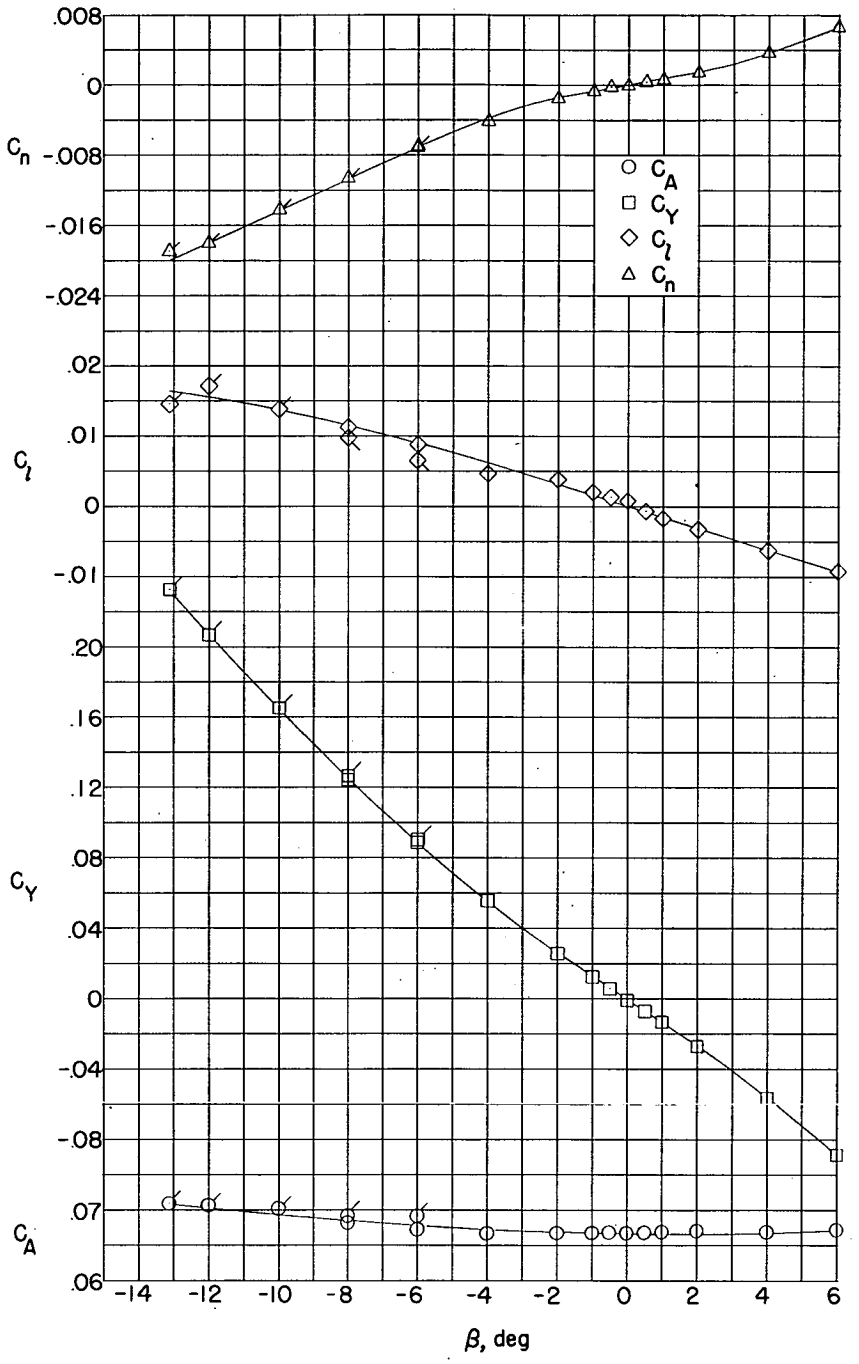

(c) Lateral characteristics in body-axis system at $\alpha = 0^{\circ}$.

Figure 16.- Concluded.

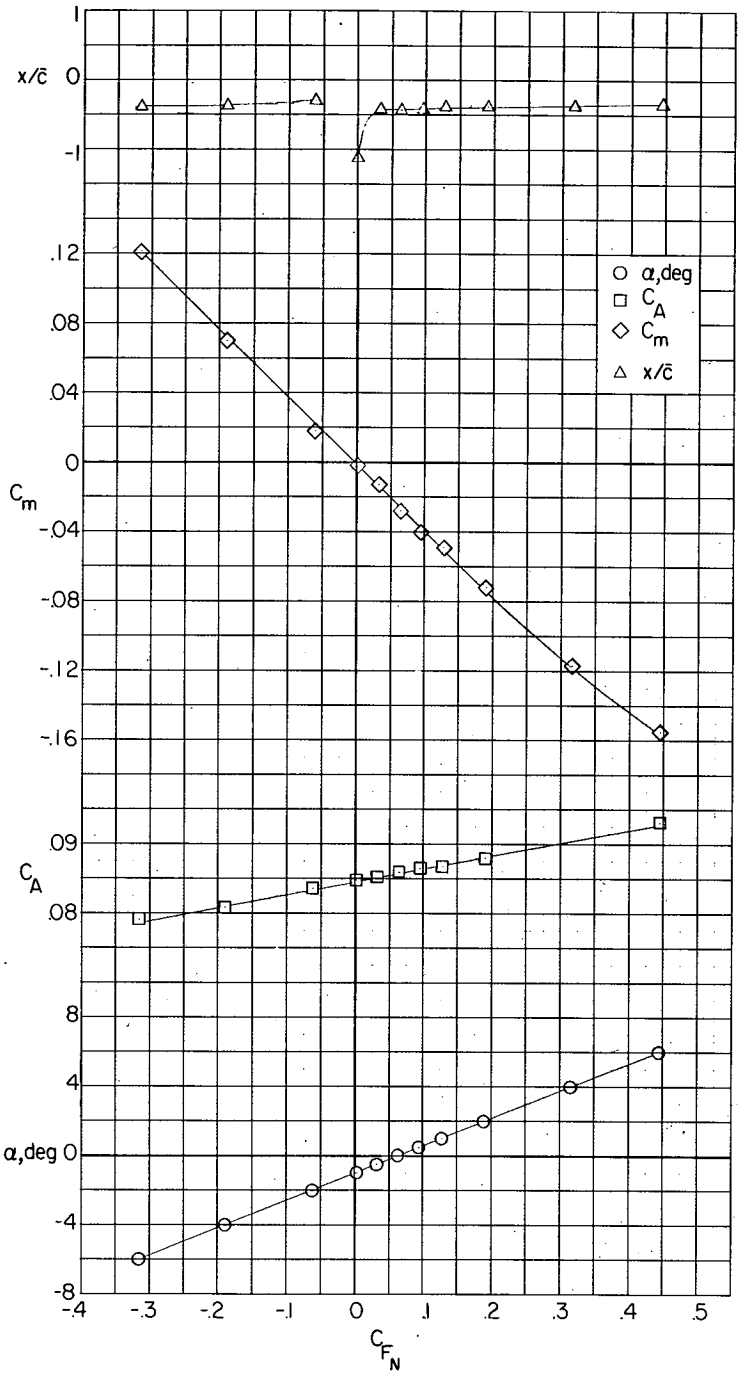

(a) Longitudinal characteristics in body-axis system at $\beta = 0^{\circ}$.

Figure 17.- Complete configuration with $i_t = 5^{\circ}$ at $M = 1.62$.

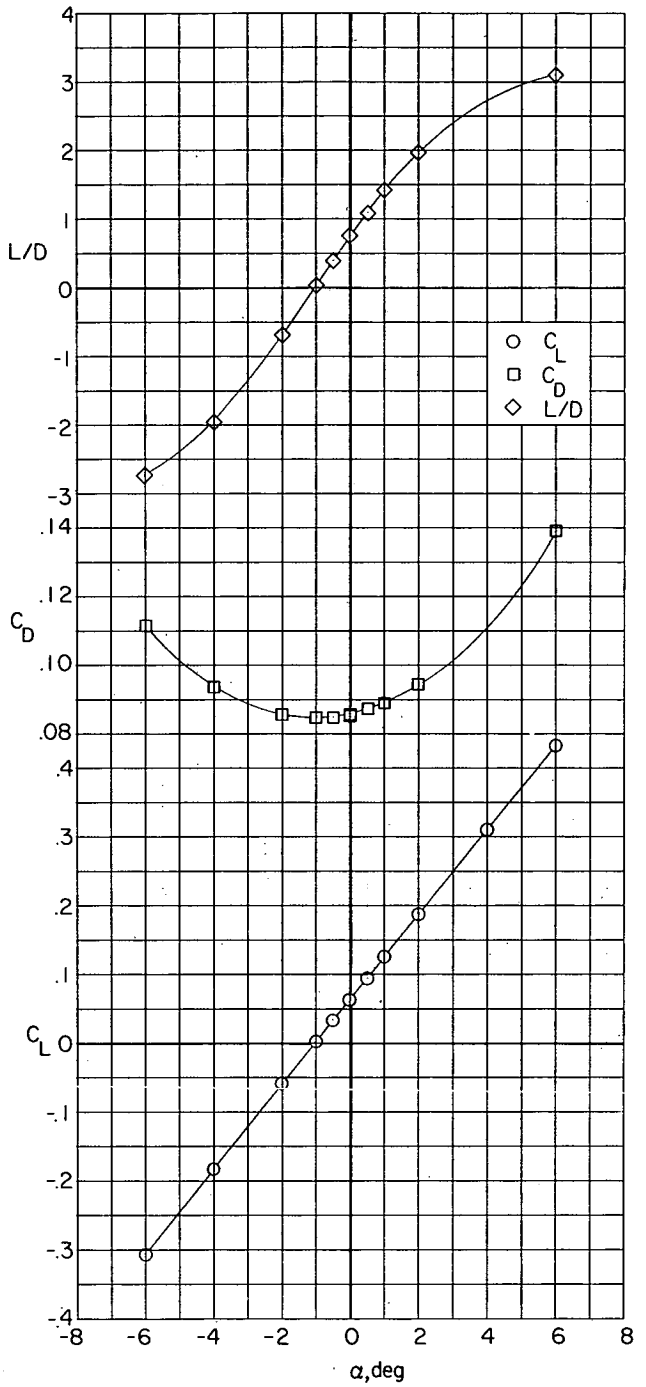

(b) Longitudinal-force characteristics in stability-axis system at $\beta = 0^{o}$.

Figure 17.- Continued.

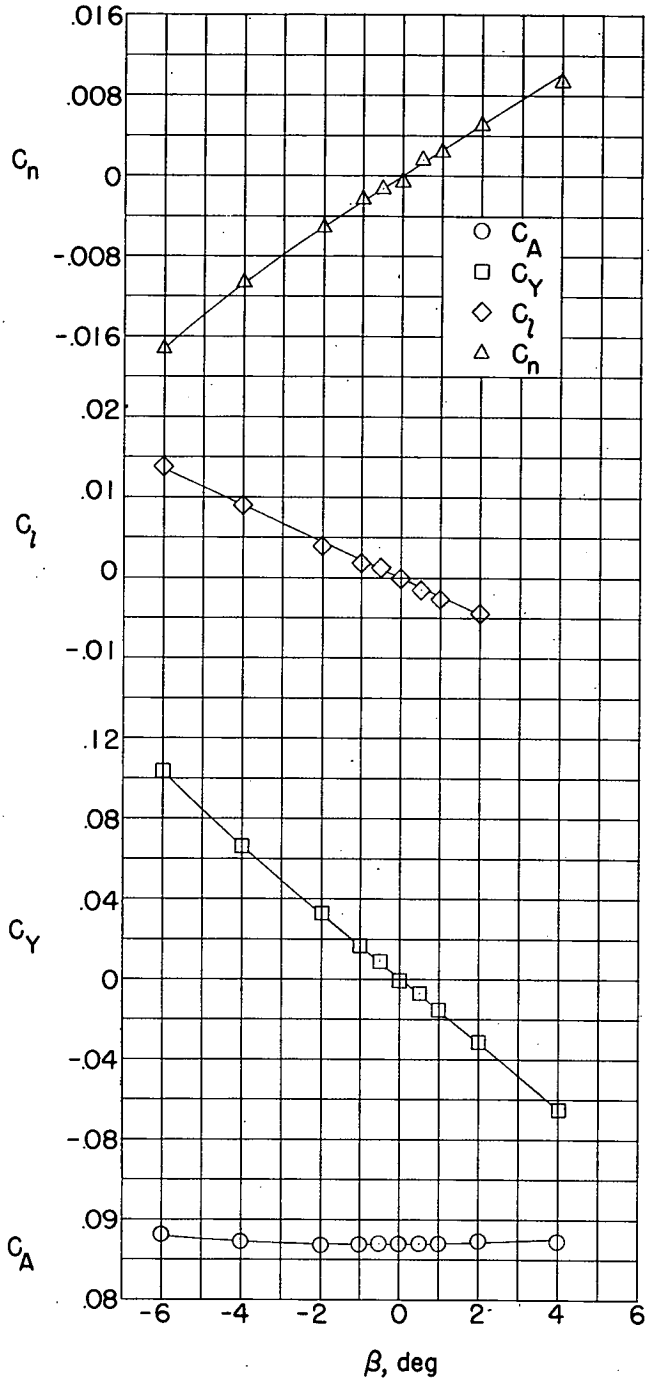

(c) Lateral characteristics in body-axis system at $\alpha = 0^\circ$.

Figure 17.- Concluded.

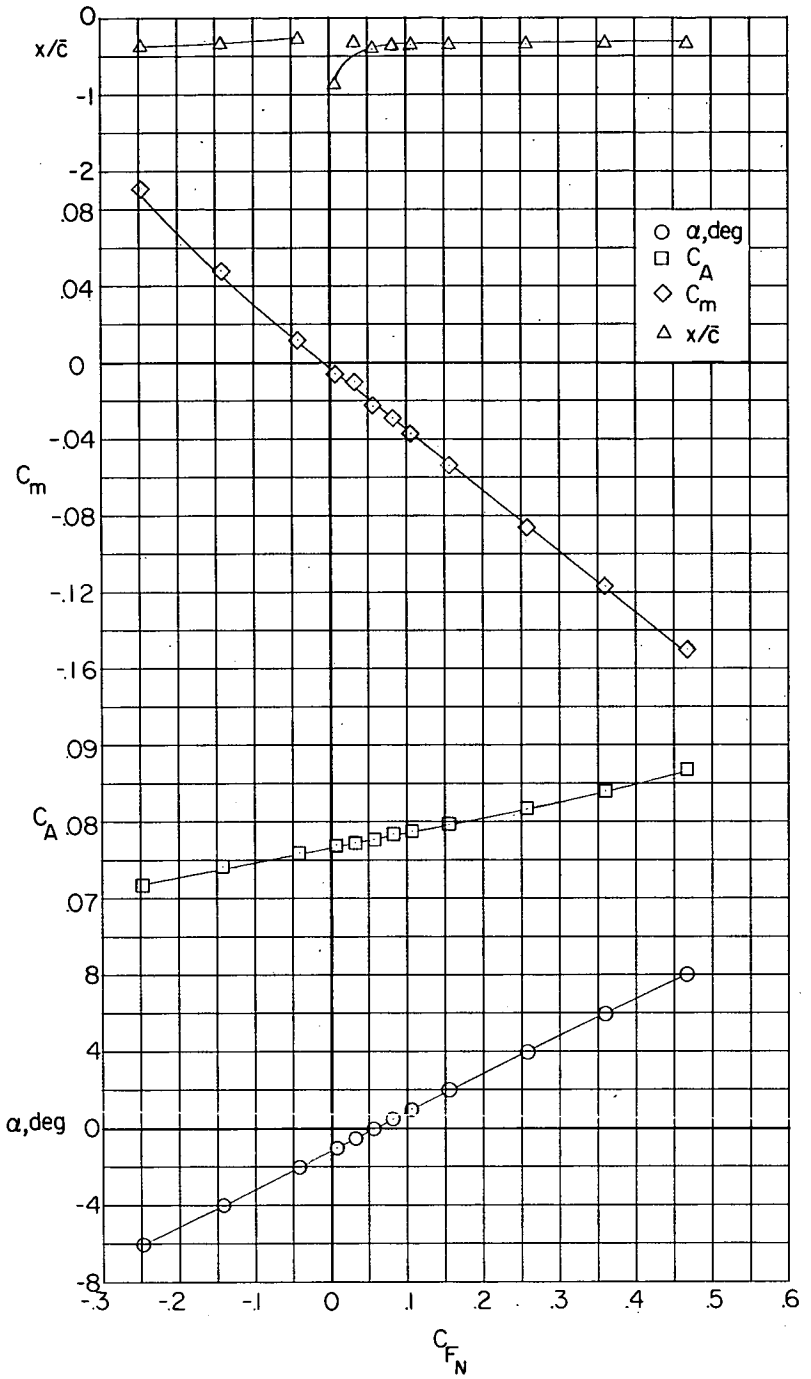

(a) Longitudinal characteristics in body-axis system at $\beta = 0^{\circ}$.

Figure 18.- Complete configuration with $i_t = 5^{\circ}$ at $M = 1.94$.

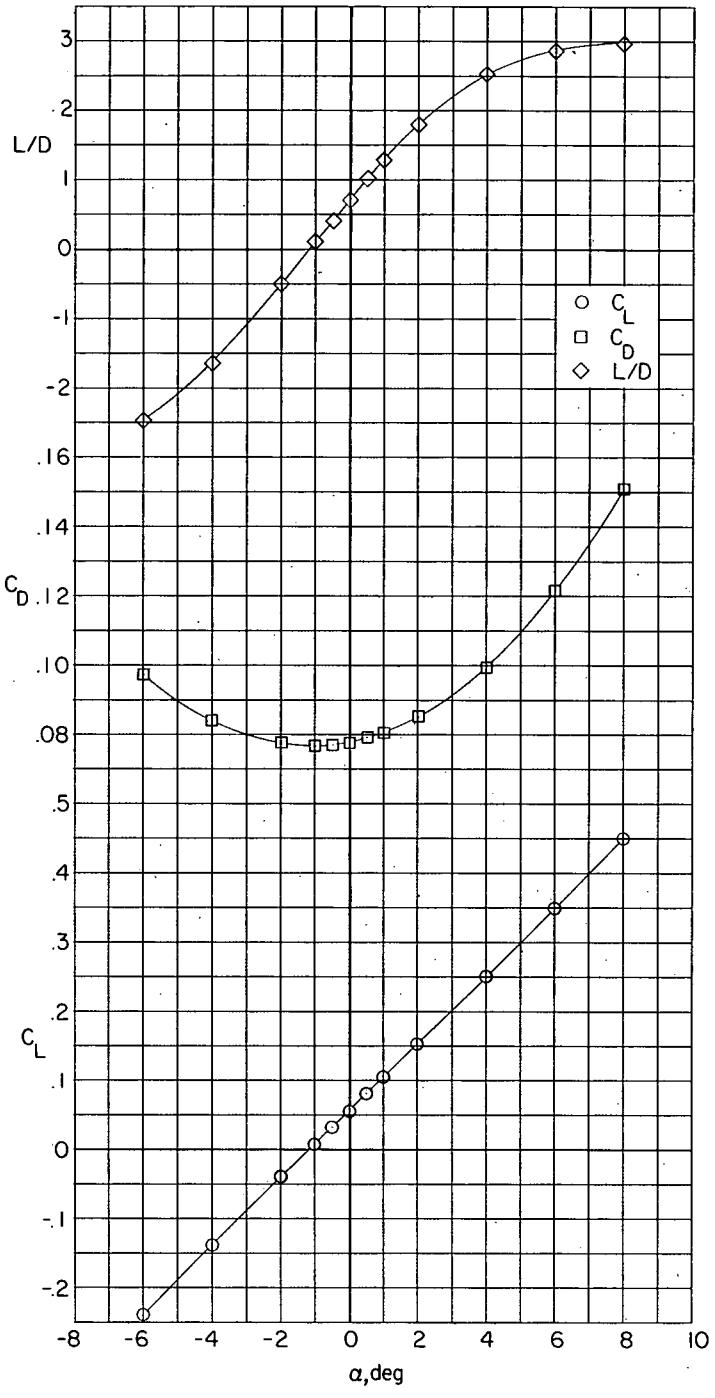

(b) Longitudinal-force characteristics in stability-axis system at $\beta = 0^{\circ}$.

Figure 18.- Continued.

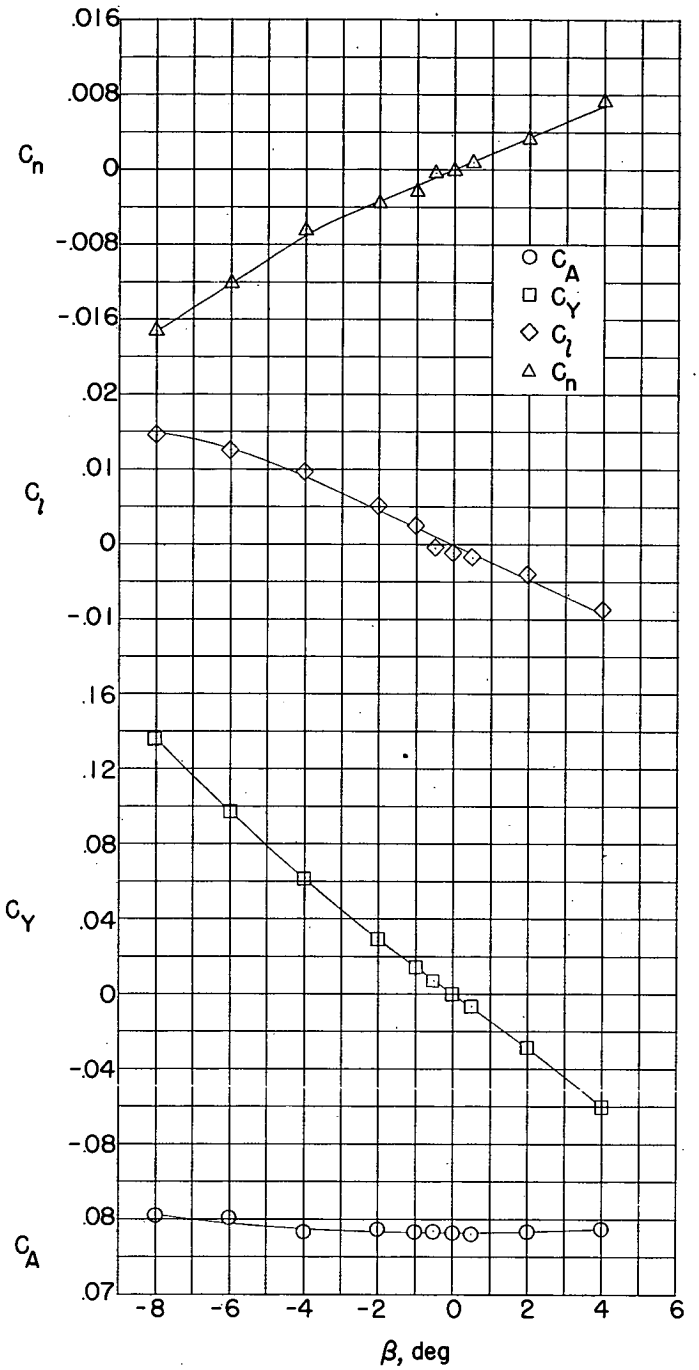

(c) Lateral characteristics in body-axis system at $\alpha = 0^\circ$.

Figure 18.- Concluded.

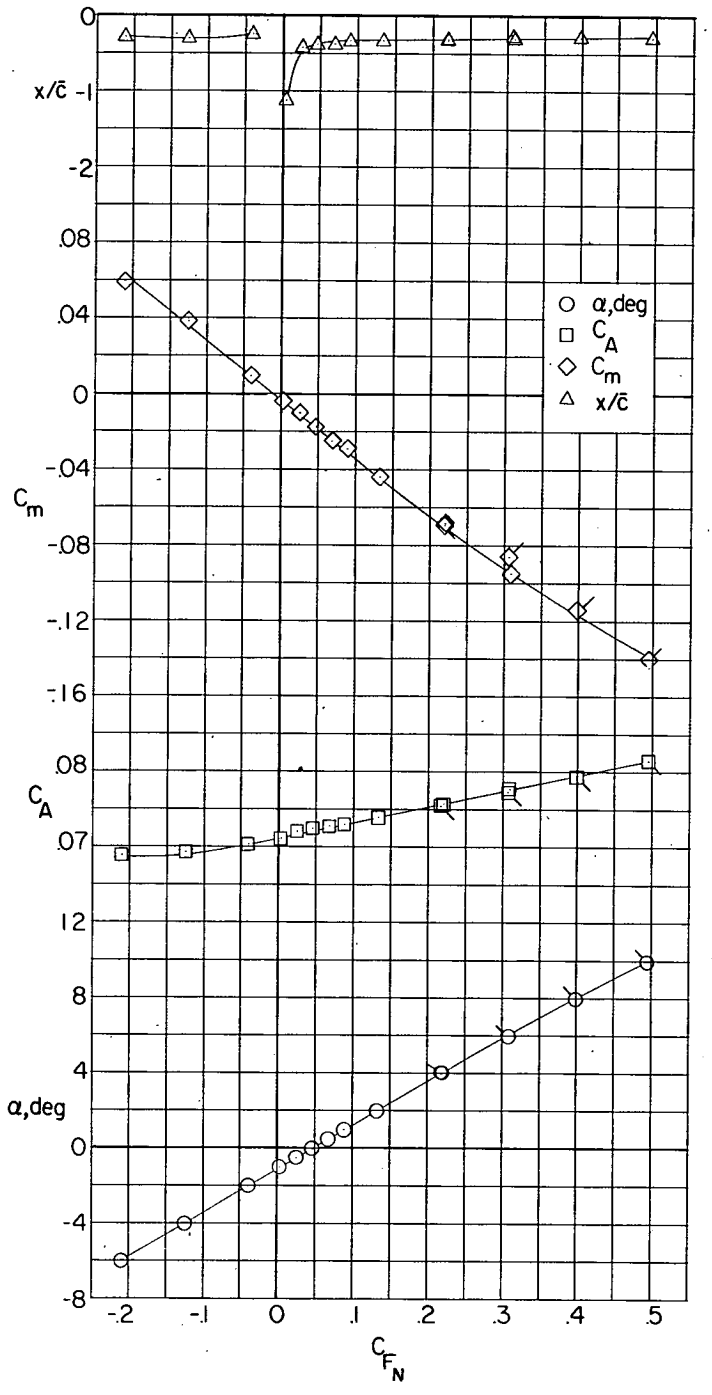

(a) Longitudinal characteristics in body-axis system at $\beta = 0^{\circ}$.

Figure 19.- Complete configuration with $i_t = 5^{\circ}$ at $M = 2.22$.

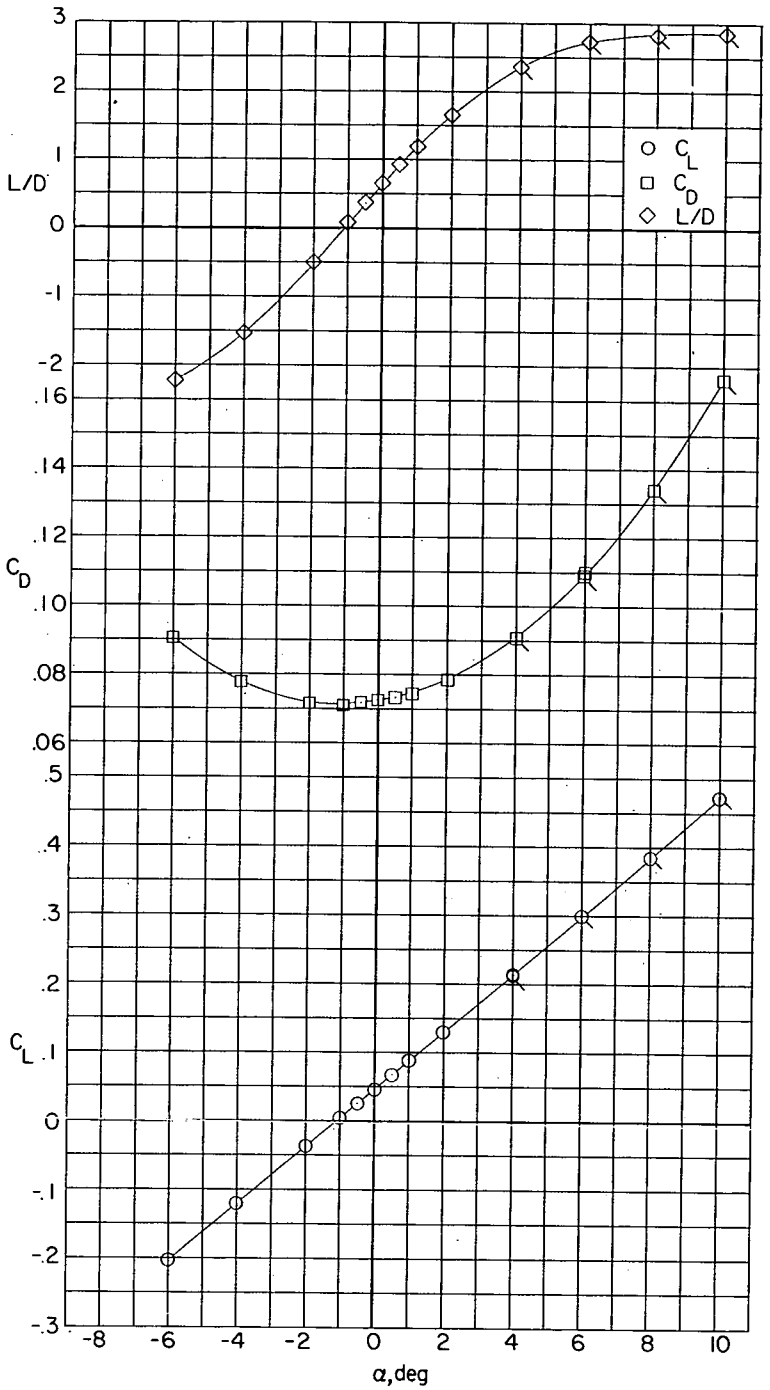

(b) Longitudinal-force characteristics in stability-axis system at $\beta = 0^{\circ}$.

Figure 19.- Continued.

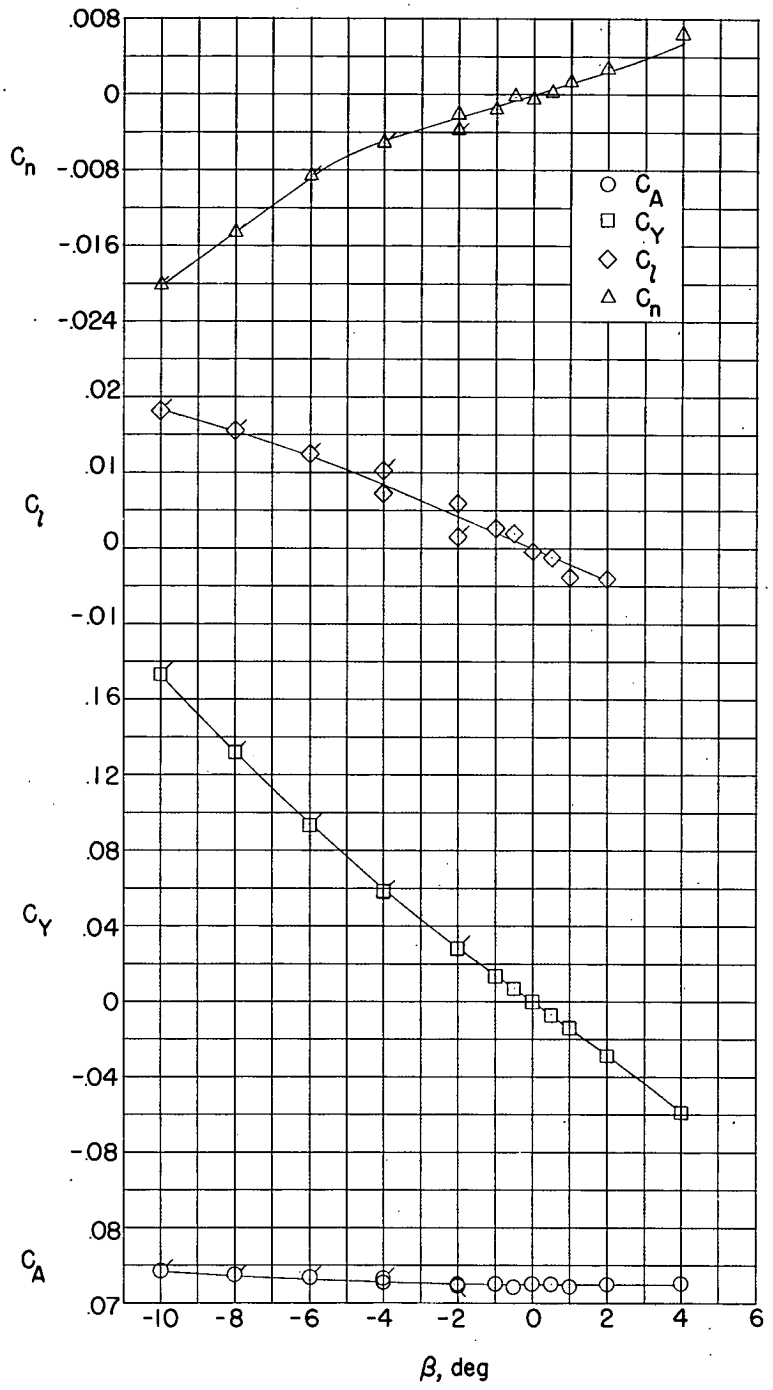

(c) Lateral characteristics in body-axis system at $\alpha = 0^\circ$.

Figure 19.- Concluded.

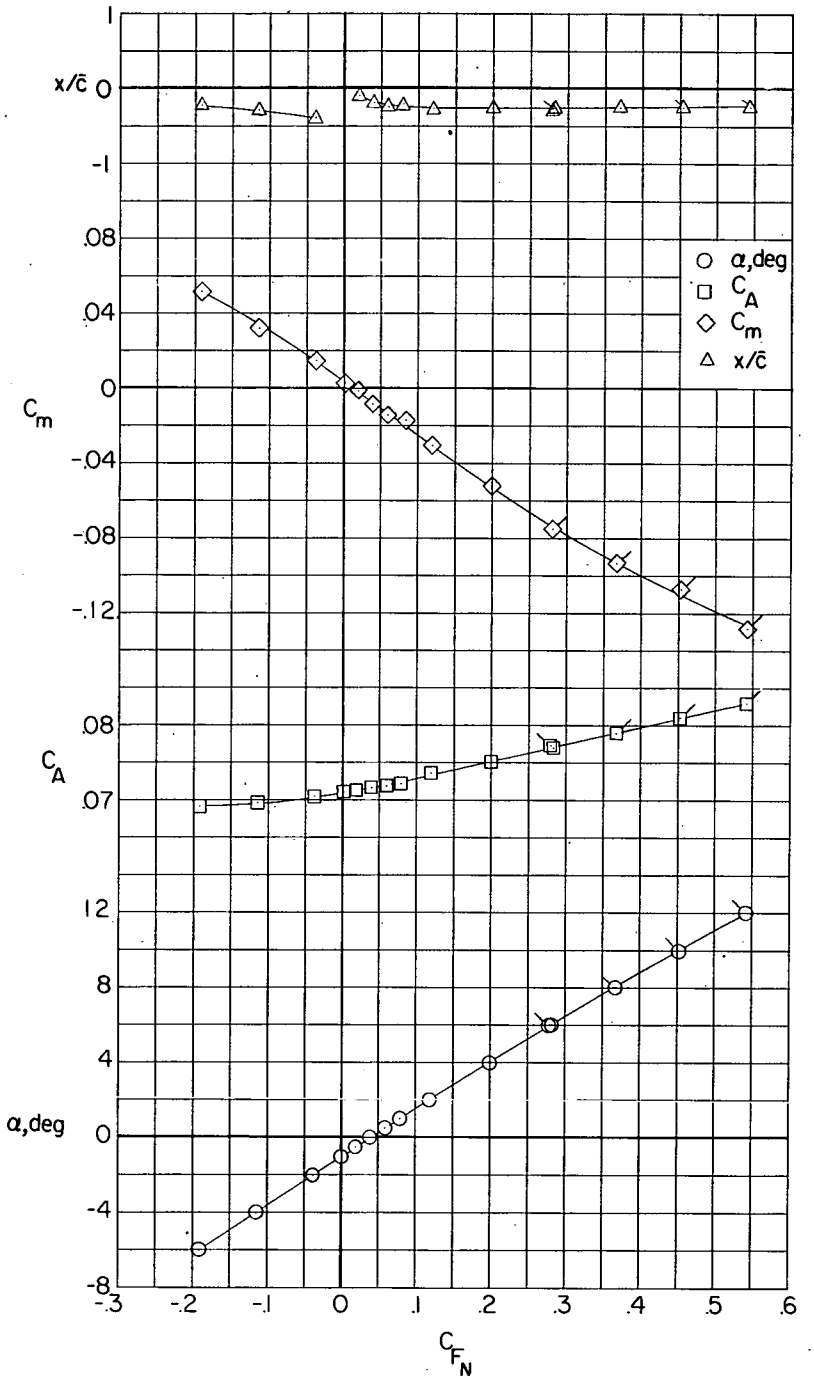

(a) Longitudinal characteristics in body-axis system at $\beta = 0^{\circ}$.

Figure 20.- Complete configuration with $i_t = 5^{\circ}$ at $M = 2.40$.

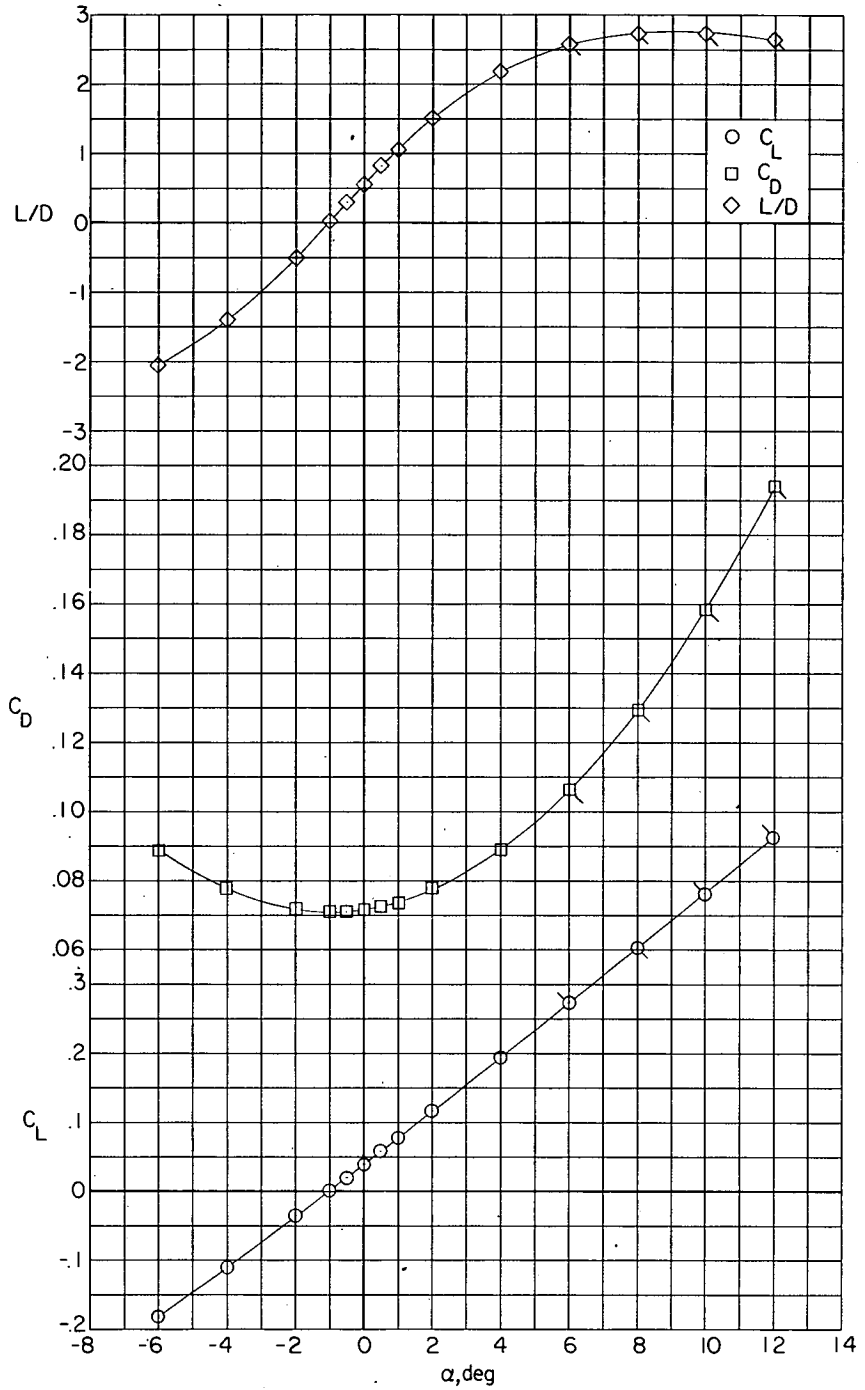

(b) Longitudinal-force characteristics in stability-axis system at $\beta = 0^{\circ}$.

Figure 20.- Continued.

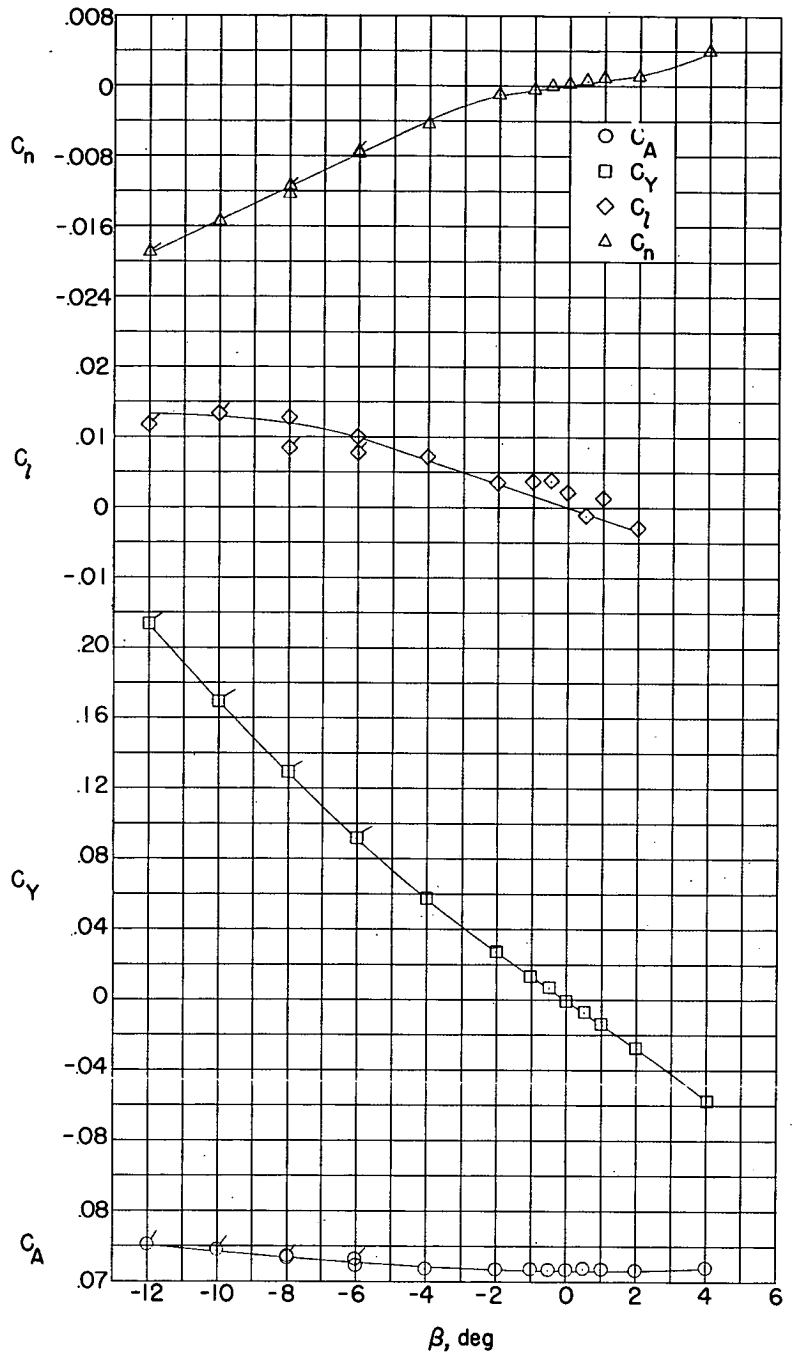

(c) Lateral characteristics in body-axis system at $\alpha = 0^{\circ}$.

Figure 20.- Concluded.

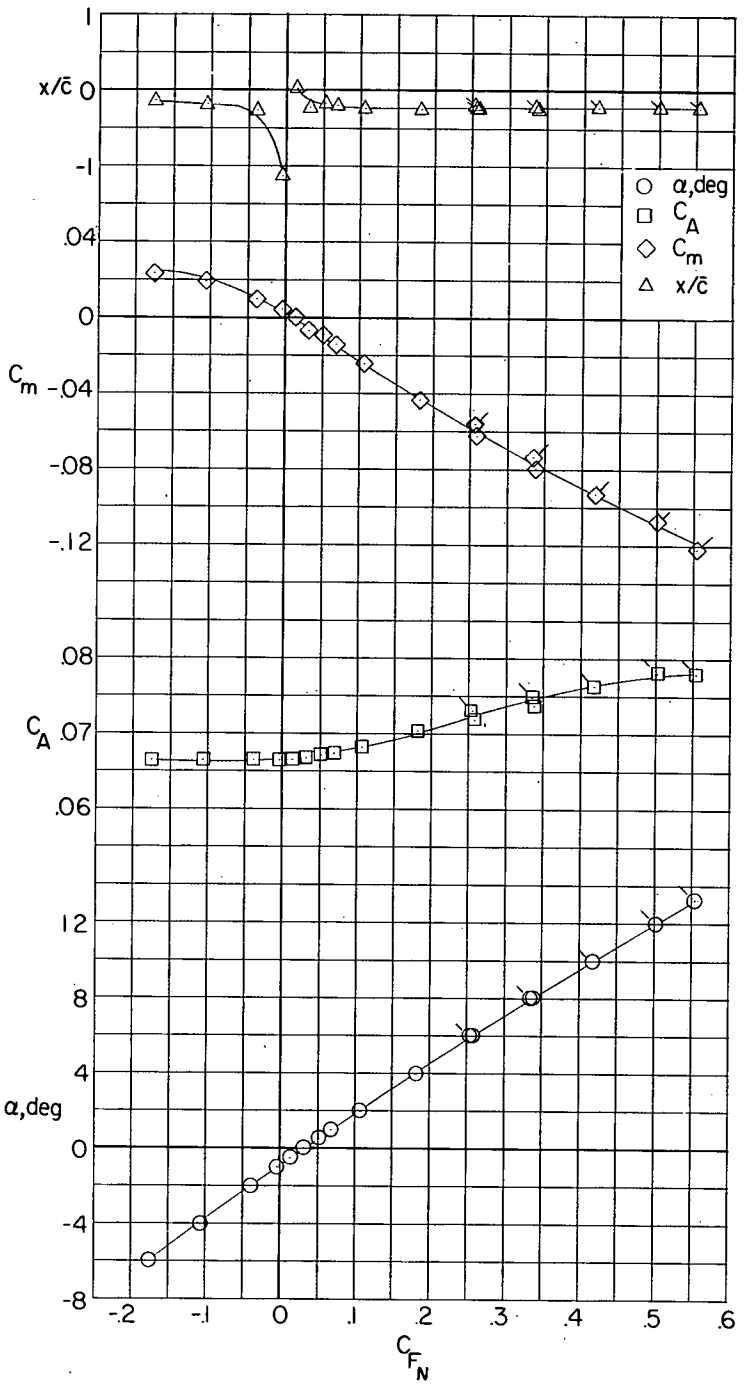

(a) Longitudinal characteristics in body-axis system at $\beta = 0^{\circ}$.

Figure 21.- Complete configuration with $i_t = 5^{\circ}$ at $M = 2.62$.

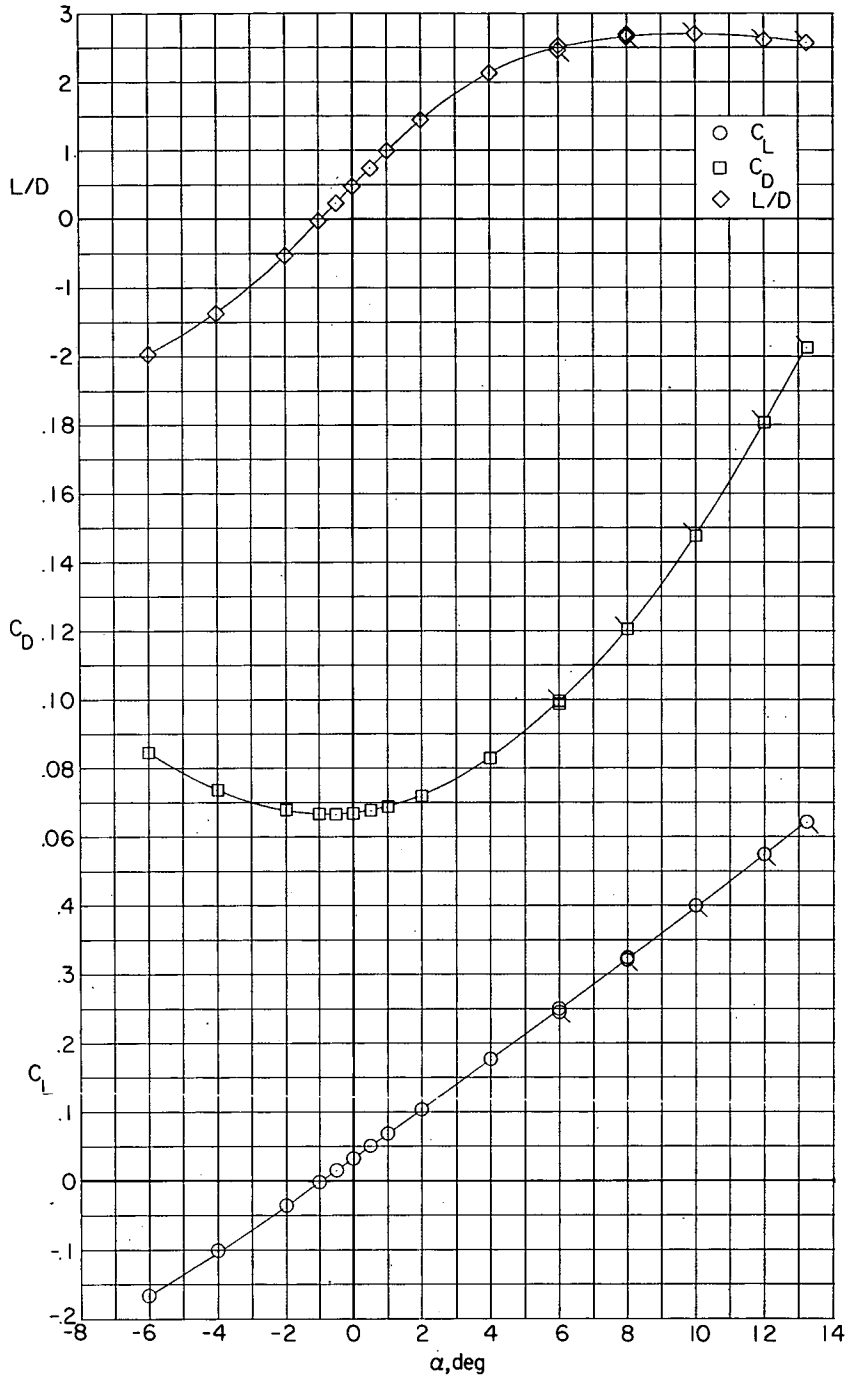

(b) Longitudinal-force characteristics in stability-axis system at $\beta = 0^{\circ}$.

Figure 21.- Continued.

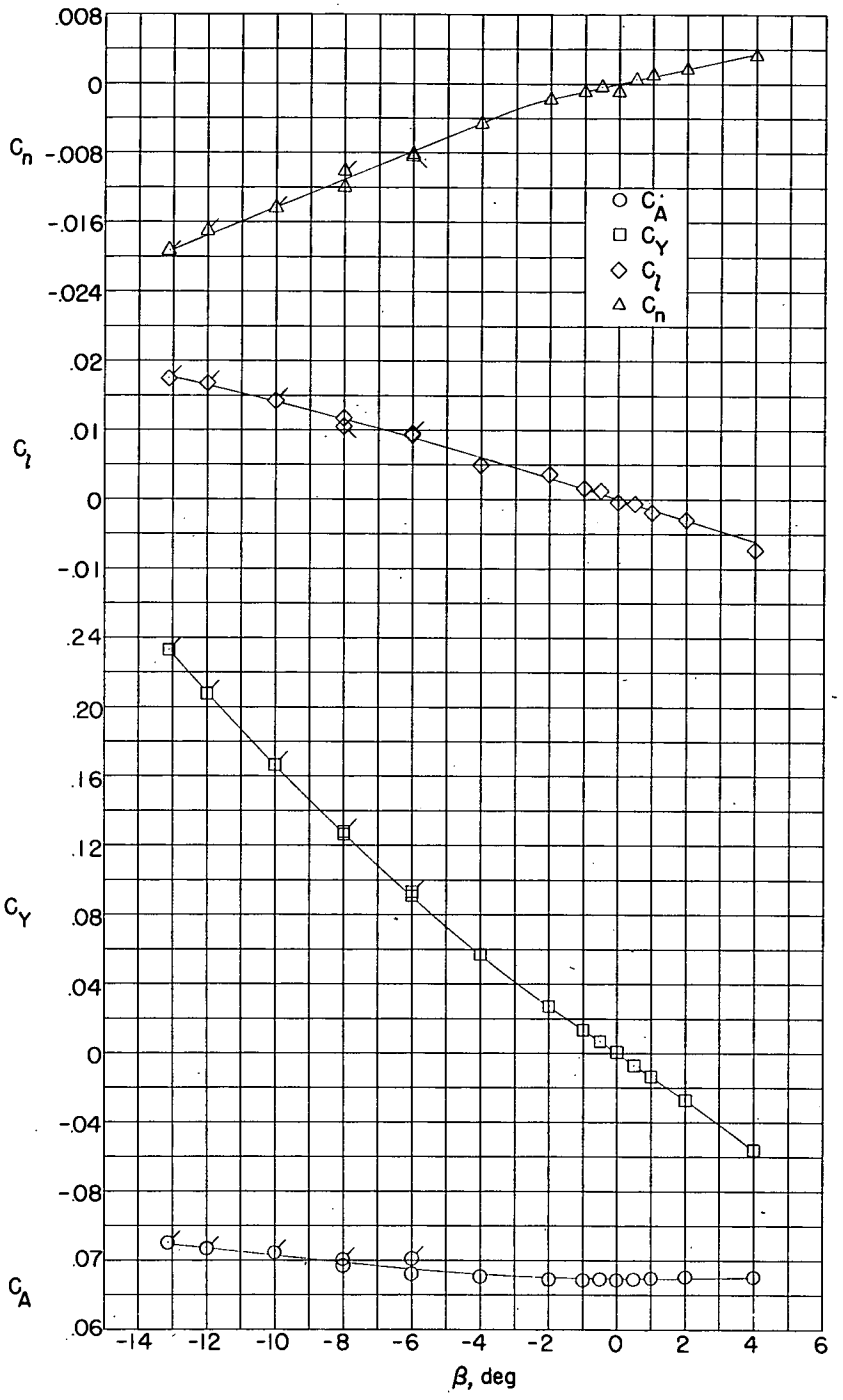

(c) Lateral characteristics in body-axis system at $\alpha = 0^{\circ}$.

Figure 21.- Concluded.

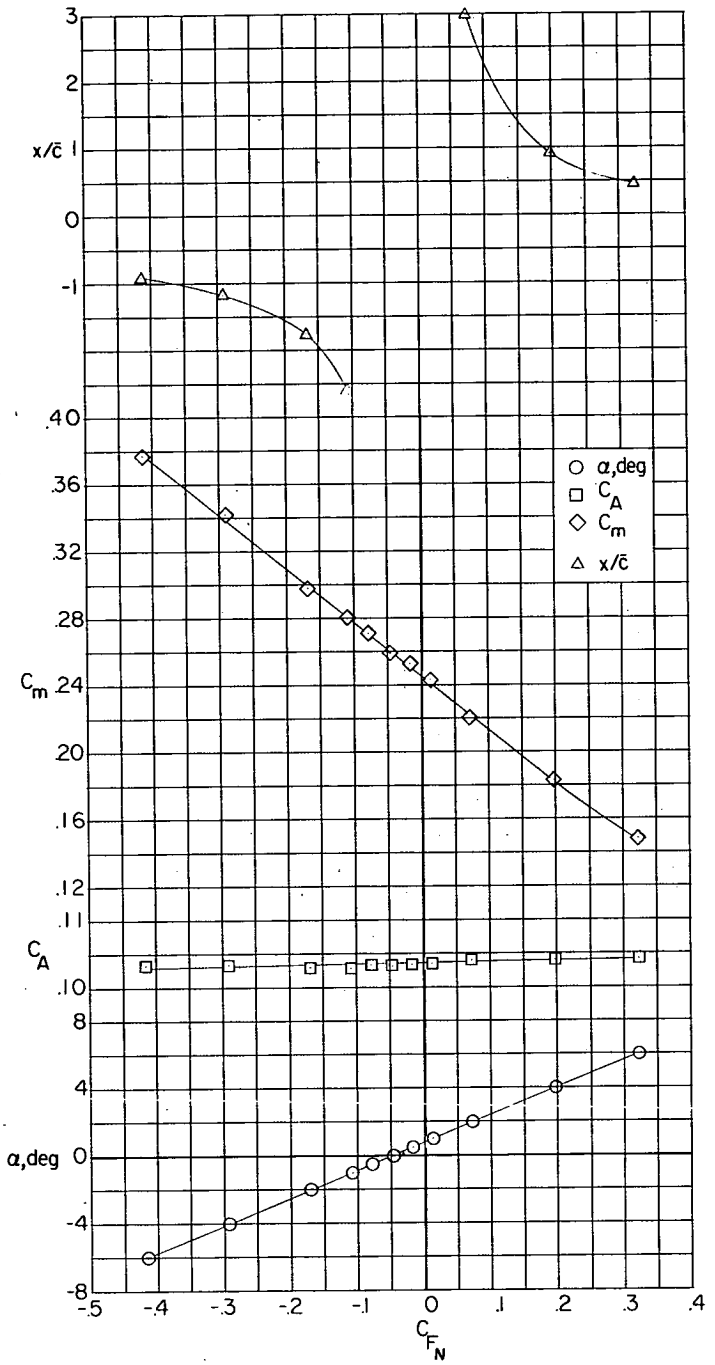

(a) Longitudinal characteristics in body-axis system at $\beta = 0^{\circ}$.

Figure 22.- Complete configuration with $i_t = -10^{\circ}$ at $M = 1.62$.

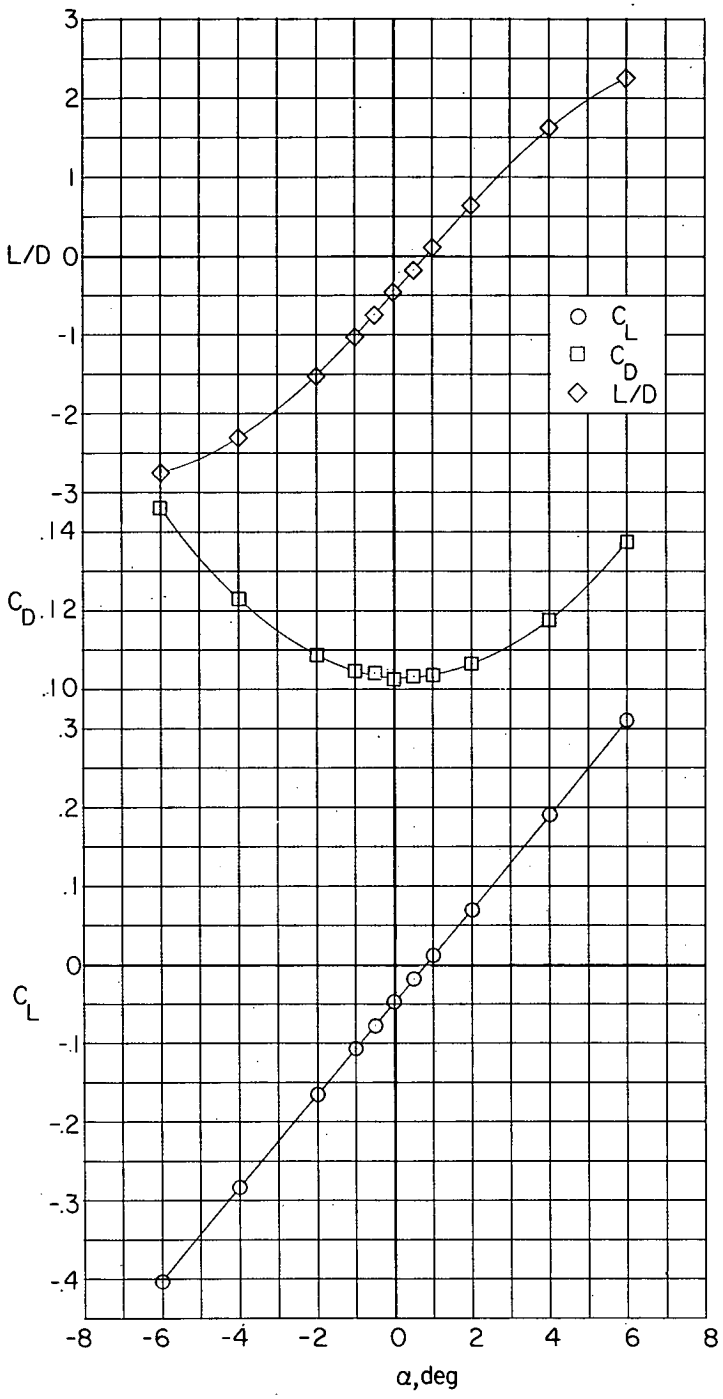

(b) Longitudinal-force characteristics in stability-axis system at $\beta = 0^{\circ}$.

Figure 22.- Continued.

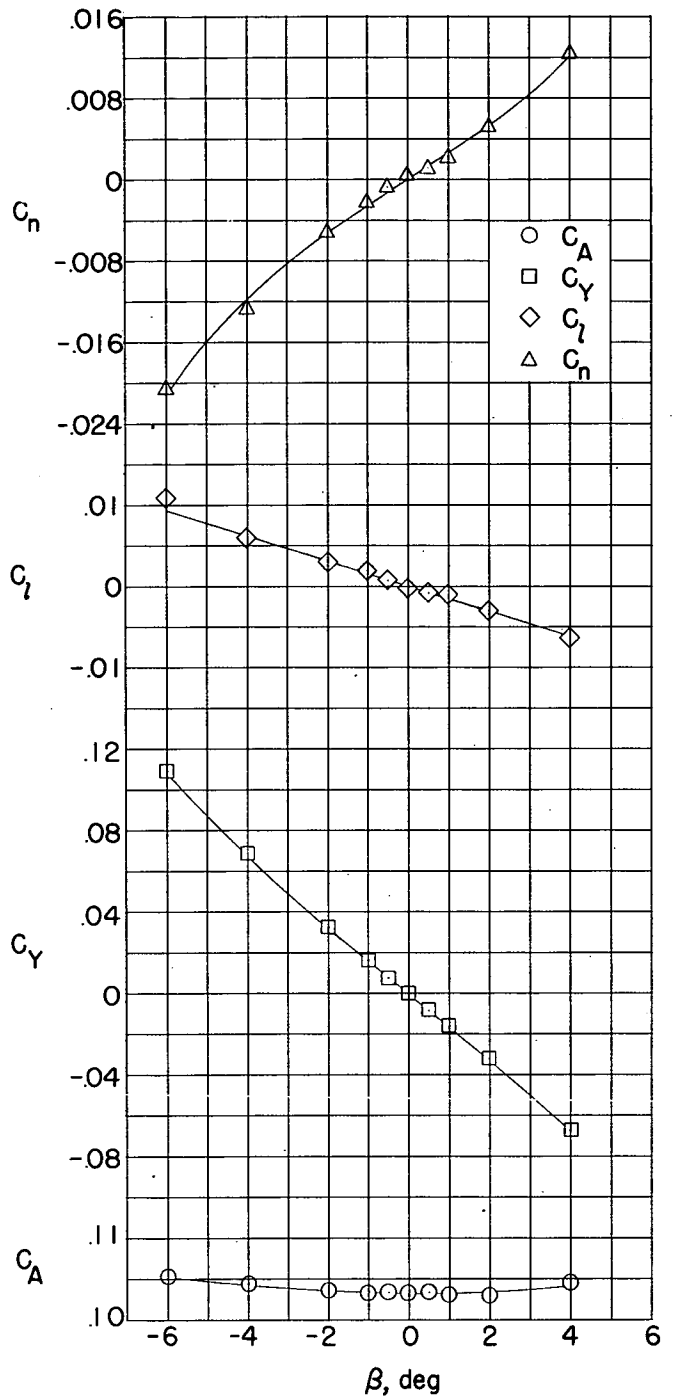

(c) Lateral characteristics in body-axis system at $\alpha = 0^{\circ}$.

Figure 22.- Concluded.

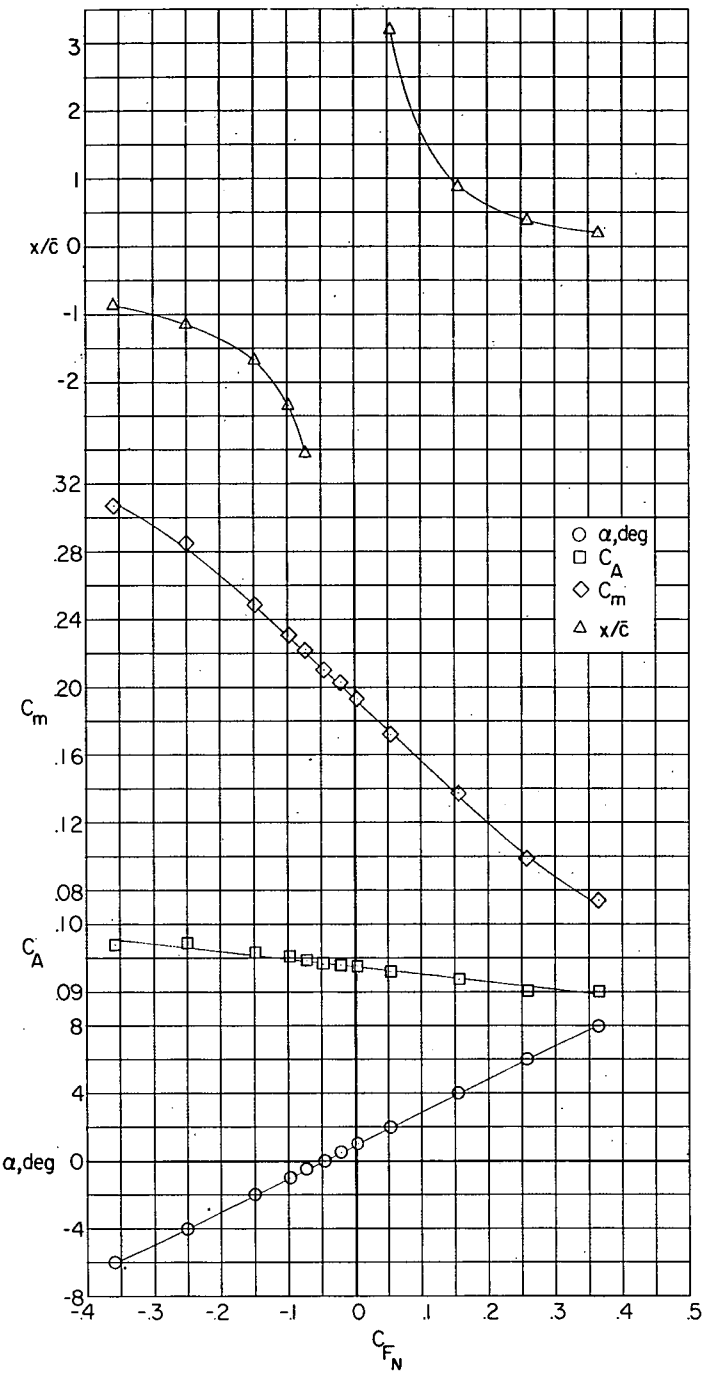

(a) Longitudinal characteristics in body-axis system at $\beta = 0^{\circ}$.

Figure 23.- Complete configuration with $i_t = -10^{\circ}$ at $M = 1.94$.

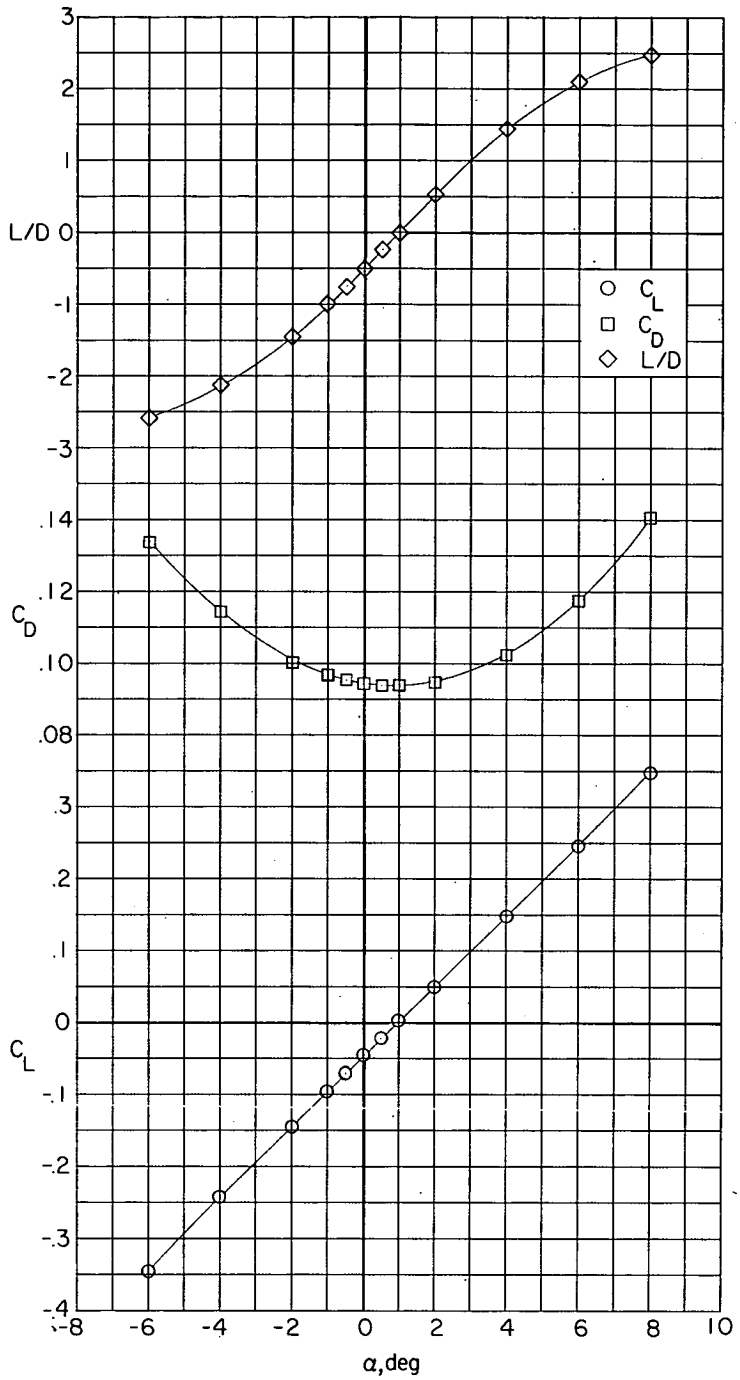

(b) Longitudinal-force characteristics in stability-axis system at $\beta = 0^{\circ}$.

Figure 23.- Continued.

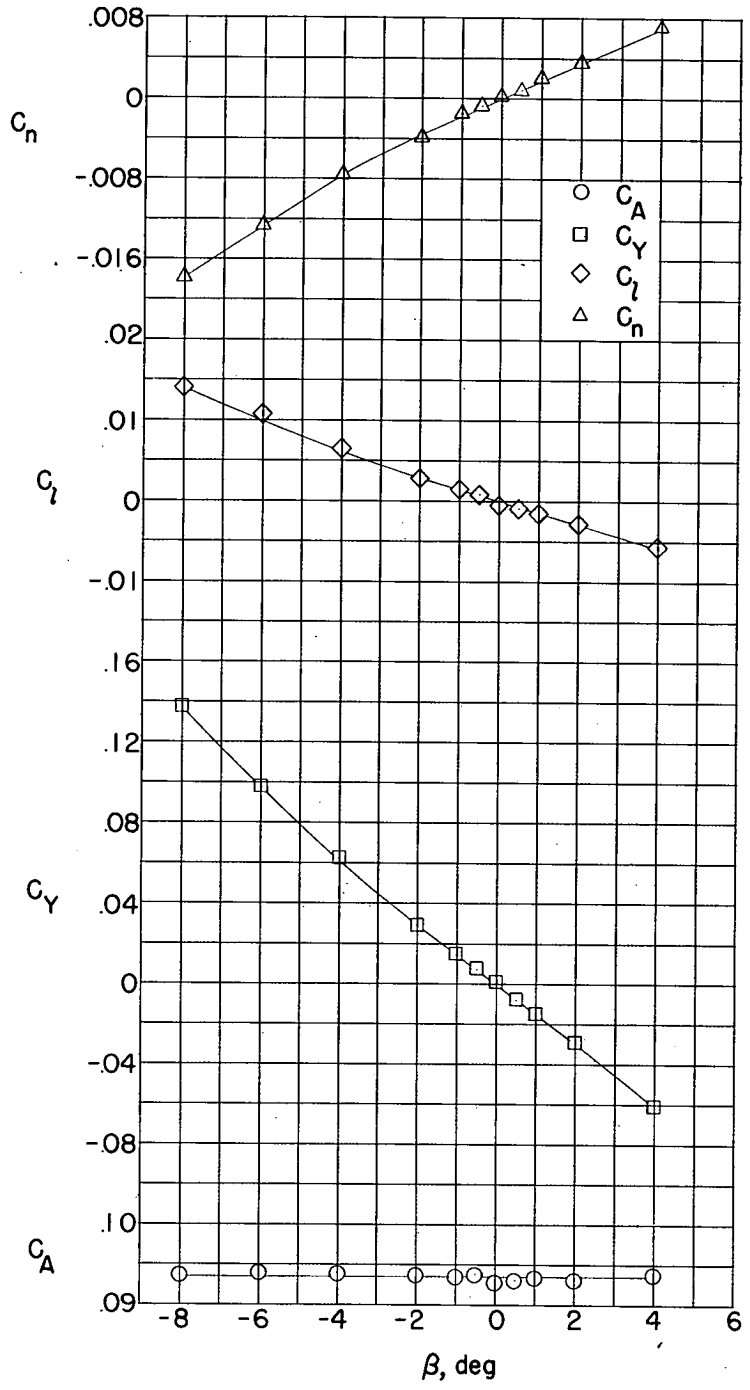

(c) Lateral characteristics in body-axis system at $\alpha = 0^\circ$.

Figure 23.- Concluded.

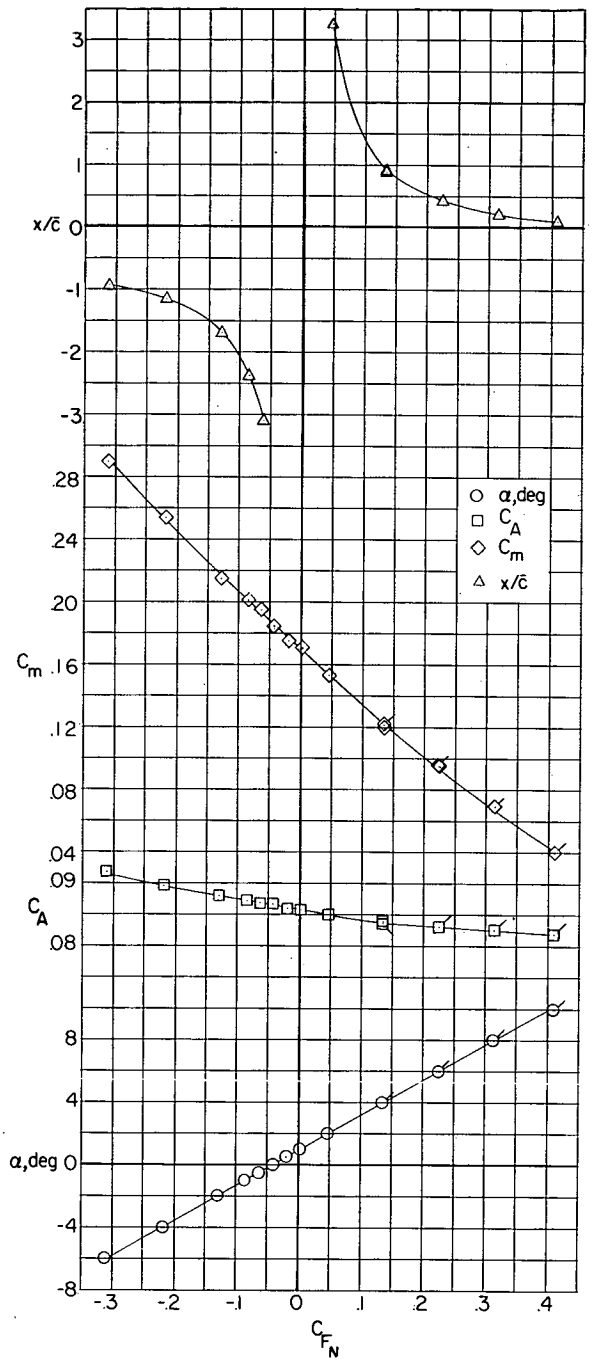

(a) Longitudinal characteristics in body-axis system at $\beta = 0^{\circ}$.

Figure 24.- Complete configuration with $i_t = -10^{\circ}$ at $M = 2.22$.

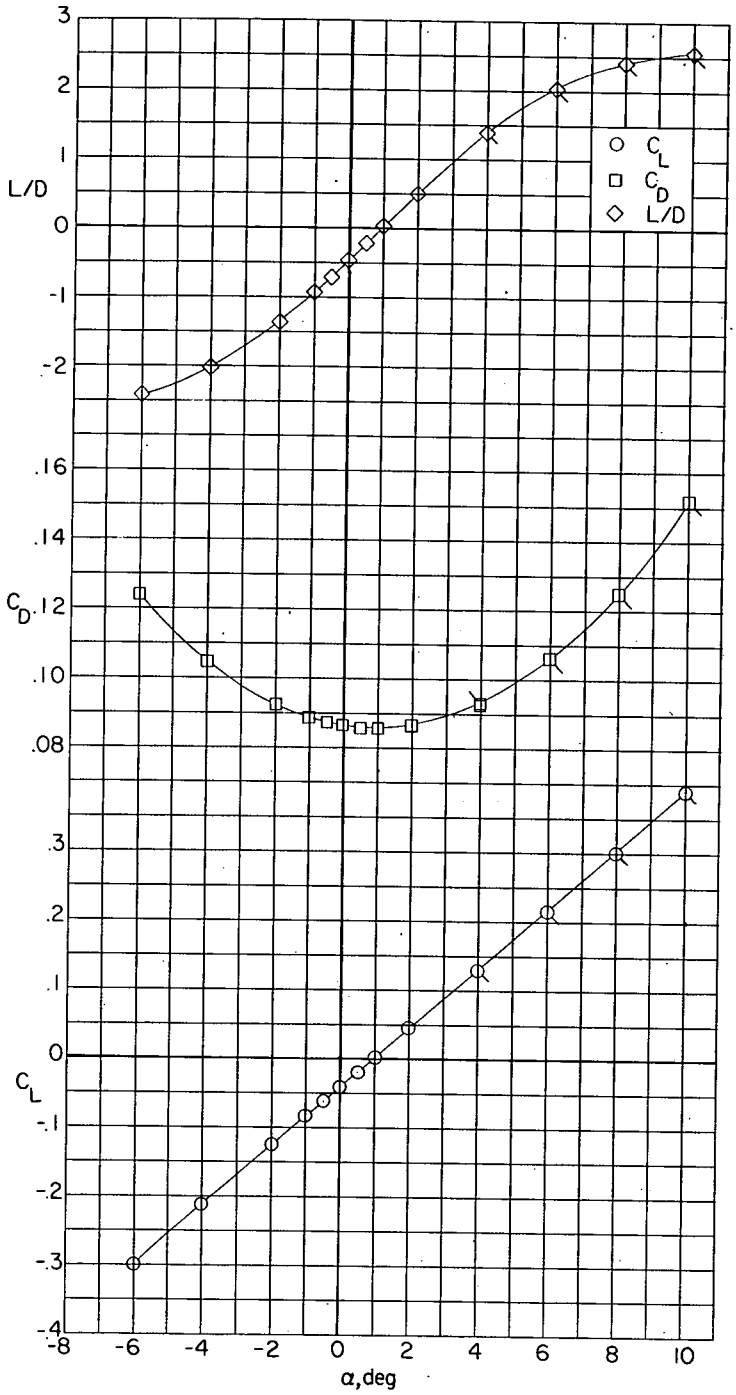

(b) Longitudinal-force characteristics in stability-axis system at $\beta = 0^{\circ}$.

Figure 24.- Continued.

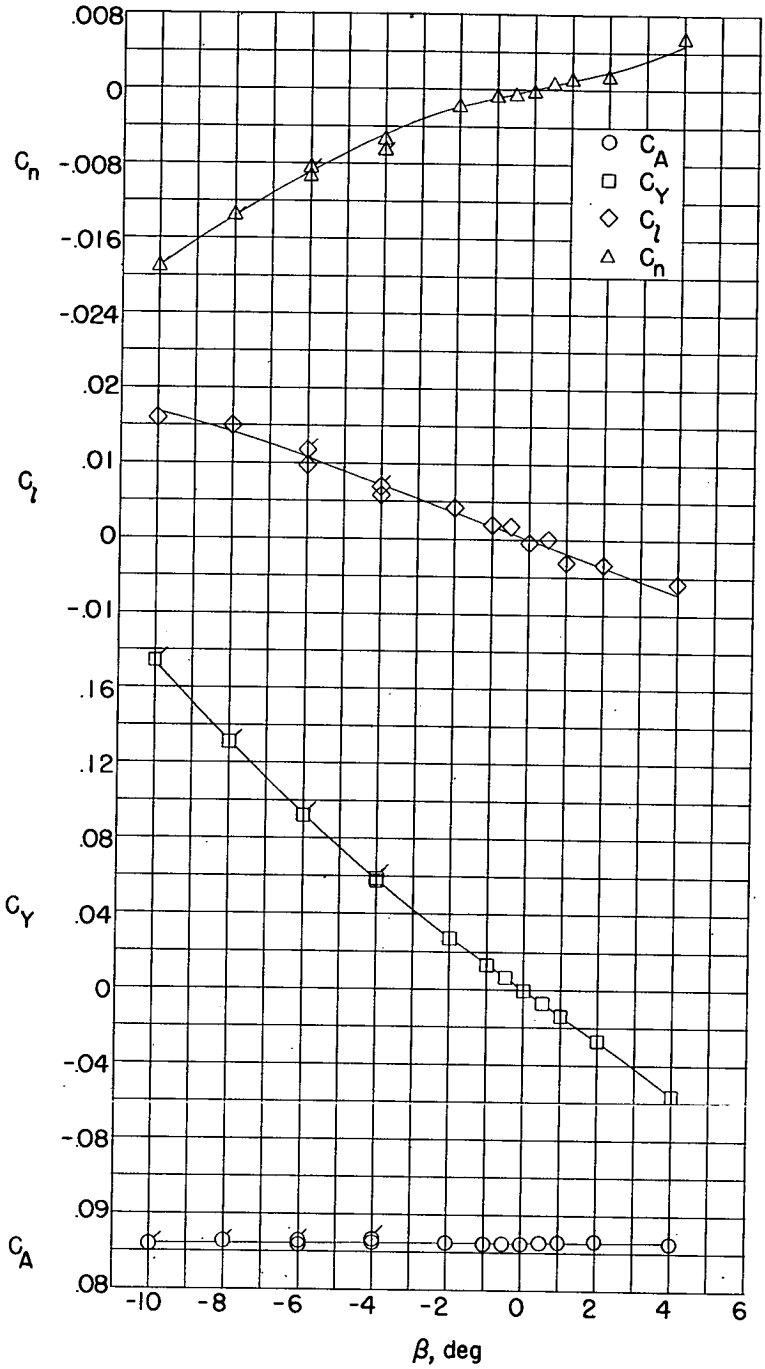

(c) Lateral characteristics in body-axis system at $\alpha = 0^{\circ}$.

Figure 24.- Concluded.

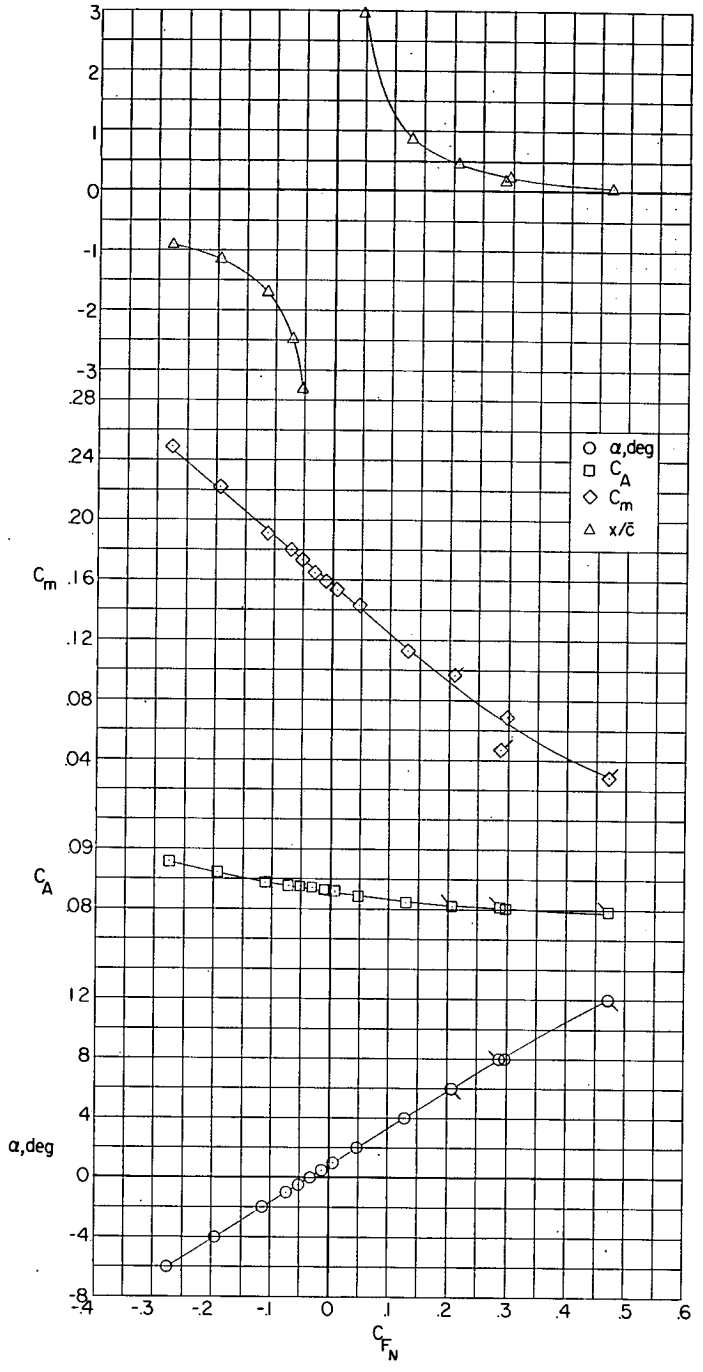

(a) Longitudinal characteristics in body-axis system at $\beta = 0^\circ$.

Figure 25.- Complete configuration with $i_t = -10^\circ$ at $M = 2.40$.

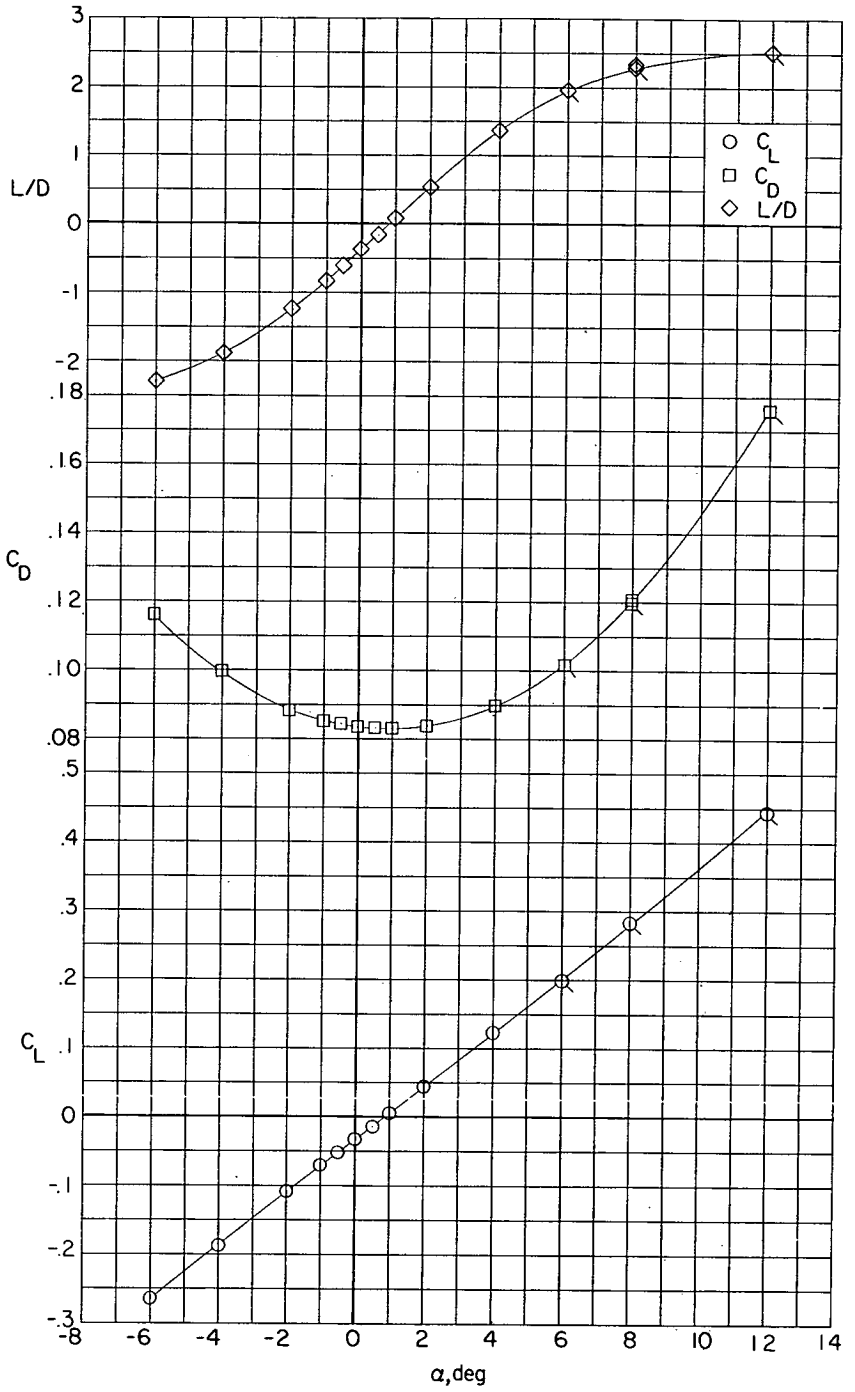

(b) Longitudinal-force characteristics in stability-axis system at $\beta = 0^{\circ}$.

Figure 25.- Continued.

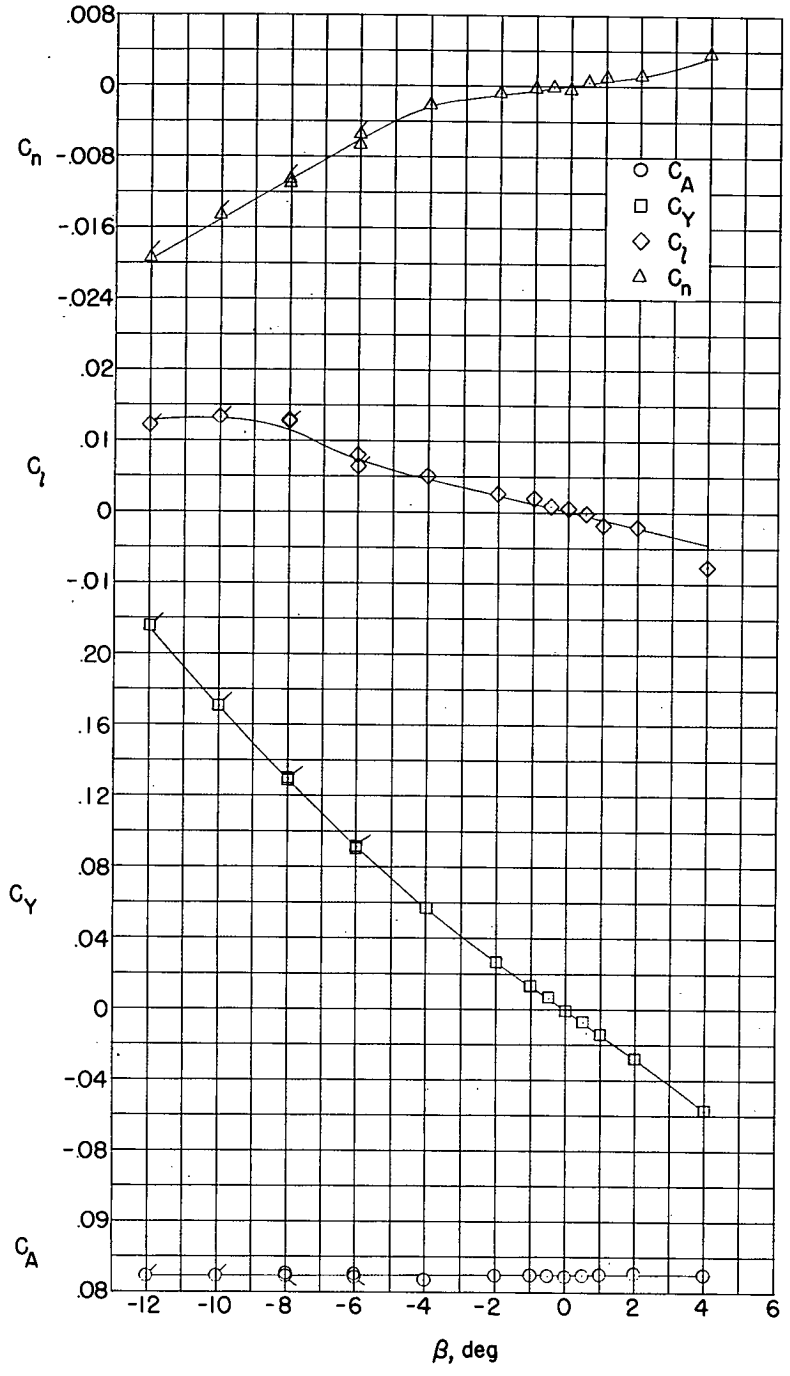

(c) Lateral characteristics in body-axis system at $\alpha = 0^{\circ}$.

Figure 25.- Concluded.

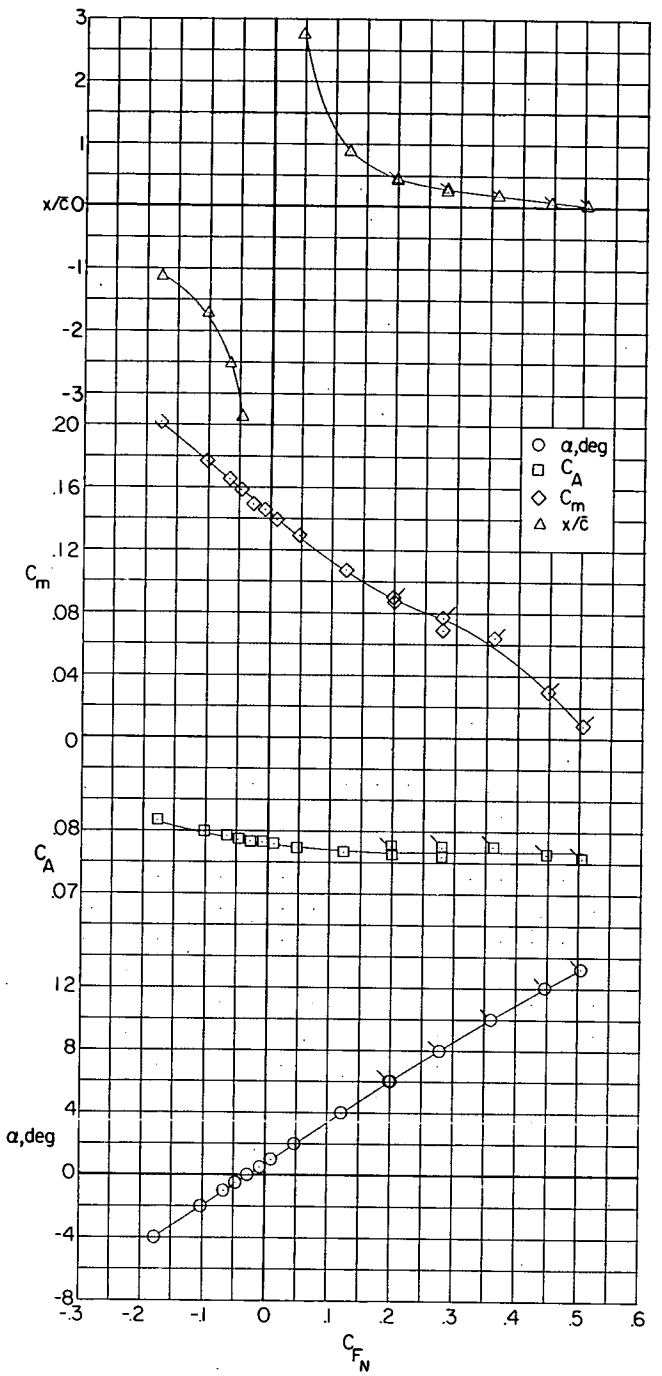

(a) Longitudinal characteristics in body-axis system at $\beta = 0^\circ$.

Figure 26.- Complete configuration with $i_t = -10^\circ$ at $M = 2.62$.

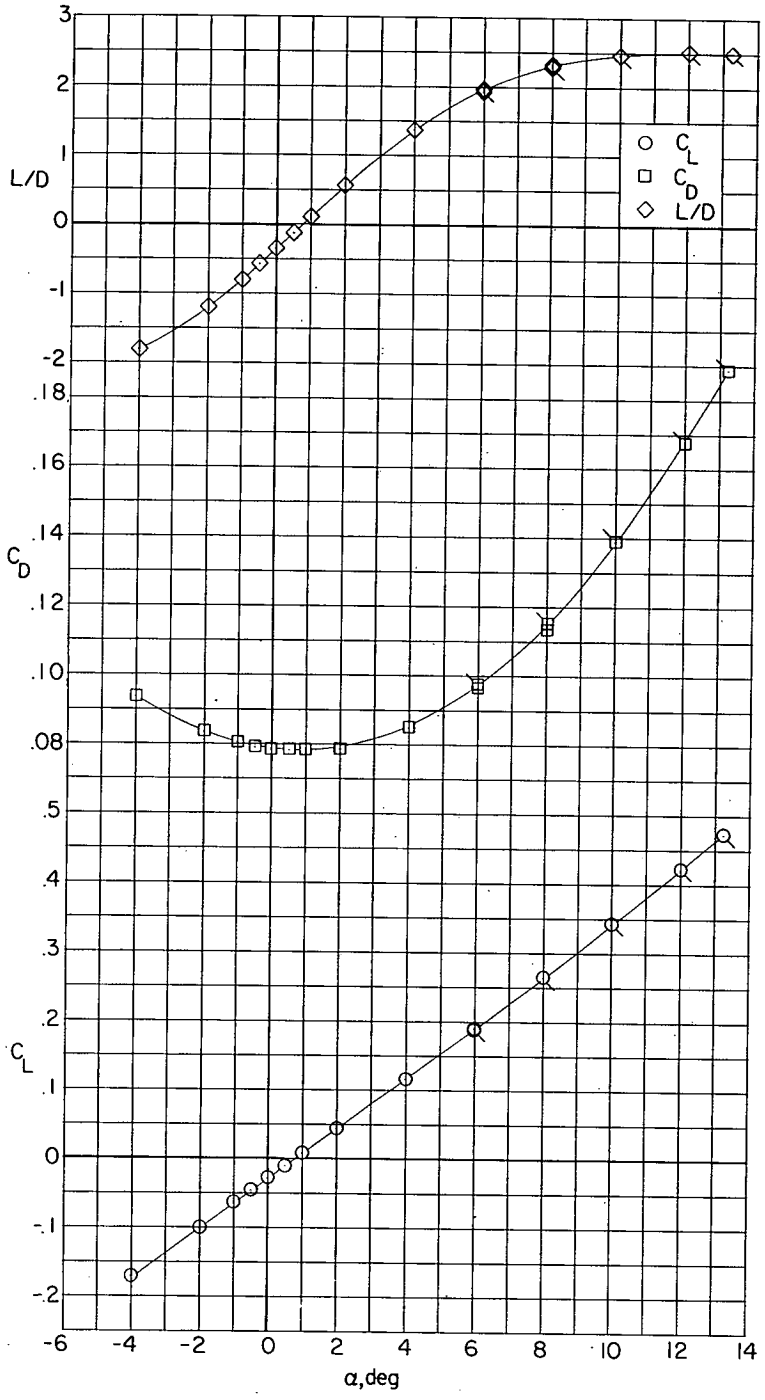

(b) Longitudinal-force characteristics in stability-axis system at $\beta = 0^{\circ}$.

Figure 26.- Continued.

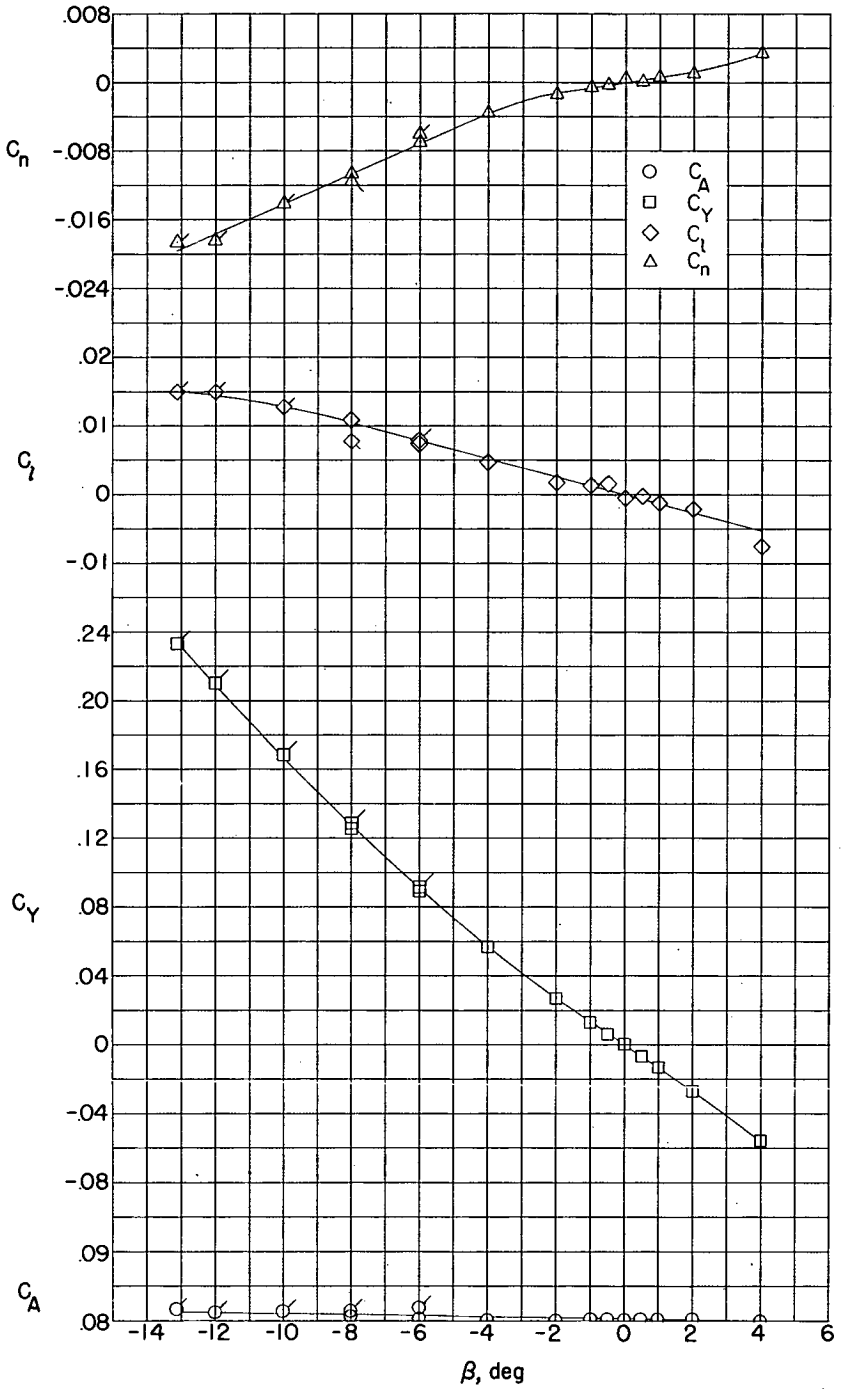

(c) Lateral characteristics in body-axis system at $\alpha = 0^{\circ}$.

Figure 26.- Concluded.

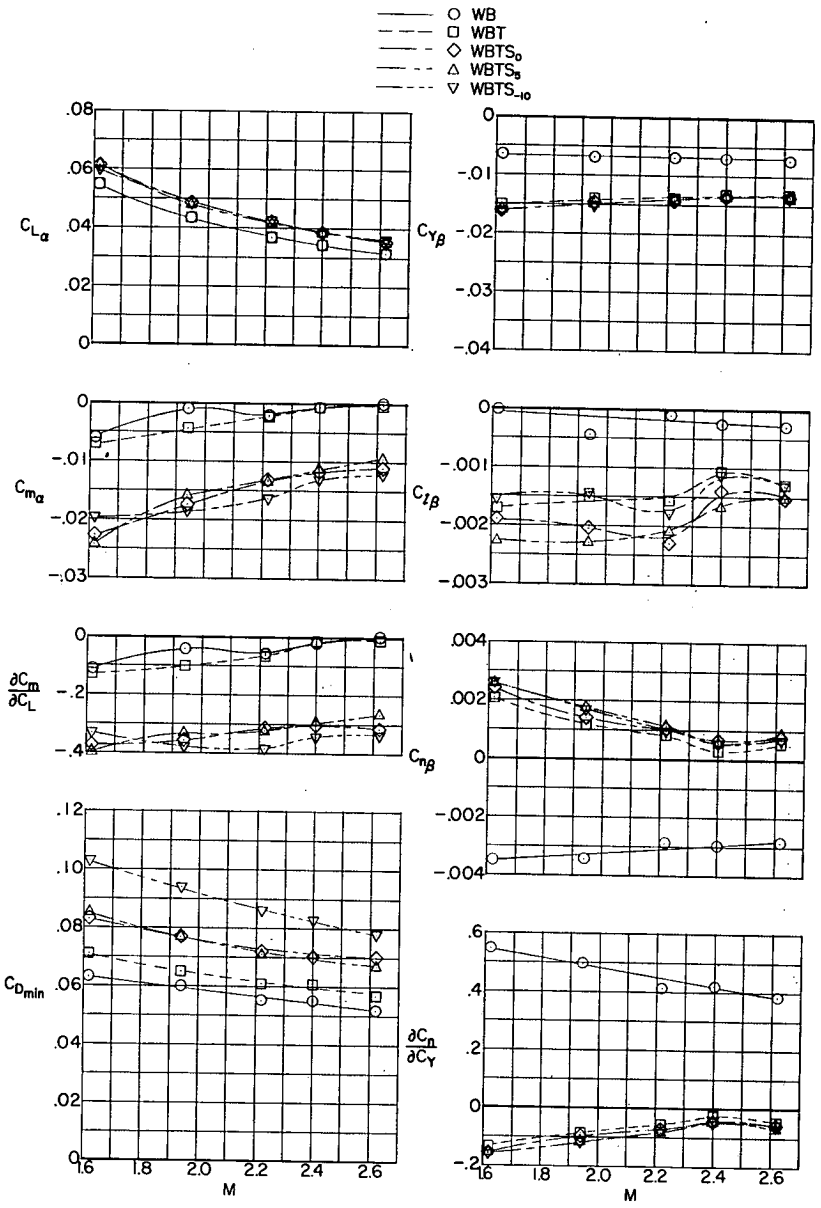

(a) Longitudinal and lateral stability derivatives of X-1E. Longitudinal derivatives through $\alpha = 0^{\circ}$ at $\beta = 0^{\circ}$. Lateral derivatives through $\beta = 0^{\circ}$ at $\alpha = 0^{\circ}$.

Figure 27.- Plot of static longitudinal and lateral stability derivatives and minimum drag of configurations tested against Mach number.

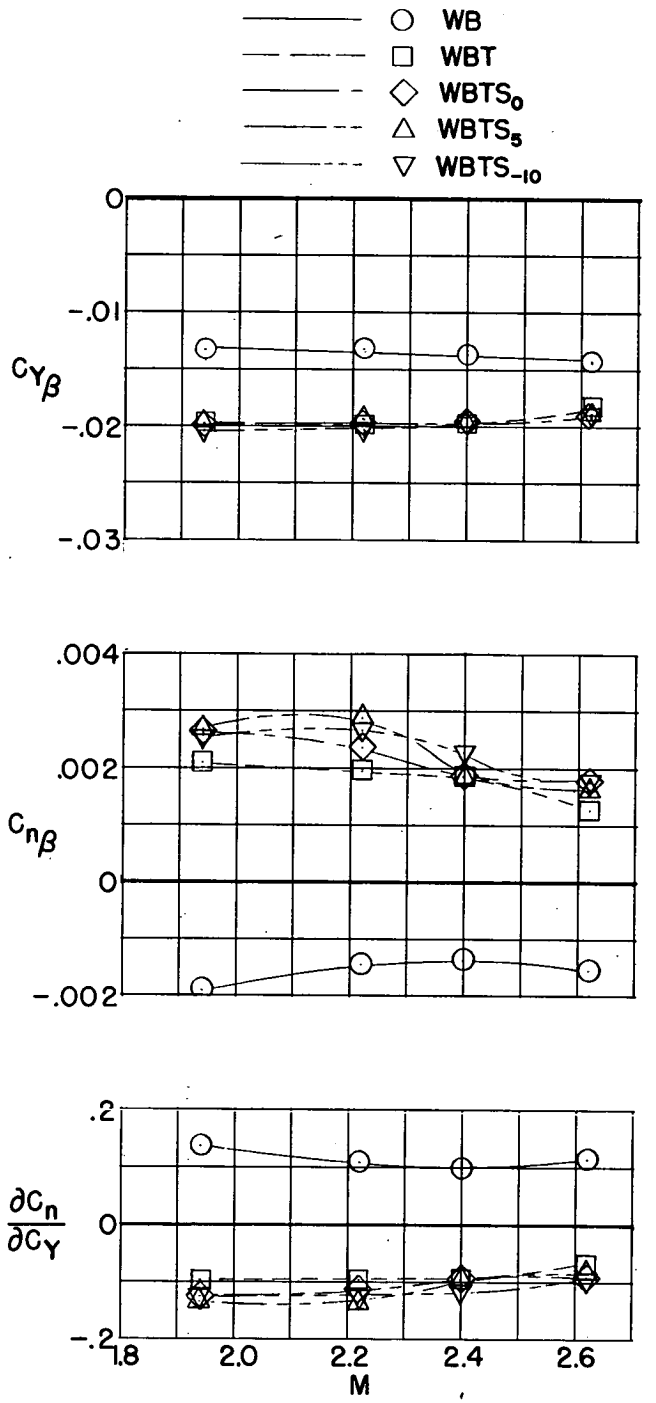

(b) Lateral stability derivatives of X-1E through $\beta = -8^\circ$, $\alpha = 0^\circ$.

Figure 27.- Concluded.

NACA - Langley Field, Va.